

**SYNTHESIS AND CHARACTERIZATION OF Pt-Sn/C
CATHODE CATALYSTS *via* POLYOL REDUCTION
METHOD FOR USE IN DIRECT METHANOL FUEL CELL**

By

Lynwill Garth Martin



Thesis presented in partial fulfilment of the requirements for the degree of

Doctor of Philosophy (Chemistry)

at the

University of the Western Cape

Supervisor: Prof. Ivan R Green

Co- supervisor: Prof. Bruno G Pollet

September 2013

DECLARATION

I declare that SYNTHESIS AND CHARACTERIZATION OF Pt-Sn/C CATHODE CATALYSTS via POLYOL REDUCTION METHOD FOR USE IN DMFC is my own work, that it has not been submitted for any degree or examination in any other university, and that all the sources I have used or quoted have been indicated and acknowledged by complete references.

Full name: .Lynwill G Martin....

Date 23/08/2013

Signed.....



Acknowledgments

First and foremost I would like to thank God almighty for providing me with his mercy and grace to awake each day in order to complete the proposed work. If it were not for His Grace I would have never been able to accomplish this not alone finish this degree. Through all the obstacles and challenges and disappointments God has remained faithful and true.

- I would also like to extend my sincere and deep appreciation to my supervisor **Prof Ivan R. Green**, for his guidance and constant encouragement throughout my research work since joining UWC in 2009. Throughout the project he provided encouragement, sound advice, and lots of ideas. The many discussions we had was a major source of learning. It is an honour and a privilege to be his last PhD student after an academic career that lasted 38 years all whom were spent at UWC.
- I'm indebted to thank **Prof Bruno G. Pollet** for his help and constant support to carry out my research. I was delighted to having him as my co-supervisor since joining HySA Systems in March 2012. I have learned a lot in these few months and I'm grateful to him for imparting his electrochemistry knowledge and for his suggestions during the final part of my project.
- I'm grateful to **Prof. V. Linkov** (SAIAMC Director) and **Dr. L. Khotseng** (ECCR Director) for their kind help for providing financial support and the necessary infrastructure to carry out the research work.
- I'm thankful to **Dr. Huaneng Su** and **Dr. Poitr Bujlo** for assisting with MEA preparation and DMFC testing.
- I wish to thank my lab mates Cecil, Jonathan, Olivia, Wafeeq, Oko, Ncumisa, Tobeka and the rest of the SAIAMC students for their co-operation, fruitful discussion in the labs and computer room.
- I'm extremely thankful to **Dr. H. Abbo** and **Dr. S. Titinchi** for their continuous help with experiments during the initial stages of the project.
- My heartfelt thanks to my friend **Marvin Piet** who helped with the preliminary experiments of the catalysts synthesis while busy with his MSc studies.
- I would like to extend a warm-hearted thank you to **Dr. Subelia Botha** and **Mr. Adrian Josephs** (Electron Microscopy Unit, Department of Physics, University of the Western Cape) for helping and teaching me how to operate the TEM.
- I want to express my heartfelt gratitude to my parent **Godfrey & Linda Martin** whose support, encouragement, limitless love and affection has made my world a beautiful place. I thank them

for all the sacrifices they have made to help me to achieve this degree. Thanks mom and dad you truly are the BEST.

- My heartfelt thanks to my **Ousus Gwyneth** and her husband **Charlton** my **Stranddienste** family my Canadian Family **Ray & Sandra Robyn**. Thanks guys for all the prayers and encouragement during this time I could not have done it without you supporting me.
- My Fiancè (now wife) **Brewine**, for the last few months you have been the best, encouraging me daily to give my best in this final stage of my PhD studies. This is for you and our future together, I LOVE YOU
- Lastly to my Saviour, Healer, Redeemer, Refuge, Deliverer, Counsellor and Friend and Lord the one who made everything possible. Without you in my life Lord all of this would have been for nothing. You give meaning to my life Lord. I honour you for all the blessings and favour in my life. I give you all the honour and all the Glory this is All for YOU.



ABSTRACT

KEYWORDS: Platinum-tin; Methanol resistant; Polyol method; Cathode catalyst; ORR; MOR

Direct methanol fuel cells (DMFCs) are attractive power sources as they offer high conversion efficiencies with low or no pollution. One of the major advantages DMFCs has over PEMFCs is that methanol is a liquid and can be easily stored where in the case for PEMFCs storing hydrogen requires high pressures and low temperatures. However, several challenging factors especially the sluggish oxygen reduction reaction (ORR) and the high cost of Pt catalysts, prolong their commercialization. With the aim to search for more active, less expensive more active ORR catalysts and methanol tolerant catalysts than pure Pt, this dissertation focuses on the development of low loading Pt electrocatalyst and the understanding of their physical and electrochemical properties.

Pt-Sn/C electrocatalysts have been synthesized by a modified polyol reduction method. The effect of temperature, pH, water, sonication and addition of carbon form were studied before a standard polyol method was established. From XRD patterns, the Pt-Sn/C peaks shifted slightly to lower 2θ angles when compared with commercial Pt/C catalyst, suggesting that Sn is alloying with Pt. Based on HR-TEM data, the Pt-Sn/C nanoparticles showed small particle sizes well-dispersed onto the carbon support with a narrow particle distribution. The particle sizes of the different as-prepared catalysts were found to be between 2-5 nm. The Pt-Sn/C HA Slurry pH3 catalysts was found to be the best as-prepared catalyst and was subjected to heat-treatment in a reducing atmosphere at 250-600 °C which led to agglomeration yielding nanoparticles of between 5-10 nm. The Methanol Oxidation Reaction (MOR) on the as-prepared Pt-Sn/C HA Slurry pH3 catalyst appeared at lower currents (+7.11 mA at 860 mV *vs.* NHE) compared to the commercial Pt/C (+8.25 mA at +860 mV *vs.* NHE) suggesting that the Pt-Sn/C catalyst has ‘methanol tolerance capabilities’. Pt-Sn/C HA Slurry pH3 and Pt-Sn/C 250 °C catalysts showed better activity towards the ORR than commercial Pt/C with specific and mass activities higher than Pt/C at +0.85 V *vs.* NHE. The Tafel slopes of Pt-Sn/C HA Slurry pH3 catalyst was -62 and -122 mV dec⁻¹ for the low and high current regions respectively and suggests that the ORR mechanism is similar to that of commercial Pt/C indicating that the ORR kinetics was not negatively influenced by the addition of tin. It was found that the electrochemical oxidation reduction reaction follows first order kinetics of a multi-electronic ($n=4\bar{e}$) charge transfer process producing water. All the Pt-Sn/C catalysts showed resistance towards MOR and it was found for the heat-treated catalysts that an increase in temperature resulted in an increase in methanol tolerance. The synthesized Pt-Sn/C HA Slurry pH3 catalysts were also tested in a fuel cell environment. Electrodes were prepared by either spraying on Toray carbon paper with the Asymtek machine or by

spraying directly on the membrane with a hand spray gun the catalysts coated membrane (CCM) technique. Polarization curves obtained in DMFC with CCM showed superior performance than electrode prepared by spraying on the carbon paper with the machine. In our study, the Pt-Sn/C catalyst appears to be a promising methanol tolerant catalyst with activity towards the ORR in the DMFC.



Project Outputs

Publications

1. Lynwill G. Martin, I.R Green X. Wang, S. Pasupathi and B.G. Pollet “*Pt-Sn/C as a possible Methanol Tolerant Cathode Catalyst for DMFC*”, *Electrocatalysis* 4, (2013)144-153
2. Lynwill G. Martin, Ivan R. Green and Bruno G. Pollet, “*The Effect of Heat Treatment and pH adjustment on Pt-Sn/C for DMFC*, (being prepared for Journal of Power Sources).
3. Lynwill G. Martin, Ivan R. Green and Bruno G. Pollet, “*Modification of Polyol Reduction Method for Pt-Sn/C Catalyst for DMFC*”, (being prepared for Int. J. Hydrogen Energy).

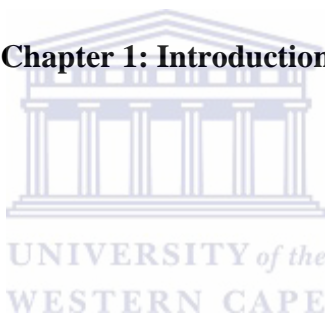
Posters and Talks

1. L.G Martin I.R Green, Synthesis of Pt-Sn/C nanoparticles as possible cathode catalysts for DMFC via Polyol Method, *Zing Hydrogen & Fuel Cell Conference, 1 – 5 December 2011, Cancun, Mexico* (Invited Talk)
2. L.G Martin, I.R Green & B.G Pollet, Pt-Sn/C catalysts as possible methanol tolerant cathode catalysts, *South African & South-Korean Hydrogen Workshop, 11-13 July 2012, Zebula Game Lodge, Bela Bela, South-Africa* (Poster)
3. L.G Martin, I.R Green & B.G Pollet, Electrochemistry of Pt-Sn/C catalysts for use in DMFC, *2nd International Symposium on Electrochemistry, 19-21 July 2012, University of the Western Cape, Bellville, South Africa* (Poster)
4. L.G Martin I.R Green & B.G Pollet, The Effect of Heat Treatment and pH adjustment on Nanoparticle Size and ORR Activity for Pt-Sn/C Catalysts for DMFC, *Zing Hydrogen & Fuel Cell Conference, 12 – 15 July 2013, California, USA* (Poster)

Table of contents

Declaration.....	II
Acknowledgements.....	III
Abstract.....	V
Project Outputs.....	VII
Table of Contents.....	VIII
List of Figures.....	XII
List of Tables.....	XV
Abbreviations.....	XVIII

Chapter 1: Introduction



1.1 Introduction	1
1.2.1 Basics of fuel cells	1
1.3 Basic elements and materials	2
1.3.1 Electrodes	2
1.3.2 Electrolyte	2
1.3.3 Gas Diffusion Layers (GDL)	3
1.3.4 Bipolar plates	3
1.4 Classification of fuel cells	4
1.4.1 Alkaline Fuel Cells (AFC)	5
1.4.2 Phosphoric Acid Fuel Cells (PAFC)	5
1.4.3 Molten Carbonate Fuel Cells (MCFC)	6
1.4.4 Solid Oxide Fuel Cells (SOFC)	6
1.4.5 Polymer Electrolyte Membrane (PEM) Fuel Cells	6
1.4.6 Direct Methanol Fuel Cell (DMFC)	7
1.5 Advantages of DFMCs	8
1.6 Issues involving the DMFC	8

1.7 Aims and Objective of this Study	9
References	11

Chapter 2: Literature review

2.1 Introduction	12
2.2 Catalysis	12
2.2.1 Homogeneous Catalyst	13
2.2.2 Heterogeneous Catalyst	13
2.2.3 Enzymes	13
2.2.4 Electrocatalyst	13
2.3 Electrocatalyst materials	14
2.4 Electrocatalyst for ORR	14
2.4.1 ORR kinetics	15
2.4.2 Criteria for suitable electrocatalysts for ORR	19
2.4.3 Pt Metal as Electrocatalyst	20
2.4.4 ORR mechanism	22
2.5 Pt Alloy Catalysts	22
2.5.1 Pt Alloy Mechanism	22
2.6 Pd and other non- Pt electrocatalysts	25
2.7 Metal Oxides	26
2.8 Methods for the synthesis of supported metal nanoparticles	26
2.9 Polyol Reduction Method	28
2.10 Other methods to prepare nanoparticles	30
References	32



Chapter 3: Experimental Methods and Background Theory

3.1 Catalyst Synthesis	37
3.2 Material Characterization	38
3.2.1 Electron Microscopy (EM)	38
3.2.2 X-Ray Diffraction (XRD)	40
3.2.3 Energy dispersion spectroscopic analysis in transmission electron microscope	40
3.2.4 Inductively coupled plasma – atomic emission spectroscopy	41

3.3 ELECTROCHEMICAL CHARACTERIZATION	41
3.3.1 <i>Glassy carbon (GC) preparation</i>	41
3.3.2 Cyclic Voltammetry (CV)	42
3.3.3 Rotating disc electrode (RDE) experiments	43
3.3.4 Brief theory of electrochemical kinetics	45
3.4 Single Cell DMFC experiments	47
3.4.1 MEA preparation	47
3.4.2 Single cell testing	48
References	49

Chapter 4: Results and Discussion I

Synthesis of Pt-Sn/C catalysts via the polyol reduction method

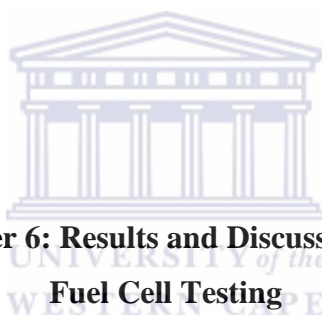
4.1 Introduction	50
4.2 Experimental	50
4.2.1 Synthesis	50
4.2.2 Acid Method	54
4.2.3 Slurry Sonication Method	55
4.2.4 Metals Boiled Method (HA Method)	55
4.3 Standard acid dropped method (STD)	55
4.4 Slurry method	62
4.5 Metals heated first (HA Method)	68
4.6 Metal heated first and then carbon added in slurry form (HA Slurry method)	68
4.7 Heat-treatment of Pt-Sn/C HA Slurry pH3 catalyst.	72
4.8 Comparison of Pt-Sn/C with other Pt-Sn/C catalysts used as cathode catalyst.	78
4.9 Conclusions	80
References	81

Chapter 5: Results and Discussions II

Electrochemical Characterization of Pt-Sn/C electrocatalysts

5.1 Introduction	83
5.2 Test protocol for electrocatalyst	83

5.3 Electrochemical method validation of 3mm Pt disc	85
5.3.1 Electrochemical Surface Area (ECSA)	85
5.3.2 Methanol oxidation reaction (MOR)	86
5.3.3 Oxygen reduction reaction (ORR)	87
5.4 Electrochemistry studies of commercial Pt/C thin-films	90
5.5 Electrochemical characterization of Pt-Sn/C STD catalysts	95
5.5.2 Methanol Oxidation of Pt-Sn/C STD catalysts	96
5.5.3 Oxygen Reduction Kinetics of Pt-Sn/C Catalyst	99
5.6 Electrochemical characterization of Pt-Sn/C HA, Slurry HA Slurry catalysts	100
5.7.1 Electrochemical characterization of Pt-Sn/C HA pH 3 and heat-treated samples	103
5.7.2 Effect of particle size on ORR for Pt-Sn/C HA Slurry pH3 catalysts	109
5.7.3 Methanol oxidation and methanol tolerance studies of Pt-Sn/C HA Slurry pH3 and HA Slurry pH3 heat-treated samples	110
5.8 Accelerated durability studies	113
5.9 Conclusions	117
References	119



Chapter 6: Results and Discussions III
Fuel Cell Testing

6.1 Introduction	122
6.2 Testing of Pt-Sn/C electrocatalysts in a fuel cell environment	122
6.3 Conclusions	128
References	129

Chapter 7
Conclusions and Recommendation

7.1 Conclusions	130
7.2 Recommendations	131

List of figures

Fig. 1.1 Schematic Diagram of DMFC operating principal

Fig. 2.1: Diagram displaying the activation energy pathways with and without a catalyst

Fig. 2.2 Models for the adsorbed states of oxygen on the catalyst surfaces

Fig. 2.3 Different reaction pathways for the reduction of oxygen in acidic medium

Fig. 2.4 Simplified schematic of the ORR pathway based on the scheme of Wroblowa

Fig. 2.4 Proposed mechanism of the ORR of alloying Pt with Fe-group metals

Fig. 2.5 Schematic depiction of various methods for producing supported metal catalysts (a) Impregnation (b) Precipitation (c) Colloidal (d) Ion-Exchange Methods

Fig. 2.6 Chemical reaction for the polyol reduction method

Fig. 3.1 Cyclic voltammogram of Pt/C (Alfa Aesar) in N₂ saturated 0.5 M H₂SO₄ at 20 mV s⁻¹.

Fig. 3.2 illustration of polarization curve corrected to obtain kinetic current in activation controlled region

Fig. 4.2 Preliminary results of polyol method after changes were made

Fig. 4.3 XRD patterns of Pt-Sn/C synthesized with STD method, b) comparison of Pt-Sn/C STD pH3 with 20% Pt/C.

Fig. 4.4 TEM images of high and low magnification of a) Pt-Sn/C STD pH3, b) Pt-Sn/C STD pH5 and c) Pt-Sn/C STD.

Fig. 4.5 Histogram of Pt-Sn/C STD method catalyst particle size distribution a) STD pH5, STD, c) STD pH3.

Fig. 4.6 Change in zeta potential of Pt-Sn colloid and carbon support on changing the pH from acidic to alkaline and vice versa.

Fig. 4.7 Filtered solution of polyol reaction (a) without pH adjustment (b) with pH adjustment to pH5 and (c) with pH adjustment to pH3.

Fig. 4.8 EDX spectra of as prepared Pt-Sn/C catalyst, a) STD, b) STD pH5, c) STD pH3.

Fig. 4.9 XRD patterns of Pt-Sn/C synthesized with Slurry method, b) comparison of Pt-Sn/C Slurry pH3 with 40% Pt/C

Fig. 4.10 TEM image and EDX spectrum of Pt-Sn/C Slurry STD.

Fig. 4.11 (a) Low and high magnification TEM images of Pt-Sn/C Slurry pH3, (b) histogram of particle size distribution of Pt-Sn/C Slurry pH3 catalyst.

Fig. 4.12 XRD patterns of Pt-Sn/C HA pH3 compared to commercial 40% Pt/C (JM).

Fig. 4.13 TEM, EDX and particle size histogram of Pt-Sn/C HA pH3 catalyst.

Fig. 4.14 XRD patterns of Pt-Sn/C HA pH3 compared to commercial 40% Pt/C (JM).

Fig. 4.15 Low and high TEM images of Pt-Sn/C HA Slurry pH3

Fig. 4.16 a) HAADF-STEM image of Pt-Sn/C HA Slurry pH3 b) corresponding EDX spectra of area O₂ analyzed with STEM catalysts

Fig. 4.17 (a-d) XRD patterns of Pt-Sn/C HA Slurry pH3 showing the effect of heat treatment at different temperatures on the catalyst crystalline character.

Fig. 4.18 Pt-Sn/C HA Slurry pH3 heated at 600 °C indicating some of the new peaks formed due to heat-treatment.

Fig. 4.19 (a) Low and high TEM images of Pt-Sn/C HA Slurry pH3 250 °C and corresponding particle size distribution histogram (b) Low and high TEM images of Pt-Sn/C HA Slurry pH3 350 °C and corresponding particle size distribution histogram.

Fig. 4.20 Low and high TEM images of Pt-Sn/C HA Slurry pH3 500 °C and corresponding particle size distribution histogram.

Fig. 4.21 Low and high TEM images of Pt-Sn/C HA Slurry pH3 600 °C indicating crystal lattice fringes and corresponding particle size distribution histogram. catalysts heated at different temperatures.

Fig. 5.1 (a) In-house EC cell (b) electrodes fabricated for the EC cell by spraying on Toray carbon paper

Fig. 5.2 CV of Pt/C using the EC cell and modified Teflon electrode for catalyst testing [1]

Fig. 5.3 Typical CV for a Pt electrode showing H desorption/adsorption region. The red line-1ar baselines are set so as to eliminate contributions to current from charge/discharge of the electrochemical double layer (Coulombic current).

Fig. 5.4 CV for methanol oxidation at Pt electrode in 0.5 M H₂SO₄ + 0.5 M MeOH as 20 mV s⁻¹.

Fig. 5.5 (a) Polarization curves recorded in O₂ saturated electrolyte of Pt electrode (b) Levich plot demonstrating linear dependence of limiting current on and theoretical values for i_{lim}

Fig. 5.6 K-L Plots used to calculate i_k from intercept and number of electrons from the slope.

Fig. 5.7 CV for 3 mm Pt electrode 20 wt.% Pt/C commercial catalysts showing the difference in ECSA.

Fig 5. 8 (a) Linear sweep voltammograms under N₂ showing the effect of subtracting background scan for 20% Pt/C (b) polarization curve of 20% Pt/C showing the effect of IR drop corrections on RDE.

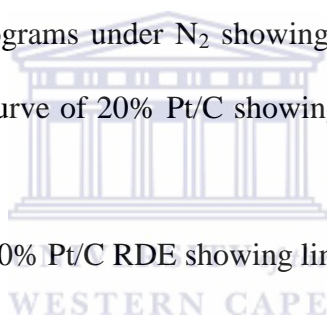


Fig 5.9 (a) Levich plot for thin film 20% Pt/C RDE showing linear relationship between limiting current and $\omega^{1/2}$.

Fig 5.10 (a) (left) iR corrected background subtracted RDE data at various rotation speeds for commercial Pt/C (a) 20% JM, (b) 40% JM and c) 46% TKK, (centre) K-L Plots;(right) mass-transported corrected Tafel plots in O₂ saturated 0.5 M H₂SO₄.

Fig. 5.11 CV of 20% Pt/C and Pt-Sn/C catalysts synthesized with the Polyol STD method recorded in 0.5 M H₂SO₄ at a scan rate of 20 mV s⁻¹ at RM.

Fig. 5.12 CVs of methanol oxidation obtained on a Pt-Sn/C electrode and compared with that of 20% Pt/C in 0.5 M H₂SO₄ solution containing 0.5 M methanol; scan rate 20 mV s⁻¹.

Fig. 5.13 (a) (a) CV of MOR tolerance obtained on a Pt-Sn/C electrode after adding various amounts of methanol (b) CV of MOR tolerance obtained on different Pt-Sn/C electrodes after adding 50 μ l methanol and compared to Pt/C in 0.5 M H₂SO₄ solution; scan rate 20 mV s⁻¹.

Fig.5.14 Polarization curves obtained with a RDE for O₂ reduction on Pt-Sn/C electrodes and compared with that of Pt/C in 0.5 M H₂SO₄ solution at 1500 rpm; scan rate 5 mV s⁻¹.

Fig.5.15 Cyclic voltammograms obtained on a Pt-Sn/C HA Slurry pH3 electrode and compared too Pt/C 0.5 M H₂SO₄ solution; scan rate of 20 mVs⁻¹.

Fig. 5.16 Polarization curves obtained with a RDE for O₂ reduction on a Pt-Sn/C electrode and compared with that of Pt/C in 0.5 M H₂SO₄ solution at 1500 rpm; scan rate 5 mV/s.

Fig.5.17 (*left*) Polarization curves obtained with a RDE for O₂ reduction on Pt-Sn/C HA Slurry pH3 electrode in 0.5 M H₂SO₄ solution at 1500 rpm; scan rate 5 mV/s, (*right*) Koutecky – Levich plots prepared from as prepared Pt-Sn/C HA Slurry pH 3 data at different potentials in mixed kinetic-diffusion controlled region.

Fig. 5.18 Mass transfer Tafel polarization curves of Pt/C and Pt-Sn/C electrodes for ORR (R.T, 1500 rpm, scan rate of 5 mV s⁻¹ in 0.5 M H₂SO₄ solution saturated in oxygen.

Fig. 5.19 CV of methanol oxidation obtained on a Pt-Sn/C electrode and compared with that of Pt/C in 0.5 M H₂SO₄ + 0.5 M methanol solution scan rate 20 mV s⁻¹ (b)

Fig 5.20 CV of methanol oxidation tolerance obtained on a Pt-Sn/C electrode after adding 50 μl methanol and compared with that of Pt/C in 0.5 M H₂SO₄ solution; scan rate 20 mV s⁻¹.

Fig. 5.21 Polarization curves for Pt/C and Pt-Sn/C HA Slurry pH3 in 0.5 M H₂SO₄ + 0.5 CH₃OH under oxygen atmosphere and at a scan rate of 5 mV s⁻¹, rotating speed 1500 rpm.

Fig. 5.22 CV of (a) 20% Pt/C (b) Pt-Sn/C HA Slurry pH3(c) 46% TKK and (d) 40% Pt/C before and after accelerated durability test at 25 mV s⁻¹ in 0.5 M H₂SO₄.

Fig. 5.23 Durability test of different Pt/C and Pt-Sn/C catalysts..

Fig. 5.24 (*top*) Pre-TEM images of (a) Pt-Sn/C, (b) TKK and (c) Pt-Sn/C 250°C (*bottom*) post TEM images

Fig. 5.25 Particle size distribution of pre -and post ADT TEM images of (a) Pt-Sn/C, (b) TKK and (c) Pt-Sn/C 250°C.

Fig. 6.1 Polarization curves of the Pt/C catalysts MEAs after conditioning. Cell temperature, 70°C; methanol concentration and flow rate, 1.0 M and 20.0 ml min⁻¹; dry oxygen, 50 ml min⁻¹ at ambient pressure.

Fig. 6.2 Polarization curves of the Pt/C and Pt-Sn/C catalysts MEAs after conditioning. Cell temperature, 70°C; methanol concentration and flow rate, 1.0 M and 20.0 ml min⁻¹; dry oxygen, 50 ml min⁻¹ at ambient pressure.

Fig. 6.3 Picture of a catalyst coated membrane (CCM).

Fig. 6.4 Polarization curves of CCMPt/C and Pt-Sn/C catalysts MEAs after conditioning. Cell temperature, 70°C; methanol concentration and flow rate, 1.0 M and 20.0 ml min⁻¹; dry oxygen, 50 ml min⁻¹ at ambient pressure.

List of tables

Table 1.1 Different types of fuel cells commonly found

Table 2.1 Preparation methods, selectivity and activity towards oxygen reduction of Pt-alloys compared to Pt.

Table 3.1 Chemicals used for this study.

Table 3.2 ICP-AES operating conditions for the determination of Pt and Sn in electrocatalysts.

Table 4.1 Values of lattice parameters and particle size for Pt-Sn/C catalyst.

Table 4.2 Values of lattice parameters, metal loading and particle size for Pt-Sn/C Slurry catalyst.

Table 4.3 Values of lattice parameters, metal loading and particle size for Pt-Sn/C Slurry catalysts.

Table 4.4 Values of lattice parameters, metal loading and particle size for Pt-Sn/C HA Slurry

Table 4.5 Values of lattice parameters, metal loading and particle size for Pt-Sn/C HA Slurry

Table 4.6 Comparison of different Pt-Sn/C catalyst physical properties used for fuel cell applications

Table 5.1 Parameters in the Levich equation.

Table 5.2 Electrochemical parameters found for crystalline Pt electrode.

Table 5.3 Electrochemical properties of commercial Pt/C catalyst.

Table 5.4 Electrochemical properties of Pt-Sn/C and Pt/C catalysts from ORR data

Table 5.5 Electrochemical properties of Pt-Sn/C Slurry and HA catalysts constructed from CVs and MOR experiments.

Table 5.6 Electrochemical properties of Pt-Sn/C and Pt/C catalysts from ORR data

Table 5.7 ORR kinetic properties of Pt-Sn/C HA Slurry pH3 catalysts series.

Table 5.8 MOR properties of Pt/C and Pt-Sn/C HA Slurry pH3 series catalysts.

Table 5.9 Summary of catalyst properties and ADT data

Table 6.1 DMFC polarization data

Table 6.2 DMFC polarization data of Pt/C and Pt-Sn/C with CCM



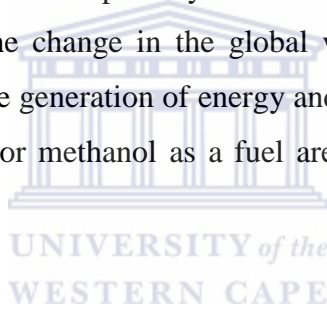
Abbreviations

AFC	Alkaline Fuel Cell
ADT	Accelerated Degradation Test
CH₃OH	Methanol
CCM	Catalyst Coated membrane
CO₂	Carbon dioxide
CV	Cyclic Voltammetry
DMFC	Direct Methanol Fuel Cell
EG	Ethylene Glycol
FC	Fuel cell
GDE	Gas Diffusion Electrode
GDL	Gas Diffusion Layer
H₂	Hydrogen gas
HCl	Hydrochloric acid
H₂O	Water
H₂PtCl₆	Chloroplatinic acid
H₂SO₄	Sulphuric acid
ICP	Inductively coupled plasma
MEA	Membrane electrode assembly
MOR	Methanol oxidation reaction
N₂	Nitrogen gas
NaCl	Sodium chloride
NaOH	Sodium hydroxide
NHE	Normal Hydrogen Electrode
O₂	Oxygen
ORR	Oxygen reduction reaction
PAFC	Phosphoric acid fuel cell
PEMFC	Proton exchange membrane fuel cell
RDE	Rotating disc electrode
STD	Standard
TEM	Transmission electron microscope
XRD	X-ray diffraction

Chapter 1

1.1 INTRODUCTION

The world's increasing demand for energy and the rapid depletion of fossil fuels together with the increase in levels of greenhouse gasses have directed large scale research efforts into the development of alternative clean green energy sources. Energy technologies like wind power, solar cells and nuclear power have received enormous attention in the recent past. However, most of these non combustion power generation forms have limitations to provide the prescribed levels of power consistently and on demand. Nuclear power generation is currently in a state of flux since many countries are in fact downscaling their dependence on this type of controversial energy source. These drawbacks have prevented the wide spread use of these alternative technologies as a primary source of energy. Solar energy for instance depends on sunlight and with the change in the global weather pattern extended days of cloudy skies can severely limit the generation of energy and power availability. In this regard fuel cells that employ hydrogen or methanol as a fuel are becoming more appealing as an alternative energy source [1-2].



1.2. Basics of fuel cells.

A fuel cell is an electrochemical device which consumes fuel and oxidant with the help of electrocatalyst to produce energy. Like other electrochemical devices a fuel cell consists of a positive electrode (cathode), a negative electrode (anode) and an ion-conducting electrolyte. The production of energy involves the oxidation of a fuel and the reduction of an oxidant which is fed to the anode and cathode compartments. This process generates an ion flow through the electrolyte resulting in the flow of electrons through the external circuit. In a fuel cell, electricity can be produced continuously as long as the reactant is available and supplied into the system. Additionally, fuel cells have very little or low emission compared to traditional combustion systems. When hydrogen and oxygen are used as fuel and oxidant respectively, zero emission is possible to be achieved as water is the only by product in the reaction. In the case where methanol or any other carbon containing fuels are used, CO₂ emission is reduced due the high efficiency of the fuel cell and the absence of combustion avoids the production of NO_x and other pollutants.

The discovery of fuel cells can be dated back to 1839 by Sir William Grove and in his prototype fuel cells sulphuric acid was used as electrolyte. Although high efficiency and environmental benefits were promised by the fuel cell concept, developing the early prototype into a commercial product turned out to be much more challenging than anticipated. The main problem associated with the development of fuel cells is to develop appropriate materials and manufacturing techniques to enable fuel cells to become more competitive with existing power generation methods in terms of cost per kWh.

1.3. Basic elements and materials

1.3.1 Electrodes

The electrodes are the elements or reaction sites at which the electrochemical reaction takes place inside the fuel cell. Fuel is oxidized at the anode and the oxidant (usually oxygen or air) is reduced at the cathode. The electrodes are normally constructed out of porous material (graphite) to facilitate a high area to volume ratio. The catalyst (mainly Pt or any other rare earth metallic element) is then coated on the electrodes inner surface in order to reduce the activation energy of the electrochemical reaction. Electrodes are usually the most expensive element of a fuel cell due to the high cost of the catalyst. The most important functions of the electrodes are:

- To provide physical active sites for the electrochemical reaction to occur.
- To separate the gas phase (H_2 or O_2) from the electrolyte.
- To transport the ionic species to complete the chemical reaction (mass and charge transport).

Electrodes are seriously affected by poisoning mainly due to impurities existing in the gasses. As a result of this, before use, the fuels need to undergo a cleaning and reforming process.

1.3.2 Electrolyte

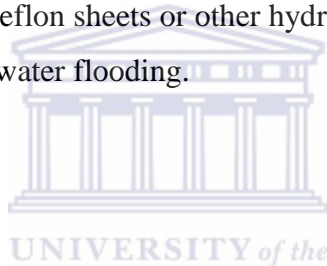
The electrolyte is an integral part of the fuel cell that separates the anode from the cathode in order for the reduction and oxidation reaction (redox) to occur at different sites of the cell. The electrolyte must inhibit the flow of reactants from one side to the other side of the cell and in addition need to be impermeable to electrons since they have to flow through an

external circuit. To balance the electrochemical reactions, the electrolyte must be able to transport ionic species (H^+ , OH^-) from the cathode to the anode or vice versa. The most important functions of the electrolyte can be summarised as follows:

- To separate the anode from the cathode.
- To avoid fuel cross-over from the anode to the cathode.
- To avoid electrical conduction.

1.3.3 Gas Diffusion Layers (GDL)

Gas diffusion layers (GDL) are used in low temperature fuel cells to distribute and supply the fuel and air to the surface of the electrodes. They can also be used to remove the exhausted reactants and the reaction products. The GDL are usually made of carbon cloth or carbon paper and can be modified with Teflon sheets or other hydrophobic materials to increase their hydrophobic character and avoid water flooding.



1.3.4 Bipolar plates

One individual cell (one electrolyte sandwiched between two electrodes) usually provides low voltages (~ 1 V). To increase the electrical power output, single cells can be connected in series or parallel configuration in so called fuel cells stacks. The bipolar plates are the elements used to separate adjacent fuel cell units.

The main functions of the bipolar plates are:

- To deliver the reactant gasses to the electrodes.
- To remove waste heat.
- To conduct electrons within an internal circuit as part of the electrochemical reaction.

Bipolar plates are commonly made from graphite due to its high electrical conductivity and high resistance to corrosion. They can also be made from metal to increase their conductivity and reduce their size.

1.4 Classification of fuel cells

During recent years fuel cell development underwent important changes and improvements. Earlier, fuel cells prototypes required operation at high temperatures in order to achieve high performances and this required very resistant and expensive materials. Nowadays there are a huge variety of fuel cells being employed in different application areas. Fuel cells with different composition, capabilities and working principles were investigated and could be classified under groupings viz., electrolyte materials and operating temperatures. Table 1 illustrates several different types of fuel cells commonly found today [1-4].

Table 1. Different types of fuel cells commonly found.

Fuel Cell	Electrolyte	Application	Operating Temperature
Alkaline fuel cell (AFC)	KOH solution	Space, military	<120°C
Phosphoric acid fuel cell (PAFC)	H ₃ PO ₄	Stationary, transportation	180~200°C
Molten carbonate fuel cell (MCFC)	Immobilized liquid molten carbonates	Stationary	~650°C
Solid oxide fuel cell (SOFC)	ceramics	Stationary, auxiliary power	550~1000°C
Proton exchange membrane fuel cell (PEMFC)	Ion exchange membranes	Portable, stationary, transportation	<120°C
High temperature proton exchange membrane fuel cell (HT-PEMFC)	Polybenzimidazole (PBI)-H ₃ PO ₄	Portable, stationary, transportation	~180°C
Direct Methanol Fuel Cell (DMFC)	Ion exchange membranes	Portable, stationary,	50-90°C

1.4.1 Alkaline Fuel Cells (AFC)

Alkaline fuel cells were one of the first cell technologies developed and used in the US space program. AFC make use of a solution of potassium hydroxide in water as the electrolyte and a variety of non-precious metals as catalysts for the cathode and anode. High temperature AFC operate between 100 – 250 °C and low temperature AFCs at roughly 23 -70 °C. In AFC the ionic charge is compensated for by the transport of OH- groups from the cathode to the anode through the electrolyte. The high performance of AFCs is due to the rate at which chemical reactions takes place in the cell and have shown efficiencies near 60% in applications. The disadvantage of AFCs is that they are easily poisoned by carbon dioxide which even in low concentration influences the performance of the fuel cell [1-3].

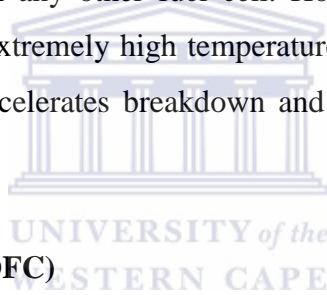
1.4.2 Phosphoric Acid Fuel Cells (PAFC)

Phosphoric acids fuel cells are commercially the most advanced fuel cell system due to its relatively simple construction and a combination of the thermal and chemical stability. These types of fuel cells use liquid phosphoric acid as an electrolyte. The acid is stored in a Teflon silicon carbide matrix and a porous carbon electrode containing a platinum catalyst is employed due to the highly corrosive nature of H₃PO₄. The PAFC is considered as the first generation of modern fuel cells and is typically used for stationary power generation although some PAFCs have been used to power large city busses. PAFCs are more tolerant to impurities than PEM cells (see 1.3.5 below) which are easily poisoned by CO that binds to the catalyst at the anode thereby decreasing the cell efficiency.

The fact that PAFCs requires an expensive platinum catalyst raises the cost of the fuel cell. Another problem associated with PAFC is electrode flooding and drying and this has been recognized as the major cause of the declining cell performance. Migration of H₃PO₄ between the matrix and the electrodes during cell load cycling is a further contributing factor responsible for these problems. Recent studies have shown that by introducing H₃PO₄ into polymer bearing functional groups like alcohols, amides, imines or ethers the cell performance can be improved. The acid-base system not only exhibits a high conductivity but also mechanical stability at elevated temperatures (>100°C), for example the polybenzimidazole (PBI)/H₃PO₄ systems [3-5].

1.4.3 Molten Carbonate Fuel Cells (MCFC)

Molten Carbonate Fuel Cells were developed for natural gas and coal based power plants and to be employed for industrial and electrical utility applications. MCFCs are high temperature fuel cells that use a molten carbonate salt mixture suspended in a porous chemically inert ceramic lithium aluminum oxide (LiAlO_2) matrix representing the electrolyte. At these extremely high temperatures, non precious metals can be used as catalysts for both anode and cathode thereby reducing the cost dramatically. Unlike alkaline, phosphoric acid and PEM fuel cells, MCFCs do not require an external reformer to convert more energy dense fuels to hydrogen. These fuels are converted into hydrogen due to the high temperature at which MCFC operates. This process is known as internal reforming which further reduces the cost. MCFCs are not affected by CO or CO_2 poisoning. They can use CO_2 as fuel making MCFCs suitable for fuelling with gasses made from coal. Another big advantage is that MCFCs are more resistant to impurities than any other fuel cell. However, the main disadvantage of MCFCs is their durability. The extremely high temperature at which these cells operate and the corrosive electrolyte used accelerates breakdown and corrosion thereby decreasing the cell life [1-3].



1.4.4 Solid Oxide Fuel Cells (SOFC)

Solid oxide fuel cells (SOFCs) use a hard ceramic compound as the electrolyte. SOFCs operate at temperatures around $1000\text{ }^\circ\text{C}$ and there is therefore no need for precious metal catalysts to reduce costs. SOFCs also have similar abilities to the MCFCs to reform fuels internally. SOFCs are also the most sulphur resistant fuel cell type. Additionally they are not poisoned by CO which can then be used as a fuel. Operating at these high temperatures does however have certain disadvantages. It results in a very slow start up and requires enormous thermal shielding to protect personnel and retain heat. It is therefore not suitable for transportation and portable devices. The high operating temperatures also place strict requirements on materials used for SOFC [1-3].

1.4.5 Polymer Electrolyte Membrane (PEM) Fuel Cells

Polymer electrolyte membrane (PEM) fuel cells also known as proton exchange membrane fuel cells operate at relatively low temperature (around $80\text{ }^\circ\text{C}$), have high power density and

are thus suitable for automobile applications. PEMFCs use solid polymer membranes which are able to conduct protons in the electrolyte. The electrolyte is sandwiched between two electrodes, which contain Pt-based catalysts to speed up the oxidation and reduction processes taking place. PEMFCs require only hydrogen, oxygen from the air and water to operate and involve no corrosive fluids like some fuel cells. These cells are fuelled with pure hydrogen supplied from storage tanks. PEMFCs are used for transportation and some stationary applications. Hydrogen storage is however, a big stumbling block in using these fuel cells in vehicles. Hydrogen must be stored onboard in pressurized tanks as a compressed gas and due to the low energy density of the gas it creates problems when it comes to powering vehicles over long distances. Recent work on PEMFCs has been mainly focusing on developing high temperature ion exchange membranes so that fuels can be operated at higher temperatures. This new development provides the benefit of decreasing or even replacing loading of noble metals which enables the fuel cells to be self-sustainable and avoids the requirements of cooling and purifying systems [1-5].

1.4.6 Direct Methanol Fuel Cell (DMFC)

The DMFC is also a PEMFC as it uses a proton exchange membrane as electrolyte. The only difference between the PEMFC and the DMFC is that the latter uses methanol as a fuel instead of hydrogen. Fig. 1 is a schematic drawing of a fuel cell which demonstrates the basic principles in the operation of a DMFC. The DMFC works by oxidizing methanol to CO₂ and water. Methanol releases 6 protons and electrons per molecule during its oxidation and its high energy density makes methanol a suitable fuel for fuel cells. DMFC works at low and intermediate temperatures (60 – 90 °C) and are fed a dilute aqueous solution of methanol and water. The hydrogen ions flow through the PEM to the cathode where air or oxygen is introduced. At the cathode the hydrogen ions react with oxygen to form water and the movement of the free electrons through an external circuit from the anode to cathode creates a current that can be used to power an electrical device. The maximum voltage attainable from the overall reaction in the DMFC in theory is 1.18 V. In practice this maximum output is not achieved due to poor electrode kinetics and ohmic losses of the electrolyte [5-7].

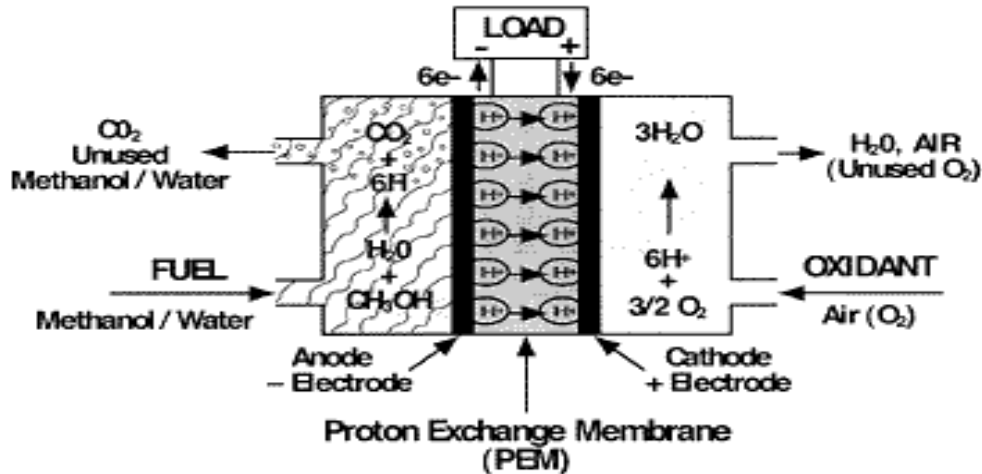
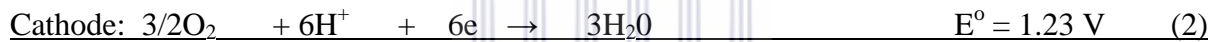


Fig. 1 Schematic Diagram of DMFC operating principal [2].

The relevant electrode reactions are:



1.5 Advantages of DFMCs

There are several advantages in using methanol as a fuel. Methanol is a liquid and can be fed directly into the fuel cell. Steam reforming of the fuel is not necessary, methanol is easier to store when compared to hydrogen which needs low temperature and high pressures. Also the energy density of methanol is much higher than that of compressed hydrogen. The DMFC operates at moderate temperatures and therefore does not need sophisticated cooling systems to remove excess heat formed as a result of the reactions occurring in the fuel cell. Because of this advantage DMFCs can be used as portable systems and is ideally suitable for applications in laptops, cellular phones and other small items [8-9].

1.6 Issues involving the DMFC.

There are still some problems involved in DMFC technologies which need to be addressed before the commercialization stage. One problem associated with the anode is the sluggish

methanol oxidation reaction. During methanol electro-oxidation various surface intermediates (CO_{ads} , COH_{ads} , CHOO_{ads}) are formed which poison the catalyst. The intermediate species are not easily oxidized and are adsorbed strongly onto the catalyst surface preventing fresh methanol molecules from adsorbing and undergoing further reaction. The switch from Pt to a bimetallic Pt/Ru as anode catalyst provided some improvement in the methanol oxidation rates and is currently being used as anode catalyst for DMFC systems. Another big challenge for DMFC development is the methanol cross-over problem which leads to decreased overall cell lifetime and efficiency. In this case methanol diffuses (permeates) through the membrane from the anode to the cathode side which negatively influences the ORR taking place on the cathode side. The reaction of methanol at the cathode results in a loss of fuel and cathode voltage and is referred to as a mixed potential. Methanol that crosses over reacts with oxygen at the cathode resulting in a loss of current. Besides, the cathode catalyst, which comprises of pure platinum, is fouled by methanol oxidations intermediates similar to the anode. Therefore, typically, low methanol concentrations (1-2 M; 4-8 Vol.%) are used to combat this problem. If methanol cross-over was not an issue, much higher methanol concentrations could be used [1,9].

There is therefore a need for the development of a cathode catalyst with high methanol resistance capabilities as well as selectivity towards the Oxygen Reduction Reaction (ORR) to overcome the challenges faced with the commercial deployment of DMFC.

1.7 Aims and Objective of this Study

The oxygen reduction reaction (ORR) takes place on the cathode side of the DMFC and is currently the area of biggest concern for DMFC development. Therefore, considerable time and R&D funding have been channelled into the development of a new cathode electro catalyst as is evident by the increased number of publications appearing on DMFC focusing on the cathode [10]. At present Pt/C is mostly used as cathode catalyst for oxygen reduction in DMFC's but due to several problems viz., high over potential under typical experimental conditions (300-400 mV), corrosion at high potentials of 0.8 V vs NHE, high cost of Pt and sluggish kinetics for oxygen reduction on Pt, its practical application have been rather limited. One of the possible ways to overcome these challenges is to alloy Pt with suitable metals supported on carbon [1,11]. Several reports exist in literature where Pt has been alloyed with metals such as Cu, Ni, Fe, Pd, Cr for ORR as cathode catalyst and have been studied extensively. However, very few reports are available where the Pt-Sn/C system has been

used as a cathode catalyst in fuel cells [11,12]. Jeyabharathi *et al.* [12] reported that the *as*-prepared Pt-Sn/C catalyst shows a mixed behaviour when compared to the catalyst subjected to heat treatment. The methanol tolerance increases with increase in temperature whereas the ORR activity remains intact. They clearly demonstrated that heat treatment of the catalyst has a significant outcome on the ORR activity as well as a resistance of the Pt-Sn/C catalyst towards methanol. Because of this finding, it is of interest to our research group to extend and investigate the possibility of using the Pt-Sn alloy system as a possible methanol tolerant cathode catalyst.

The main objectives of this PhD study were to develop an improved Pt-Sn/C catalyst for the oxygen reduction reaction and may be divided into the following sections.

- Synthesis of a range of Pt-Sn/C cathode catalysts via the polyol reduction method.
- Study the influence of temperature, change in pH, addition of water, sonication, Pt:Sn ratio and addition of the carbon matrix support either as is, or in slurry form to generate a large number of synthetic protocols.
- Heat treatment of the catalyst under inert conditions in a tube furnace from 250-600°C.
- Evaluate all the synthesized catalysts electrochemical and physical properties by means of X-Ray Diffraction (XRD), Transmission Electron Microscopy (TEM), Energy Dispersive X-Ray (EDX), Cyclic Voltammetry (CV), Methanol Oxidation Reaction (MOR), Oxygen Reduction Reaction (ORR).
- Compare the activities of the synthesized catalysts with the 20%, 40% commercial Pt/C (JM) and 46% Pt/C (TKK).
- Test the catalyst in a working fuel cell.

REFERENCES

1. J. Larminie, A. Dicks, Fuel Cell Systems Explained, John Wiley & Sons, Chichester, 2000
2. R.O. Hayre, W. Colella, S.K. Cha, F.B. Prinz, Fuel Cell Fundamentals, John Wiley & Sons, New York, 2009
3. K. Kordesch G. Simader, Fuel Cells and their Applications, Wiley-VCH, Weinheim, 1996
4. Z. Wang, H. Rivera, X. Wang, E. Smotkin. *J. Power Sources*.177 (2008) 386
5. J.S. Newman, K.E. Thomas-Alyea, Electrochemical Systems, John Wiley & Sons, Inc., Hoboken, New Jersey. 2004
6. S. Srinivasan, R. Mosdale, P. Stevens, C. Yang, *Annu. Rev. Energ. Env.* 24 (1999) 281.
7. B.D. McNicol, D.A.J. Rand, K.R. Williams, *J. Power Sources* 100 (2001) 47
8. G. Pérez, E. Pastor, C.F. Zinola, *Int. J. Hydrogen Energy*. 34 (2009) 9523
9. E. Antolini, T. Lopes, E.R. Gonzalez, *J. Alloys Comp.* 461 (2008) 253
10. ISI Web of Science (<http://isiknowledge.com>)
11. A.K. Shuka, R.K. Raman, *Annu. Rev. Mater. Res.* 33 (2003) 155
12. C. Jeyabharathia, P. Venkateshkumarb, J. Mathiyarasua, K.L.N. Phania, *Electrochim. Acta* 54 (2008) 448

Chapter 2

Literature Overview

2.1 INTRODUCTION

Chemical reactions require a specific amount of energy to able them to proceed to completion at a reasonable rate. This energy barrier is described as the activation energy and can cause potential problems for some reactions if it is too high. Catalysts are substances that lower this activation energy, thus causing an increase in the rate at which the reaction occurs [1]. The general definition for a catalyst is that it is a substance that can cause a change in the rate in a chemical reaction without itself being consumed in the reaction. Changing the reaction rate by use of a catalyst is called catalysis. Fig. 2.1 gives a schematic representation of how the catalyst influences the activation energy of a chemical reaction. The activation energy, which is the minimum amount of energy needed for a specific reaction, is lowered when a catalyst is added. A new mechanism or reaction pathway is provided by which the reaction may then proceed when a catalyst is employed in a reaction. There are several different types of catalyst that can be used in a variety of chemical reactions [1-4].

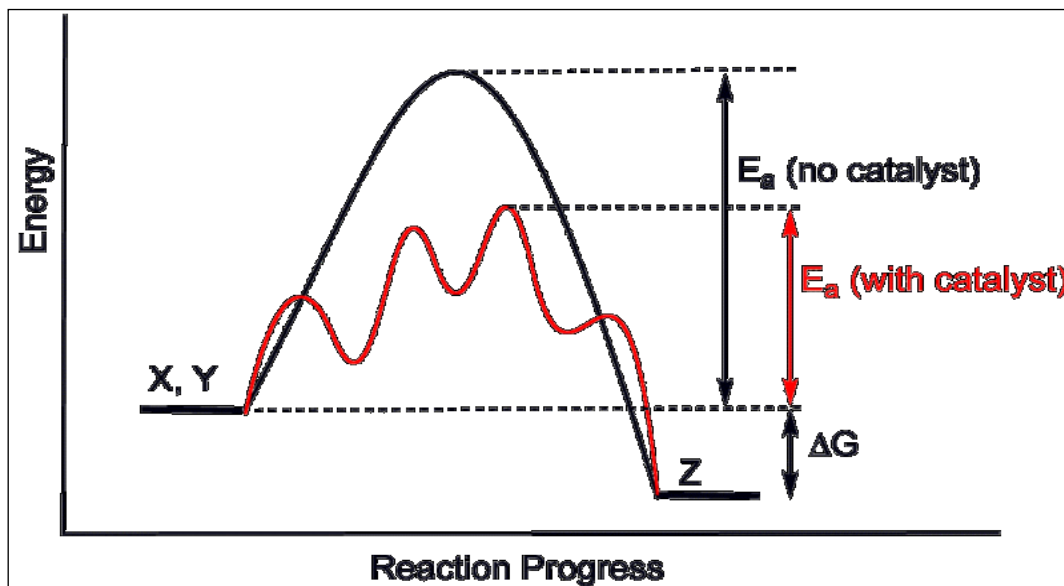


Figure 2.1: Diagram displaying the activation energy pathways with and without a catalyst [2].

2.2 Catalysis

2.2.1 Homogeneous Catalyst

Homogeneous catalysts function in the same phase as the reactant. These types of catalyst are typically dissolved in a solvent and added to the substrate which is also in liquid form. For example the hydrolysis of esters is catalyzed by the presence of a small amount of base (KOH or NaOH). In this reaction, it is the hydroxide ion, OH^- that reacts with the ester and the concentration of the hydroxide ion is greatly increased over that of pure water by the addition of the base. Although some of the hydroxide ions provided by the base are used up in the first part of the reaction, they are regenerated in a later step from water molecules. This in fact ensures that the net amount of hydroxide ion present is the same at the beginning and end of the reaction and for this reason the base is considered to be a catalyst [3-5].

2.2.2 Heterogeneous Catalyst

A heterogeneous catalyst functions in a different phase to that of the reactant. The most common heterogeneous catalyst occurs as a solid catalyst and liquid reactants. An example of this type of catalyzed reaction is the hydrogenation of vegetable oil in the presence of a nickel catalyst. In this reaction, vegetable oil is in a liquid form and the Ni catalyst is in the solid phase. Heterogeneous catalysts are normally supported which means the catalyst is dispersed on a secondary material to increase its surface area of contact that enhances the effect [3-5].

2.2.3 Enzymes

Enzymes are a special type of catalyst that lowers the activation energy for a variety of important biological and physiological processes. They are usually proteins which are composed of a chain of amino acids. Enzymes largely act as homogeneous catalysts although there are some that may act as a heterogeneous catalyst as well [6].

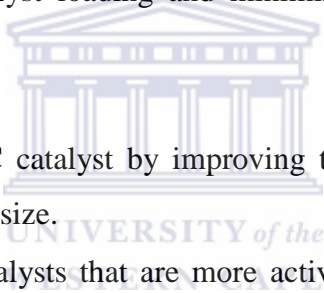
2.2.4 Electrocatalyst

Electrocatalysts are metal based catalysts that are used in half reactions in fuel cells. These substances reduce the activation energy required for the reduction or oxidation of molecules allowing energy to be generated. One common type of fuel cell electrocatalyst is based upon

nanoparticles of platinum that are supported on slightly larger carbon particles (Pt/C). An electrocatalyst is unique in that it does not only lower the activation energy but goes a step further than other catalysts by lowering the excess energy consumed by a redox reaction activation barrier [3-5].

2.3 Electrocatalyst materials

DMFC and PEMFC catalysts are often based on expensive metal material like Pt and it is therefore most desirable to find new catalysts in order to reduce their costs as much as possible. A very small amount of Pt nanoparticles supported on carbon is needed for the facile hydrogen oxidation reaction in PEMFC. In contrast, in the case of DMFC a much higher Pt loading is needed for both anode and cathode catalyst. This is necessary due to the very poor reaction kinetics and poisoning caused by the high methanol crossover. The strategy involved to reduce catalyst loading and minimize cost has followed three basic principals which are: [7-10].

- 
- Optimize the current Pt/C catalyst by improving the dispersion/distribution and by also decreasing Pt particle size.
 - Develop new Pt-alloy catalysts that are more active than pure Pt and also resistant towards methanol crossover in the case of DMFC.
 - Develop new Pt-free catalysts that are less expensive than Pt even if they are less active than the current Pt catalyst.

Several research groups have successfully achieved the one strategy of increasing Pt dispersion by reducing the Pt particle size. In some cases these improved Pt nanoparticles are smaller than the best commercial catalyst. It has been found that maximum dispersion is achieved at around 1.1 nm and any further decrease in diameter will have no improved effect on the Pt dispersion. At these small particle sizes, agglomeration seems to have manifested itself as a problem because of the large surface area and surface energy of the nanoparticles which will negatively influence the catalyst activity. So, there is a compromise between dispersion and durability [1].

The second strategy to reduce the Pt loading, namely by developing novel Pt-alloy catalysts will be discussed in detail in the following section with the specific focus on cathode

electrocatalysts which is the main topic of this thesis. The discussion will include mechanistic and application of these novel electrocatalysts for the oxygen reduction reaction in which the alloying metal is Sn.

The third strategy where Pt-free catalysts are prepared won't be looked at for this study although it is an important aspect concerning future catalyst development. With the increasing price of Pt, Pt-free catalysts will play an ever increasing and important role in fuel cell development in the future. However, South Africa is considered to be the world's largest producer of precious metals (PGM's) supplying 75% of the world's Pt [11]. It is therefore more beneficial for us to develop Pt/C and Pt-alloy catalysts since it is clear that exporting Pt is considered a huge financial benefit for the economy and for the South African hydrogen and fuel cell plan.

2.4 Electrocatalyst for ORR

2.4.1 ORR kinetics

Even although the oxygen reduction reaction (ORR) appears to be relatively simple, it is in fact quite complex. Hund's rule states that in the ground-state, O₂ possesses 2 unpaired electrons located in a doubly degenerated π^* antibonding orbital corresponding to a triplet state. When O₂ undergoes reduction, the additional electrons occupy anti-bonding orbitals, decreasing the bond order of O-O bond and thus the bond distance increases while the vibrational frequency decreases. For this reason the O₂ molecule is very stable and has relatively low reactivity in spite of its high oxidizing power [12,13]. The various adsorbed states for oxygen are represented in Fig. 2.2 and the resulting possible reaction pathways are shown in Fig. 2.3. The generally accepted 1:1 and 2:1 metal-dioxygen complex structures shown below by representative geometries **1** and **2** have been shown to give similar bonding patterns in which each exhibits one σ and one π interaction. Geometry **1** which is known as the Griffiths model, involves a side on interaction of oxygen with the metal. This type of bonding can be viewed as arising from two contributions. In the first case σ type bonding may be formed by mainly overlapping between the π orbitals of oxygen and the d_z^2 orbitals on the metal. The second contribution is where π backbond interaction between the metal d π -orbitals and the partially occupied π^* antibonding orbital on O₂ arises [14].

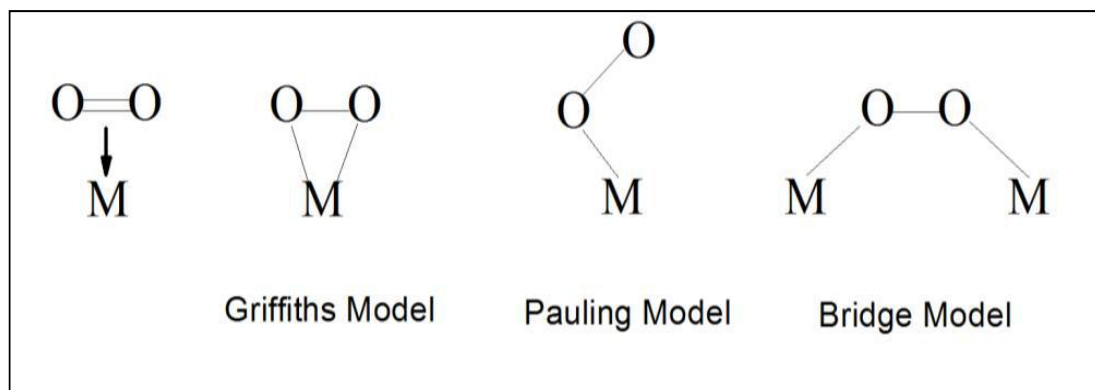


Fig. 2.2 Models for the adsorbed states of oxygen on the catalyst surfaces [18].

The Pauling model (Geometry 2) can be seen as an end-on interaction of O_2 with the metal. In this model a σ -bond is formed by the donation of electron density from the σ -rich orbital of dioxygen to an acceptor d_{z^2} orbital on the metal. The metal's two d-orbitals viz., d_{xz} and d_{yz} then interacts with the π^* orbitals of dioxygen, with a corresponding charge transfer from the metal to the O_2 molecule. The preference for either of the geometries 1 and 2 is determined by the donating abilities of the filled π and σ orbitals of the dioxygen molecule respectively [15].

Geometry 3 also known as the bridge model, is a 2:1 complex of metal-dioxygen where the bonding arises from the interaction between the d-orbital on the metal with π^* and π orbitals combinations on O_2 [15,16]. This gives rise to a singlet or triplet nature of dioxygen orbitals and determines the bridge or trans mode of interaction of dioxygen with the metal [16]. Yeager proposed this bridge-like model where two bonds interacts with two sites. This type of interaction is likely to occur on noble metals such as Pt and organic porphyrins where O_2 is reduced to water with little or no peroxide being formed [17]. The different mechanistic steps are dependent on the mode of adsorption of the oxygen molecule onto the metal surface. Depending on the mode of adsorption of the oxygen molecule on metal surface, different mechanistic steps become possible and therefore the reduction to water might occur according to pathway I or III which is desired [16-18] [Fig. 2.3].

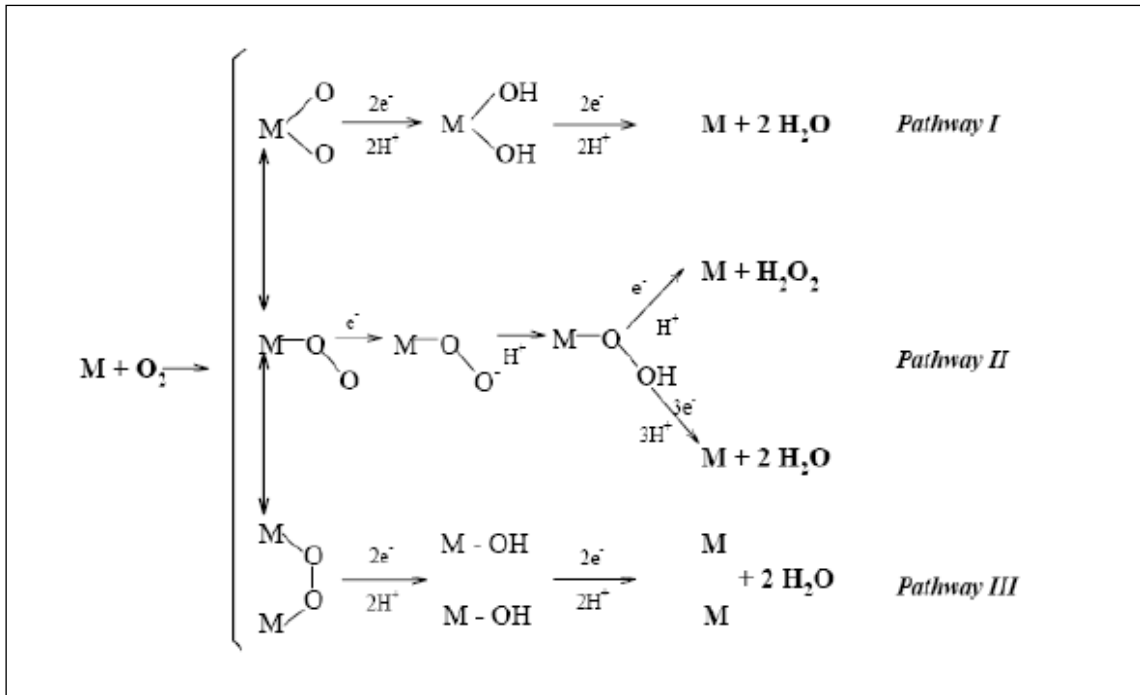
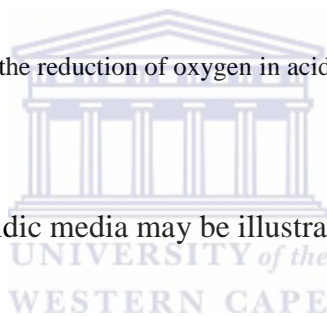
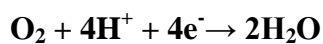


Fig. 2.3 Different reaction pathways for the reduction of oxygen in acidic medium [18].



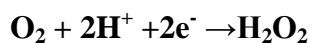
The ORR reaction pathway in acidic media may be illustrated as follows:

Direct 4 electron reduction



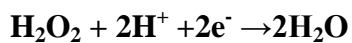
$$E^\circ (\text{O}_2/\text{H}_2\text{O}) = 1.23\text{V}$$

Indirect reduction



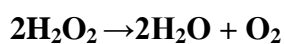
$$E^\circ (\text{O}_2/\text{H}_2\text{O}_2) = 0.682\text{V}$$

Further reduction



$$E^\circ (\text{H}_2\text{O}_2/\text{H}_2\text{O}) = 1.77\text{V}$$

Or chemical decomposition



Based on these facts several authors have proposed different schemes for the ORR pathway [19-21]. Damjanovic et al., came up with the first proposed scheme and later Wroblowa et al., modified their proposed scheme, making it easier to understand the complicated reaction pathway for the reduction of O_2 on the metal surface which is presented in Figure 2.4 [19,20].

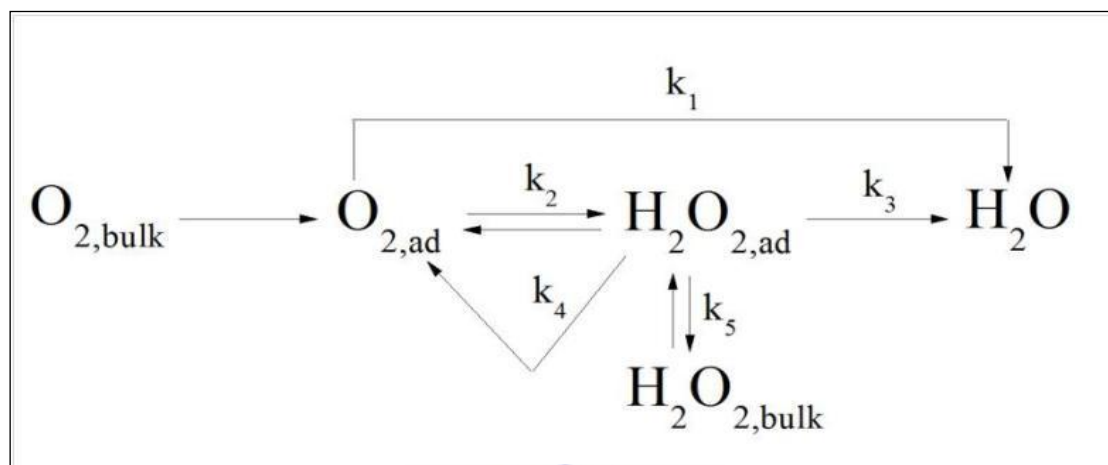


Fig. 2.4 Simplified schematic of the ORR pathway based on the scheme of Wroblowa [20].

This scheme holds true for both basic and acidic environments and all the electrode materials. The above Fig. 2.4 illustrates that pre-adsorbed oxygen can be electrochemically reduced to either $H_2O_{2,ad}$ with rate constant k_2 (the $2e^-$ pathway) or directly to water with rate constant k_1 (the $4e^-$ pathway). The adsorbed H_2O_2 can subsequently undergo further changes and can be electrochemically reduced to water with rate constant k_3 , desorbed into the bulk of the solution (k_5) or catalytically decomposed on the electrode surface (k_4). The different reaction pathways are influenced by the different adsorption rates, the pH of the electrolyte, the presence or absence of adsorbing anions and on the catalyst material [20-24]. Reduction of oxygen on the electrocatalyst takes place by the formation of a high energy intermediate, H_2O_2 . This intermediate gets further reduced to H_2O and can probably be attributed to the high stability of the H-O bond which has a dissociation energy of 494 kJ mol^{-1} . In contrast, the O-O bond in H_2O_2 only has a value of 146 kJ mol^{-1} . In fuel cells in order to avoid corrosion and obtain maximum efficiency of carbon supports and other materials by peroxide, a four electron reduction is desired. The two electron reduction is of interest for the production of hydrogen peroxide. It is therefore important to find suitable electrocatalysts that can promote the direct four electron reduction of oxygen [21,22].

2.4.2 Criteria for suitable electrocatalysts for ORR

Electrocatalysts used in fuel cells for ORR are normally comprised of noble metals immobilized on a conductive support and should have the following characteristics:

- high electronic conductivity
- chemical and structural stability under operating conditions (high temperature, low and high pH)
- ability to decompose intermediate species formed during the reduction process
- chemical and thermochemical compatibility to electrolyte
- tolerant to contaminants e.g halide ions, methanol, NO_x, CO_x, SO_x and have a low cost.

The literature is full of reports where noble and non-noble metal based electrodes have been investigated for the reduction of oxygen [25-27]. Pt and Pd based metal catalysts still appear to be the best noble metals, whereas in the case of non-noble metal electrocatalysts, transition metal chalcogenides and pyrolyzed macrocyclic compounds are two of the most widely studied electrocatalysts for oxygen reduction [28].

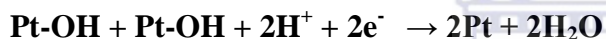
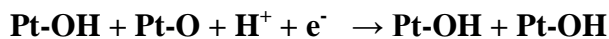
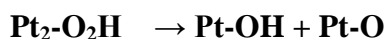
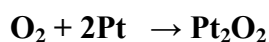
2.4.3 Pt Metal as Electrocatalyst

Platinum exhibits good activity and chemical stability under fuel cell operating condition and is therefore a promising electrocatalyst for ORR. However, Pt is very expensive and not that easy to obtain in large quantities [1]. The ORR consists of several processes namely; oxygen diffusion, adsorption, charge transfer, desorption and back diffusion. One of the key factors of the charge transfer process is the work function, because the work function is the minimum energy needed to remove an electron from the material surface. However the work function of Pt with high catalytic activity for the ORR is higher than other transition metals and therefore makes Pt a suitable electrocatalyst for ORR in fuel cells [29]. Oxygen reduction generally takes place at high positive potentials and at these high potentials most other metals will dissolve and give rise to similar situations to that prevailing at the cathode and consequently only noble metals and some of their alloys offer realistic possibilities among metallic systems to overcome these challenges. Pt is the most familiar oxygen reduction

catalyst used in fuel cells and has been investigated extensively as the pure metal [30], as nanoparticles [31], alloys [32,33], and as polycrystalline and single crystal surfaces [34,35]. To date, Pt/C is the most efficient electrocatalyst for oxygen reduction but, the cost associated with the Pt/C electrocatalyst is the main quintessential hurdle for the commercialization of electrochemical devices. To reduce the Pt loading at the cathode, thereby reducing the cost has led to various synthetic approaches being adopted to disperse Pt on suitable supports to increase the surface area of catalytic interaction [1-3]. Among the various support materials currently available, carbon is the most attractive because of several unique features. Carbon has good electronic conductivity, is chemically and mechanically stable, is abundant and has a low cost [36-38]. Several methods were developed for synthesizing Pt supported catalysts and those include the impregnation method [39,40], electrodeposition [41-43], the use of reducing agents such as borohydride to reduce Pt salts [44,45], formaldehyde [46], colloidal route [47], polyol reduction [48,49], microwave-assisted polyol reduction method [50] and sputtering techniques [51]. For the past few years Pt supported on conducting polymers, carbon nanotubes (CNT) [52,53], and carbon nanofibers (CNF) [54] have received enormous attention in the search for an efficient electrocatalyst. However, the preparation of CNTs and CNFs in bulk quantities and stability of polymers at high potentials remain a matter for concern for commercialization. The overall observations made from the ORR measurements on Pt/C catalyst are: Sluggish kinetics for ORR on Pt. Formation of the OH⁻ species at +0.8 V due to water oxidation as well as corrosion under acidic condition on the Pt hinders the oxygen reduction in such a way that the kinetics is not facile. The OH⁻ species also influences the availability of molecular oxygen thereby reducing the ORR activity [55,56]. Studies have shown that the optimum particle size of Pt for ORR should be between 3- 5 nm [56-58]. A debate however still exists in literature regarding the optimum particle size. What is clear however is that the ORR is structure sensitive and that particle size, distribution and structural effects are key components in the Pt/C catalyst activity [56]. Pt catalysts are sensitive towards contaminants [59]. Strongly adsorbing halides (Cl⁻, Br⁻, I⁻), air borne contaminants of both an organic (benzene) and an inorganic (CO, NO₂, SO₂) nature, significantly reduce the Pt catalyst activity in the operational potential window. Water is the exclusive reaction product of the ORR on Pt at the cathode at potentials of between +0.6 V - +1.0V and in the presence of strongly adsorbing halides or any other contaminants, the ORR pathway changes and ample amounts of H₂O₂ are formed. This product leads to the reduction in cell voltage, degrades the Pt sites and also the Pt catalyst life span [58-60].

2.4.4 ORR mechanism

Oxygen reduction on Pt occurs by a parallel mechanism with direct four-electron reduction as the dominant step. However, due to the large number of possible steps and some remaining uncertainties regarding the correct mechanism, a detailed mechanism still defies formulation. The main steps in the mechanism of oxygen reduction on Pt are given below [61].



It was found that there is a direct relationship between the binding ability of O and OH and the oxygen reduction activity. Further investigations showed that at high potentials adsorbed oxygen is stable and that proton and electron transfer was impossible. It was therefore proposed that the origin of the overpotential for Pt was the O and -OH adsorption and that both dissociative and associative path may contribute to the ORR depending on the metal and the electrode potential [62]. Pt shows two Tafel slope regions which is in good agreement with the reports by Yeager [17]. A Tafel slope of 120 mV dec⁻¹ below +0.8 V vs NHE may be attributed to Langmuir kinetics, while a Tafel slope of 60 mV dec⁻¹ can be explained assuming Temkin conditions in the presence of surface Pt-OH, a surface poison to the O₂ adsorption [63]. Reports have shown that the formation of Pt-OH beyond +0.8 V is caused by the reaction of H₂O with Pt causing inhibition of the O₂ reduction thereby resulting in a low Tafel slope of and not due to the interaction of O₂ with Pt as previously assumed [64]. So taking these facts into consideration a significant improvement of ORR electrocatalyst could be possible if certain changes were made to the Pt catalyst. Firstly, by inhibiting the formation of adsorbed oxygenated species (primarily Pt-OH) beyond +0.8 V, which is a known surface poison and secondly, by changing the electronic and short-range atomic order around Pt to induce alternative lower energy pathways for improved ORR kinetics. Pt alloy catalysts could offer a solution to all the challenges faced with Pt/C as electrocatalyst for

ORR at the cathode seeing that by adding a second metal the geometry and electronic effect of the catalyst will be changed which will influence the ORR mechanism [17,63-65]

2.5 Pt Alloy Catalysts

High surface Pt alloys for ORR in PAFC were originally developed by United Technology Corporation (UTC) in the 1980s. The development started with binary Pt-V/C alloys and later accumulated to ternary alloys with reported mass activities 2-3 times higher than that of Pt/C [66]. Later, other commercial companies such as TKK and Johnson Matthey (JM) also patented a number of binary, ternary and quaternary alloys that were claimed to have better catalytic activity and improved performance and stability over the standard Pt/C [67]. Mukerjee *et al.*, was the first to apply Pt-alloys in PEMFC in the early 1990s and several other groups also reported improved performance of Pt alloy catalyst vs Pt/C but in all these cases the overpotential of about 300 – 400 mV was problematic [68]. Therefore to continue the search for improved oxygen reduction catalyst the focus should be on the development of Pt alloys with better stability and greater activity than Pt. Several Pt-alloy systems have been investigated as oxygen reduction catalyst for their use in fuel cells. In Table 2.1, various preparation methods and ORR activity of Pt-alloys are given as an overview. The results obtained through these studies are however, not consistent as several different groups reported different findings when the same Pt alloy catalysts were studied. For instance Landsman *et al.* [69] found an increase in mass activity of a factor of 1.5 to 2.5 at +0.9 V whereas Beard *et al.*, [70] could not find an increased activity for Pt-Co and Pt-Cr alloys. On the other hand Mukerjee *et al.* [68] and Capuana *et al.* [71] found similar activity enhancements factors of 2 to 4 when using Pt-Mn, Pt-Cr, Pt-Fe, Pt-Ni and Pt-Co alloys. In all the cases of ORR measurements reported for Pt-Ni and Pt-Co catalyst an activity enhancement of factor 3 in comparison to Pt/C catalyst was revealed [72].

2.5.1 Pt Alloy Mechanism

Various authors have suggested possible mechanisms for the enhancement of the ORR kinetics on Pt-alloy compared to pure Pt. Jalan and Taylor [74] were the first to study the ORR on Pt-alloy systems supported on carbon black.

Table 2.1 Preparation methods, selectivity and activity towards oxygen reduction of Pt-alloys compared to Pt.

Catalyst	Preparation Method	Electrolyte Medium	Catalytic activity towards O₂	Reference
Pt-Fe (3:1)/C	Polyol reduction method	Acid (fuel cell)	Excellent	Li <i>et al.</i> , 2004
Pt-M (3:1)/C; M=Ni, Co, or Cr	Incipient wetness method	Acid (fuel cell)	Excellent	Min <i>et al.</i> , 2000
Pt-Co (1:1)/C	Incipient wetness method	Acid	Comparable	Hwang <i>et al.</i> , 2007
Pt ₇₀ Co ₃₀ /C	Formic acid reduction method	Acid	Comparable	Salgado <i>et al.</i> , 2005
Pt ₈₅ Co ₁₅ /C	Borohydride reduction method	Acid	Comparable	Salgado <i>et al.</i> , 2005
Pt ₃₂ V ₁₄ Fe ₅₄ /C	Polyol reduction method	Acid	Comparable	Luo <i>et al.</i> , 2006
Pt _(100-x) Ni _x /C	Sputtering Method	Acid	Excellent	Toda <i>et al.</i> , 1999
Pt-Fe/C	Alloying	Acid	Comparable	Shukla <i>et al.</i> , 2004
Pt-Cr/C	Carbonyl Route	Acid	Good	Yang <i>et al.</i> , 2005
Pt-Ni/C; Pt/Ni = 3:1, 3:2 and 9:1	Microemulsion method	Acid	Good	Santos <i>et al.</i> , 2006

They claimed that due to the shorting of the Pt-Pt interatomic distances by alloying, the ORR improvement was possible [73]. Appelby *et al.*, claimed that dissociative adsorption of O₂ was possible due to lattice contraction as a result of alloying giving more favourable Pt-Pt distances [74]. Paffet *et al.*, proposed that the enhancement could be attributed to surface roughening brought about by an enhanced corrosion [75]. However, further studies proved that these findings were incorrect and that the enhancement does not result from surface roughening [70]. Mukerjee *et al.*, used in-situ X-Ray adsorption spectroscopy (XAS) studies to explain the enhance electrocatalyst performance on the basis of the interplay between the

electronic (Pt d vacancy) and geometric factors (Pt-Pt interatomic distances and Pt coordination number) and their effect on the chemisorption behaviour of OH species from the electrolyte [76]. From the electrocatalytic activity vs the electronic and geometric parameter plots they observed a volcano shape behaviour from the different metals studied alloyed with Pt. They investigated the alloy catalysts (Pt-Co, Pt-Fe, Pt-Ni and Pt-Cr) and found that Pt-Cr is located on top of the volcano based on the best combination of both Pt d-band vacancies and the Pt-Pt bond distances.

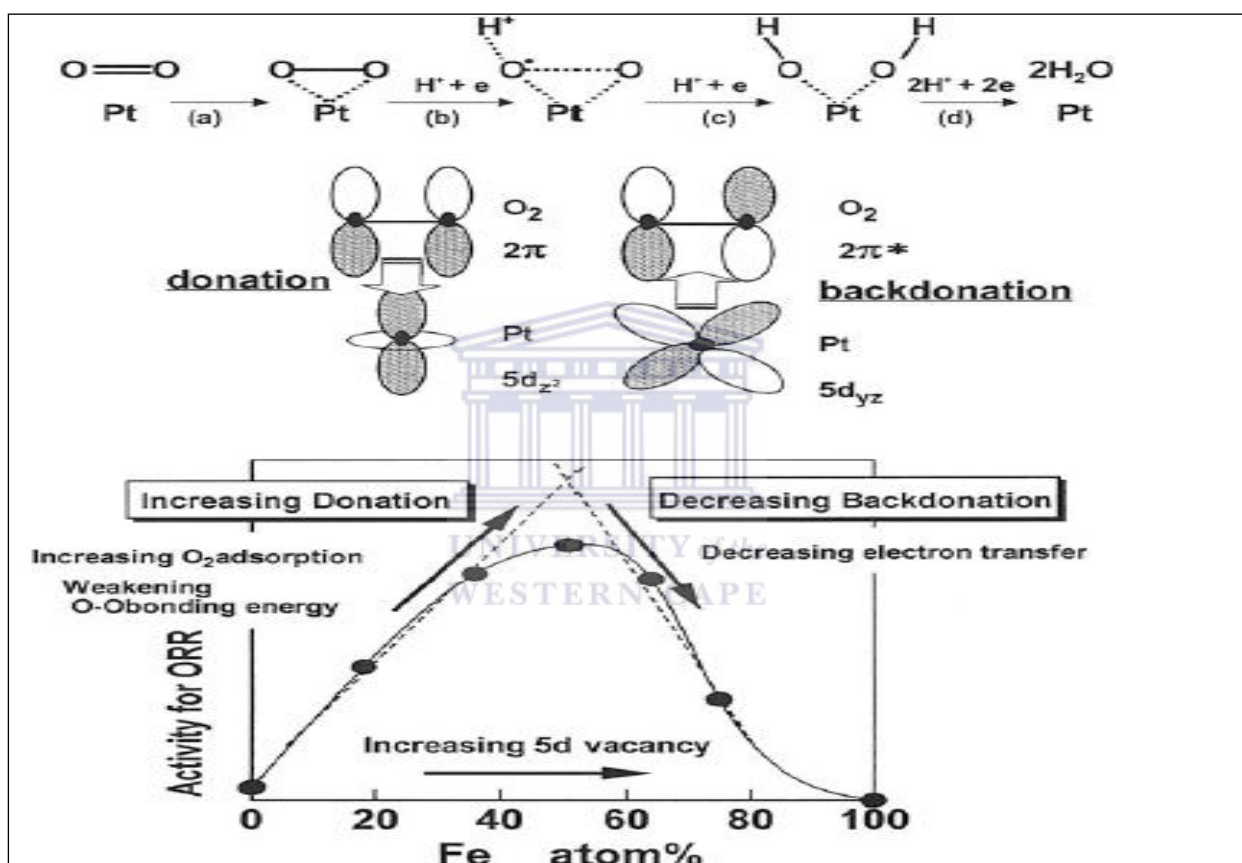


Fig 2.4 Proposed mechanism of the ORR of alloying Pt with Fe-group metals [78].

It was concluded that the optimum distance between Pt-Pt determined by XRD corresponding to the maximum performance lies between 2.71 and 2.75 Å [75-77]. Figure 2.4 shows the proposed mechanism for the enhancement of the ORR on the Pt-Fe alloy. By adding more Fe the 5d vacancies of the surface would increase seeing that Fe has 5d vacancies that Pt may interact with. The increase of 5d vacancies leads to an increased $2\bar{e}$ donation from O_2 to the Pt surface, resulting in increased $[O_2]$ and a weakening of the O-O bond. Splitting of the

bonds should occur simultaneously as \bar{e} back donated from 5d-orbitals of the surface Pt to the $2\pi^*$ orbitals of the adsorbed O_2 which is the first electron transfer, is then accompanied by H^+ binding. The first step is followed by the back donation of $3\bar{e}$ and by the additional introduction of 3 H^+ ions. The Pt-O bonding becomes stronger as the 5d vacancies of the electrode increase resulting in a lower O_2 reaction rate as back donation becomes difficult. When the content of the second metal becomes too large, the d-band vacancy may contribute to the enhancement of O-O bond splitting. Therefore the volcano shape electrocatalytic behaviour of Pt alloys can be explained as a result of the increased second element content [78]. What is evident from these studies is the role of morphology, crystallographic and electronic structural change brought about by alloying on the electrocatalyst surface for ORR. After theoretical and experimental data on Pt alloys are taken into account, it can be concluded that the Pt-M (Fe, Cr, Ni, Cu, Co) alloys have shown good activities among the various investigated bimetallic alloys compared to Pt. Particle size, Pt d-band vacancy, changes in the short range atomic order and Pt-OH inhibition are some of the reasons given for the enhanced performance by these alloys [76-78].

2.6 Pd and other non- Pt electrocatalysts

Pd has a similar electronic configuration and lattice constant to that of Pt and is consequently expected to perform similarly as Pt also bearing in mind that Pd is a row above Pt on the periodic table. Pd also has a four electron pathway for ORR similarly to Pt. Pd is additionally more abundant than Pt and less expensive viz., Pt \$1500 per ounce and Pd \$650 per ounce. Pd additionally has little or no electrocatalytic activity for methanol oxidation in acid medium [80]. All these properties strongly suggest that Pd may be a more suitable candidate as an ORR selective electrocatalyst. It was also reported that the reduction of oxygen on Pd takes place in a similar manner as that of Pt [81,82]. However, when compared to Pt, the ORR activity for Pd was less and at high potentials of about +0.8 V vs NHE. Unfortunately, Pd shows poor stability which hinders its commercial exploitation. Savagado *et al.*, studied Pd-alloy catalysts and found that there are vast improvements when elements like Co, Fe, Cr, were added when compared to Pd/C [83].

Metal containing Macrocyclic derivatives of transition metals are also a unique class of compounds that can be used as electrocatalyst for ORR. Transition metals like Fe and Co are used predominantly [84]. Studies conducted on these type of ORR catalyst have shown that a number of metal chelates will chemisorb oxygen and that the most chemically stable of this

group of compounds are metal porphyrins [85], metal phthalocyanines [84] and metal tetraazannulenes [86]. Although these reported catalysts show favourable ORR activity and high methanol tolerance these type of materials unfortunately, demonstrate very poor stability in acidic conditions. They decompose either via hydrolysis in the electrolyte and attack of the macrocycle rings by peroxide was found to be the main cause of poor performance and stability [84-86]. Heat treatment of these macrocyclic materials above 800 °C has shown to improve the stability and overall catalytic activity [87].

2.7 Metal Oxides

Metal oxides may in the current context, be considered as unique in that this group of compounds possess appreciable chemical and electrocatalytic activity which thus makes them suitable for chemical and electrochemical reactions. Transition metal oxides are able to exist in various valency states and thus may act as metal-like conducting agents providing that half-filled d-bands are present. Various metal oxides have been investigated in the past but studies have been mainly focused on pyrochlores [88], perovskites [89], amorphous [90] and spinels [91] since these materials can provide reversible pathways for oxygen reduction. Metal oxides such as IrO₂, NiO, CeO₂, ZrO₂, TiO₂, SnO₂ were also investigated for oxygen reduction [92-95]. Most transition metal oxides have been found to be unstable in the acidic environment of PEMFC and DMFC operations [96]. Oxygen reduction studies performed on spinels, pyrochlores and perovskites indicated that the intrinsic activity as well as stability of these metal oxides is less than that of Pt based materials in acidic medium. Although these materials do not exhibit significant activity, from these studies valuable experience was gained that led to the search for new materials for oxygen reduction of metal nitrides which were observed to give superior activity [93-96].

2.8 Methods for the synthesis of supported metal nanoparticles

A crucial consideration in choosing an electrocatalyst for DMFC application is the method by which the nanoparticles are prepared. It is well known that the activity of the electrocatalyst strongly depends on the particle size, particle distribution and morphology. Thus, during the synthesis of supported metal nanoparticles, control of the metal particle size and with a size distribution as narrow as possible is of the utmost importance. Furthermore, the metal dispersion needs to be stable as well. The generally regarded desired range for nanoparticles

used as electrocatalysts are between 1-10 nm. It is further known that relatively small changes in size can be accompanied by significant morphological changes and also influence changes on the valence band density [97]. Different methods have been used in the synthesis of supported metal catalysts where the major focus has been on catalytic activity and catalyst morphology [98]. For the synthesis of metal nanoparticles there are four commonly employed liquid-phase precursor methods that are used viz., ion exchange, precipitation, impregnation and colloidal. The fundamental mechanism of each method is not yet fully understood although a general understanding of the differences between each method has been presented by Li et al., as depicted in Figure 2.5 [99].

Briefly, the impregnation method involves adding the liquid metal precursor into the catalyst support which upon drying leaves the metal catalyst salt and upon pyrolysing this under reducing condition generates the Pt catalyst.

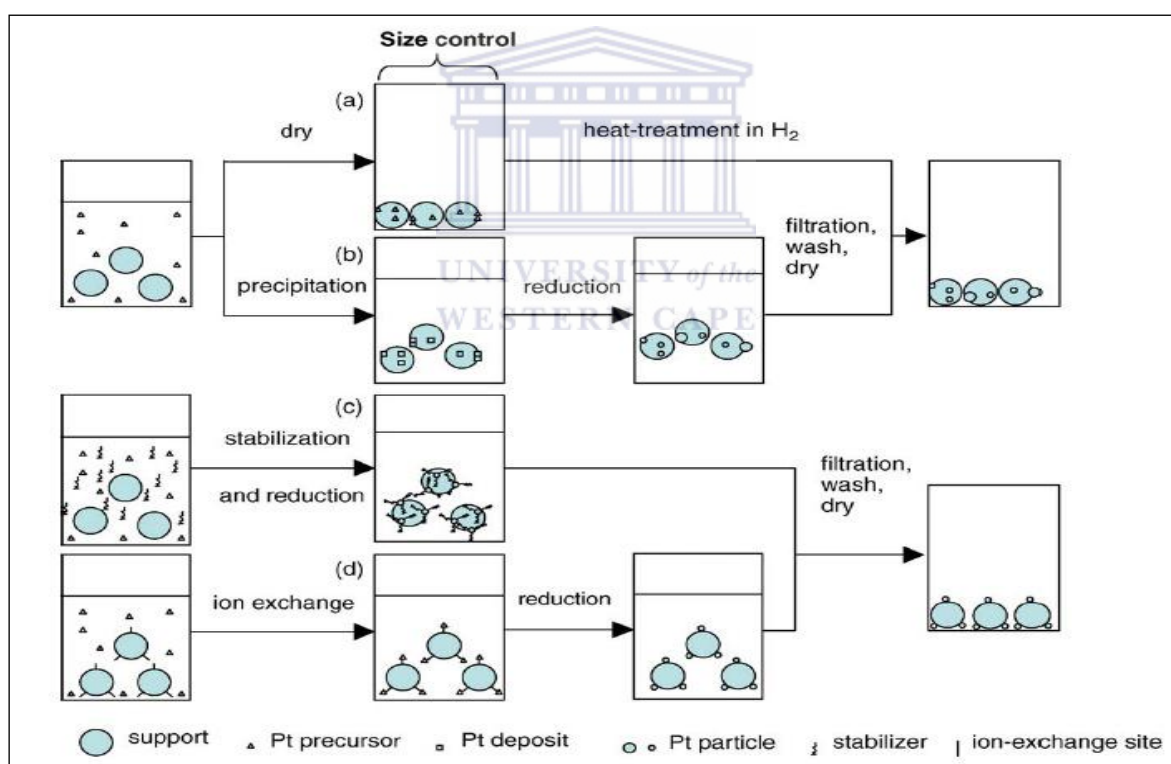


Fig. 2.5 Schematic Depiction of Various Methods for Producing Supported Metal Catalysts (a) Impregnation (b) Precipitation (c) Colloidal (d) Ion-Exchange Methods [99].

This is a simple one step preparation method, but it provides a poor control over particle size and size distribution. A variation of this method is known as incipient-wetness impregnation.

In this method a certain volume of the impregnating metal solution is chosen to match the pore volume of the carbon support. The advantage of this method is that metal is only deposited in the pore structure of the carbon support but, the particle size cannot be controlled [100]. In the precipitation method the carbon support is introduced into a liquid medium containing the Pt precursor to form a suspension. The precipitant, which is usually a hydroxide (KOH or NaOH), is added slowly to the suspension to precipitate out the metal containing complex which is subsequently subjected to a reduction step to generate the metal particles. Although higher performances than typical catalyst were observed in catalysts synthesized by this method, when compared against other deposition methods however, this method was found to be not such a reliable fabrication method [99,101]. In the ion exchange method, platinum nanoparticles are deposited on a carbon matrix without the aid of either a reducing or protective agent. Here, a Pt cation complex $[\text{Pt}(\text{NH}_3)_4]^{2+}$ interacts with the protons of the acid groups on the surface of the CNTs. Consequently, the dispersion of the Pt nanoparticles is dependent on the interaction between the Pt cation and acid group. Once this process is complete the Pt cation complex is reduced in a H_2 atmosphere. Yin et al., successfully used this method to prepare Pt nanoparticles on CNTs. They electrochemically functionalized CNTs and then immersed the CNTs in a solution of a Pt cation for 48 hours and thereafter introduced the product into a flowing stream of H_2 gas [102]. The idea behind the colloidal method is to generate the catalyst metal colloids which are stabilized by the addition of stabilizers such as polyvinyl propylene (PVP) [103]. By using ethylene glycol (EG) as reducing agent the reduction process is achieved simultaneously and in-situ. The stabilizer can act as a bridge between the catalyst support and the precipitated catalyst. Recent studies have shown that EG may be employed as a stabilizer since it breaks down to form acetate at high temperatures which is believed to stabilize the metal colloid. In this case no addition of stabilizer is desired [100,103].

2.9 Polyol Reduction Method

In the last few years the polyol reduction method has been chosen by many researchers due to it being a versatile method to generate metal colloids or clusters on the nanoscale with great uniformity and controllable composition [104,105]. This approach is also commonly known as the “Bottoms Up” method and was developed by Fievet et al., using ethylene glycol (EG) both as solvent and reducing agent [106]. It has been found that the metal precursors and carbon support co-exist in the suspension medium. It is still not clear whether the metal

particles form as a colloid and are then deposited on the support surface or alternatively form and stabilize on the surface. It has been found that EG is well able to support colloidal metal particles in solution thereby creating a well dispersed solution. EG has a relatively high viscosity and this unique property prevents the Pt from being transported too quickly to the reaction sites resulting in smaller Pt particle sizes [107]. This method has additionally been used to successfully prepare bimetallic catalysts, metal oxides and metal sulfides with narrow particle size distributions, controllable composition and alloy structures [108]. The reduction of metal precursors by the polyol method is depicted in Fig. 2.6 below.

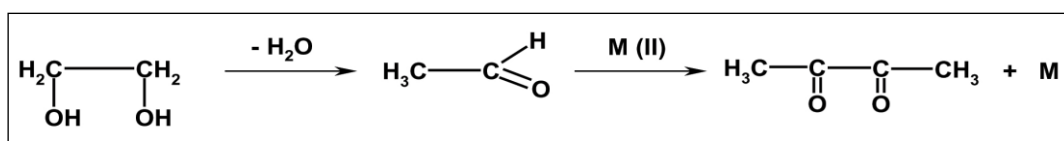


Fig. 2.6 Chemical reaction for the polyol reduction method [109].

EG is a vicinal alcohol and also a very weak acid ($\text{pK}_a = 15^{13}$) and can easily be oxidized to a dialdehyde or dicarboxylic acid. For these intermediates to form, the -OH groups of EG interact with the d-orbitals of Pt and facilitates the alcohol in its oxidation. As a result of this the aldehyde that is formed is very unstable under the conditions and is further oxidized to glycolic and eventually oxalic acid [108]. The electrons required for the oxidation of the -OH to the carbonyl groups are derived from the metal which thus reduces these precursors to their zero valent oxidation state. Binary metallic alloys can be prepared by the reduction of the corresponding metal precursors either with the polyol (EG) protocol or by reduction of one of the metal precursors with the polyol protocol while the second metal is decomposed at high temperature in solution. The size and shape of the nanoparticles can be controlled by changing the reducing agent, reaction temperature and capping agent [106-109]. Propylene 1,2-glycol and butylene 1,4-glycol were investigated previously as an alternative reducing agent to EG but it was found that when these solvents were used the metal colloids that formed were not very stable [110]. Several modifications were also performed on the polyol method. Optimum EG:Water ratios, i.e solution viscosities have been studied and it was found that 20% water in EG results in the smallest sized catalyst particles. At high temperatures the EG/Water solution breaks down to form formaldehyde which acts as a reducing agent for Pt. This method has produced small sized Pt nanoparticles down to 2 nm which is smaller than the Pt particle sizes of the commercial catalyst which is typically in the

region of 4 nm. It has been generally accepted that a higher pH leads to smaller Pt particle size but a systematic study on the influence of pH in this method has not been comprehensively studied [112].

A modified polyol method has been reported wherein the deposition and reduction step occurs in a microwave. At high pH conditions for depositions, promising results were reported with an average Pt size of 2.7 nm. However it should be noted that in these experiments the pH was not controlled throughout the duration of the reaction since it occurred in a closed system and thus the full scope of the reaction under these conditions is not very well known [113].

Based on the results gathered in studies thus far, it would be beneficial to study the effect of different aspects of the deposition procedure. Since the EG method shows promising results, it is important to study the effect of pH on this deposition procedure before and after the completion of the reaction [110-113].

2.10 Other methods to prepare nanoparticles

Various other methods have also been used to synthesize Pt nanoparticles [30] Other commonly used methods include the sulfite complex route, the Bonneman method, Adams fusion method and micro-emulsion method.

Briefly the Sulfite complex route involves the synthesis of Pt sulfite complexes in aqueous solutions. Platinum hexachloride (H_2PtCl_6) is used as metal precursor and suspended in aqueous $NaHSO_3$. Hydrogen peroxide is then used to oxidatively decompose the suspension on the carbon support. Monomodal Pt nanoparticles with a mean particle size of <3 nm can be achieved when using this method [114]. In the Bonneman method, $PtCl_2$ is suspended in tetrahydrofuran (THF) which is then treated with tetra-alkyl ammonium hydro-tri-organoborate which leads to the formation of a Pt metal colloid solution. High vacuum is then used to dry the colloidal suspension and evaporate all the solvent and the resulting waxy residue is mixed with ether. Ethanol is then added to precipitate the colloid. The average particle size obtained when using the method is between 1 -5 nm. This method is renowned for the preparation of bimetallic catalysts which require a narrow particle size distribution. However a major disadvantage of using this method is that it involves several complicated steps which involves a fair amount of time and the reagents and apparatus used are very expensive [115,116].

For the synthesis of metal catalysts without making use of a support, the Adams fusion method is typically used. This method is based on the oxidation of the metal precursors in a molten nitrate melt. The metal precursors are mixed with a solvent and heat treated and the resulting metal oxide evaporated to dryness. For the synthesis of metal powders with small particle sizes this method is suitable. The disadvantage of using this method is that during synthesis impurities in the forms of salts can easily be generated and can only be removed with a great amount of effort [117]. The micro-emulsion method generally involves the use of 2 immiscible liquids like water and cyclohexane followed by the addition of a surfactant and reducing agent, e.g. hydrazine into the micro-emulsion. After the reduction step the nanoparticles are stabilized from agglomeration by the added surfactant molecules [118]. The control of particle size and distribution in the micro-emulsion method appears to be tolerant of small variation in process parameters such as amount of surfactant and concentration of precursors solutions as proved by Barnickel and coworkers [119].



REFERENCES

1. J. Larminie, A. Dicks, Fuel Cell Systems Explained, John Wiley & Sons, Chichester, 2001.
2. www.en.wikipedia.org/wiki/Catalysis (Sept 2012)
3. J.E Huheey, E.A Keiter, R.L Keiter, Inorganic Chemistry: *Principals of structures and reactivity* 4th Ed. HarperCollins College Publishers, New York, 1993
4. R.O. Hayre, W. Colella, S.K. Cha, F.B. Prinz, Fuel Cell Fundamentals, John Wiley & Sons, New York, 2009.
5. K. Kordesch G. Simader, Fuel Cells and their Applications, Wiley-VCH, Weinheim, 1996.
6. J. McMurray, Organic Chemistry 5th Ed, Brooks/Cole, California, 1999
7. A.S. Arico, A. Stassi, E. Modica, R. Ornelas, I. Gatto, E. Passalacqua, V.J. Antonucci, *J. Power Sources* 178 (2008) 525.
8. K.D. Beard, M.T. Schaal, J.W. Van Zee, J.R. Monnier, *Appl. Catal., B* 72 (2007) 262
9. M. Min, C. Park, H. Kim, C. Kwak, A.A. Serov, H. Kweon, S. Lee, *Electrochim. Acta* 52 (2006) 1670.
10. M.H. Seo, S.M. Choi, H. J. Kim, J.H. Kim, B.K. Cho, W.B. Kim, *J. Power Sources* 179 (2008) 81.
11. www.platinum.matthey.com/production/ (September 2012)
12. H. Taube, *J. Gen. Phys.* 49 (1965) 29
13. J. S. Valentine, *Chem. Rev.* 73 (1973) 235
14. J. S. Griffith, *Proc. R. Sot. London Ser. A* 235 (1956) 23
15. L. Pauling, *Nature* 203 (1964) 182
16. K. Tatsumi and R. Hoffman, *J. Am. Chem. Soc.* 103 (1981) 3328
17. E. Yeager, *J. Electrochem. Soc.* 128 (1981) 160
18. T. Toda, H. Igarashi, H. Uchida, M. Watanabe, *J. Electrochem. Soc.* 145 (1998) 4185
19. A. Damjanovic, M. A. Gensaw, J. O. Bockries, *J. Chem. Phys.* 45 (1966) 4057
20. H. S. Wroblowa, Y. C. Pan, G. Razumney, *J. Electroanal. Chem.* 69 (1976)
21. N. A. Anastasijevic, V. Vesovic, R. R. Adzic, *J. Electroanal. Chem.* 229 (1987) 305
22. J. Zagal, *Coord. Chem. Rev.* 119 (1992) 89
23. C.H. Hamann, A. Hamnett, W. Vielstich, Electrochemistry, 1st ed., Wiley-VCH, Weinheim, 1998
24. N.M. Markovic, T.J. Schmidt, V. Stamenkovic, P.N. Ross, *Fuel Cells* 1 (2001) 105

25. P. Sotelo-Mazón, R.G. González-Huerta, J. G. Cabañas-Moreno, O. Solorza-Feria, *Int. J. Electrochem. Sci.* 2 (2007) 523
26. G. Pérez, E. Pastor, C.F. Zinola, *Int. J. Hydrogen Energy* 34 (2009) 9523
27. E. Antolini, T. Lopes, E.R. Gonzalez, *J. Alloys Comp.* 461 (2008) 253
28. A.K. Shukla, R.K. Raman, *Annu. Rev. Mater. Res.* 33 (2003) 155
29. S. Trasatti, *J. Electroanal. Chem.* 33 (1971) 351
30. H. Geins, R. Faure, R. Durand, *Electrochim. Acta.* 44 (1998) 1317
31. S. Mukherjee, S. Srinivasan, M. P. Sorioga, J. McBreen, *J. Electrochem. Soc.* 142 (1995) 1409
32. Y. Jong, K. Kwon, K. Pak, H. Chang, *Catal Today* 146 (2009) 15
33. S. I. Pyun and S. B. Lee, *J. Power Sources* 77 (1999) 170
34. Perez, H. M. Villullas and E. R. Gonzalez, *J. Electroanal. Chem.* 435 (1997) 179
35. N. M. Markovic, H. A. Gasteiger and P. N. Ross, *J. Electrochem. Soc.* 144 (1997) 1591
36. Carbon blacks, [Online], Available; <http://www.carbon-black.org> (September 2012)
37. Norton Haner, P.N. Ross, *J. Phys. Chem.* 95 (1991) 3740–3746
38. Herrero, K. Franaszczuk, A. Wieckowski, *J. Phys. Chem.* 98 (1994) 5074–5083
39. L.J. Vracar, N.V. Krstajic, M.M. Jaksic, *J. Electroanal. Chem.* 587 (2006) 99
40. B. Rajesh, J.-M. Bonard, N. Xanthopoulos, H.J. Mathieu, B. Viswanathan *J. Phys. Chem. B*, 107, (2003) 2701.
41. B. Rajesh, B., K. Ravindranathan Thampi, J.-M. Bonard, N. Xanthopoulos, *Electrochemical and Solid-State Lett.*, 7, (2003), 404
42. Z.D. Wei, S.H. Chan, L.L. Li, H.F. Cai, Z.T. Xia, C.X. Sun *Electrochim. Acta*, 50, (2005) 2279
43. O. Antoine, Y. Bultel, and R. Durand, *J. Electroanal. Chem.* 499 (2001) 85
44. Y. Guo, L. Zhuang, J. Lu, *Angew. Chem. Int. Ed.* 46 (2007) 2862
45. H. Ma, X.-Z. Xue, J.-H. Liao, C.P. Liu, W. Xing, *App. Surf. Sci.* 252 (2006) 8593
46. Z. Hou, B. Yi, H. Zhang, *Electrochemical and Solid-State Lett.*, 6 (2003) A232
47. H. Bönemann, G. Braun, W. Brijoux, R. Brinkmann, S. Tilling, K. Seevogel, K. Siepen, *J. Organometallic Chem.* 520 (1996) 143
48. Z. Liu, L.M. Gan, L. Hong, W. Chen, J.Y. Lee, *J. Power Sources* 139 (2005) 73
49. N. Shukla, E.B. Svedberg, J. Eii, *Colloids and Surfaces A: Physicochem. Eng. Aspects* 301 (2006) 113
50. C. Wang, H. Daimon, Y. Lee, J. Kim, S. Sun, *J. Am. Chem. Soc.* 129 (2007) 6974
51. K. Makino, K. Furukawa, K. Okajima, M. Sudoh, *Electrochim. Acta* 51 (2005) 961

52. H. Cui, J.-S. Ye, W.-D. Zhang, J. Wang, F.-S. Sheu *J. Electroanal. Chem.* 577 (2005) 295
53. M.S Saha, R. Li, X. Sun, *J. Power Sources* 177 (2008). 314
54. J. Zheng, M. Wang, X. Zhang, Y. Wu, P. Li, X. Zhou, W. Yuan, *J. Power Sources* 175 (2008) 211
55. C.C Liang, A.L. Juliard, *J. Electroanal. Chem.* 9 (1965) 390
56. K. Kinoshita, *J. Electrochem. Soc.*, 137(1990) 845
57. M. Min, J. Cho, K. Cho, H. Kim, *Electrochim. Acta*, 45, (2000) 4211
58. F.M Maillard, Martin, F. Gloaguen, J.-M. Léger, *Electrochim. Acta*, 47 (2002) 343
59. T.J Schmidt, H.A. Gasteiger, G.D. Stab, P.M. Urban, D.M. Kolb, R.J. Behm, *J. Electrochem. Soc.*, 145, (1998) 2354
60. S.D Gupta, S.Tryk, W. Zecevic, D. Aldred, D. Guo, R.F. Savinell, *J. Appl. Electrochem.* 28 (1998) 673
61. R.A Sidik, A.B. Anderson, *J. Electroanal. Chem.*, 528 (2002) 69
62. J.K Nørskov, J. Rossmeisl, A. Logadottir, L. Lindqvist, J.R. Kitchin, T. Bligaard, H. Jonsson, *J. Phys. Chem. B*, 108, (2004) 17886.
63. A. Damjanovic, *J. Electrochem. Soc.*, 138 (1991) 2315
64. A. Danjanovic, O.M. Bockris. *Electrochim. Acta*, 11 (1966) 376
65. M. Teliska, V.S. Murthi, S. Mukerjee, D.E. Ramaker, *J. Electrochem. Soc.* 152 (2005) 2159
66. D.A. Landsman, F.J. Luczak, US Patent 4,316,944, 1982
67. D. Thompsett, W. Vielstich, H. Gasteiger, A. Lamm (Ed.), *Handbook of Fuel Cells – Fundamentals, Technology and Applications*, vol. 3, Wiley, Chichester, UK, 2003,
68. S. Mukerjee, S. Srinivasan, *J. Electroanal. Chem.* 357 (1993) 201.
69. F.J Luczak, D.A. Landsman (1987) Ordered ternary fuel cell catalysts containing platinum and cobalt and method for making the catalysts. *US Patent* 4 677 09
70. B.C Beard, P.N. Ross, *J. Electrochem. Soc.* 137 (1990) 3368
71. G. Tamizhmani, G.A. Capuano, *J. Electrochem. Soc.*, 141 (1994) 968
72. U.A Paulus, A. Wokaun, G.G. Scherer, T.J. Schmidt, V. Stamenkovic, V. Radmilovic, N.M. Markovic, P.N. Ross, *J. Phys. Chem. B* 106 (2002) 4181
73. A.J Appleby, *Energy* 11 (1986) 13
74. V. Jalan, E.J. Taylor, *J. Electrochem. Soc.* 130 (1983) 2299
75. M.T Paffet, G.J. Beery, S. Gottesfeld, *J. Electrochem. Soc.* 135 (1988) 1431
76. S. Mukerjee, S. Srinivasan, M.P. Soriaga, J. McBreen, *J. Phys. Chem.* 99 (1995) 4577

77. S. Mukerjee, S. Srinivasan, M.P. Soriaga, J. McBreen, *J. Electrochem. Soc.* 142 (1995) 1409
78. T. Toda, H. Igarashi, H. Uchida, M. Watanabe *J. Electrochem. Soc.* 146 (1999) 3750
79. B.N Grgur, N.M. Markovic, P.N. Ross, *Can. J. Chem.*, 75 (1997) 1465
80. D.B Sepa, M.V. Vojnovic, A. Damjanovic, *Electrochim. Acta* 26 (1981) 781
81. L.J Vracar, D.B. Sepa, A. Damjanovic, *J. Electrochem. Soc.* 134 (1987) 169
82. L.J Vracar, D.B. Sepa, A. Damjanovic, *J. Electrochem. Soc.* 136 (1989) 1973
83. O. Savadogo, K. Lee, K. Oishi, S. Mitsushima, K.I. Ota, *Electrochem. Commun.*, 6 (2004) 105
84. M. Lefèvre, E. Proietti, F. Jaouen, J.P. Dodelet, *Science* 324 (2009) 71
85. H. Jahnke, M. Schonbron, G. Zimmerman, *Top Curr. Chem.* 61 (1976) 133.
86. H.X. Zhong, H.M. Zhang, G. Liu, Y.M. Liang, J.W. Hu, B.L. Yi, *Electrochem. Commun.* 8 (2006) 707.
87. P. N Vasudevan, N. Santosh, N. Mann, S. Tyagi, *Transition Met. Chem.* 81 (1990) 92
88. J. Yang, J. J. Xu, *Electrochem. Commun.* 5 (2003) 306.
89. H. Nguyen-Cong, V. de la Garza Guadarrama, J.L. Gautier, P. Chartier, *Electrochim. Acta* 48 (2003) 2389.
90. S. Mulljzr, K. Stiuebel, O. HAAS, *Electrochim. Acta* 39 (1994) 1661
91. H.S. Horowitz, J.M. Longo, J.T. Lewandowski, U.S. Pat. 4,129,525, 1978
92. K. Matsuki, H. Kamada, *Electrochim. Acta* 31 (1986) 13
93. C.C Chang, T-C Wen, H-J Tien, *Electrochim. Acta* 42, (1997) 557- 565
94. E.R Vago, E.J. Calvo, *J. Electroanal. Chem.* 388 (1995) 16
95. J. Kim, A. Ishihara, S. Mitsushima, N. Kamiya, K. Ota, *Electrochim. Acta* 52 (2007) 2492
96. V. Raghuveer, K. Kumar, B. Viswanathan, *Indian. J. Eng. Mater. Sci.* 9 (2002) 137
97. J.A van Bokhoven, J.T Miller, *J. Phys. Chem. C* 111 (2007) 0245
98. K. Lee, J. Zhang, H.Wang, D. Wilkinson, *J. Appl. Electrochem.* 36 (2006) 507
99. X.Li, I.M. Hsing, *Electrochim. Acta* 51 (2006) 5250
100. R.Yu, L.Chen, Q. Liu, J.Lin, K-L.Tan, S. Ng, H. Chan, G-Q. Xu, T.S. Hor, *Chem. Mater.* 10 (1998) 718
101. N. Rajalakshmi, H. Ryu, M.M. Shaijumon, S. Ramaprabhu, *J. Power Sources* 140 (2005) 250
102. P. Barnickel, A. Wokaun, *Molec. Phys.* 67 (1989) 1355
103. W. Chen, Y. Lee, Z.Liu, *Chem. Comm.* 21 (2002) 2588

104. S.K. Natarajan, D. Cossement, J. Hamelin, *J. Electrochem Soc.* 154 (2007) 310
105. V. Selvaraj, M. Vinoba, M. Alagar, *J. Coll. Int. Sci.* 322 (2008) 537
106. F. Fievet, J.P Lagier, M. Figlarz, *MRS Bull.* 14 (1989) 29
107. I. Elisabete I. Santiago, C. Laudemir, H. Mercedes Villulas, *J. Phys. Chem. C* 111 (2007) 3146
108. B. He, Y. Chen, H. Liu, Y. Liu, *J. Nanosci. Nanotechno.* 5 (2005) 266
109. [Online], Available: <http://www.strem.com/uploads/>
110. D.R Lide, CRC Handbook of Chemistry and Physics, 71st Ed., CRC Press: Boston, 1990
111. H.A Gasteiger, S.S Kocha, B. Sompalli, F.T Wagner, *Appl. Cat. B:* 56 (2005)
112. X. Li, W.X. Chen, J. Zhao, W. Xing, Z.D. Xu, *Carbon* 43 (2005) 2168
113. S. Knupp, W. Li, O. Paschos, T. Murray, J. Snyder, P. Haldar, *Carbon* 46 (2008) 1276
114. M. Watanabe, M. Uchida, I Satoshi, *J. Electroanal. Chem.* 229 (1987) 395
115. H. Bönemann, W. Brijoux, *Angew.Chem. Int. Ed* 30 (1991) 1312
116. H. Bönemann, P. Britz, U. Endruschat, R. Mörstel, *J. New Mater. Electrochem. Syst.* 3 (2000) 199
117. A. Marshall, B. Børresen, G. Hagenm, M. Tsykin, R. Tunold, *Mater. Chem. Phys.* 94 (2005) 226
118. Z.S Hu, S.Y Chen, S.Y Peng, *Prep. Cat. VI* 6 (1995) 197
119. P. Barnickel, A. Wokaun, W. Sager, H.F Eicke, *J. Coll. Inter. Sci.* 148 (1992) 8

Chapter 3

Experimental Methods and Background Theory

This chapter presents the details of the experimental methods and relevant background theory for the synthesis of Pt-Sn nanoparticles deposited on a carbon matrix and characterization thereof.

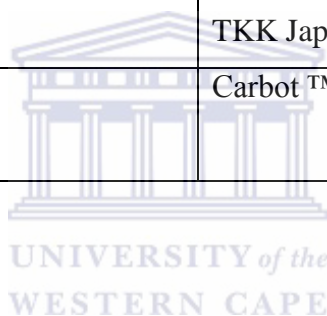
3.1 Catalyst Synthesis

All Pt-based electrocatalysts investigated for this study were synthesized via a modified polyol reduction method. In a typical experiment to a mixture of $\text{H}_2\text{PtCl}_6 \cdot 6\text{H}_2\text{O}$, a calculated amount of $\text{SnCl}_2 \cdot 2\text{H}_2\text{O}$ and Vulcan XC-72R carbon was suspended in ethylene glycol in a Shlenck tube. The pH of the solution was adjusted to about 13 with 1 M NaOH solution followed by stirring and purging with N_2 . The solution was then heated at 150°C for 4 hours and then set aside to cool to room temperature and stirred overnight. The catalyst was filtered and the filter cake thoroughly washed with ultra pure water and dried in a vacuum oven at 80°C overnight and subsequently heat treated at various temperatures under an Argon atmosphere in a tube furnace. The as prepared Pt-Sn/C catalyst powders typically had a total weight of approximately 125 mg with a metal loading of 30 wt. % (20% Pt and 10% Sn). This procedure was noted as the standard method (STD) and several changes were performed on the STD method and will be discussed in the following chapter. The chemicals used in this study are listed below.

Table 3.1 Chemicals used for this study.

Chemicals	Company
$\text{H}_2\text{PtCl}_6 \cdot 6\text{H}_2\text{O}$	Sigma Aldrich
EG	Sigma Aldrich

NaOH	Sigma Aldrich
SnCl₂.2H₂O	Sigma Aldrich
32 % HCl	KIMIX
Isopropanol	KIMIX
98 % H₂SO₄	KIMIX
20% Pt/C HiSPEC™ 3000 40% Pt/C HiSPEC™ 4000 20%Pt-10%Ru/C 46% Pt/C	Alfa Aesar TKK Japan
Carbon black Vulcan XC-72R	Carbot™



3.2 Material Characterization

3.2.1 Electron Microscopy (EM)

Electron microscopes use electron beams to create a highly magnified image of a specimen. These types of instruments can give a direct and detailed description concerning morphologies, particle size and composition of a specimen. EM has demonstrated its value in different domains of science such as chemistry, biology and material science. One of the main advantages EM has over conventional light microscopes is in terms of resolution and depth of field. The resolution of a light microscope can hardly go down to ca. 400 nm. This is due to the limitation of visible light which covers wavelengths of 400 – 800 nm. By using electron beams which have much smaller wavelengths than light, one is capable to view samples in the range of nanometers. Transmission Electron Microscopy (TEM) is performed by applying a beam of electrons transmitted through a ultra thin specimen. The electron beams that pass through will interact with the specimen and the emerging beam will contain valuable information regarding the electronic structure and crystal orientation of the sample.

The electron beam is generated in an electron gun by heating a LaB₆ or tungsten filament in a vacuum. After the electrons are accelerated in the gun (cathode) they are then rapidly moved towards the anode by applying a high voltage of 200 kV. A series of condensers is then used to focus and align the beams on the specimen which is mounted on a specimen grid [1].

Particle size and morphology of the samples in the current study were determined by TEM using a HRTEM Technai G2 F20 X-Twin MAT operating at 200 kV. Samples were prepared as follows: A spatula tip of the sample was suspended in ethanol. The mixture was then sonicated for approximately 30 minutes to ensure efficient dispersion. A micropipette was then used to extract some of the sample from the suspension which was then deposited on a S147-4 holey carbon film or 400 mesh copper grids. The copper grid was then left to dry in air. The sample was then placed in the sample tray of the microscope for analysis. The average particle size was calculated based on 150 particles.

Instrument setup :

HRTEM Technai G2 F20 X-Twin MAT 200 kV Field Emission Transmission Electron Microscope

Gunlens used: Gunlens 1

Spot size: 3

C2 aperture: 3

Objective aperture: 1

Accelerating voltage: 200 kV



3.2.2 X-Ray Diffraction (XRD)

Structural properties of Pt-Sn/C electrocatalysts obtained were investigated by XRD on a Bruker AXS D8 Advanced instrument operating with a copper tube with Cu-K_α ($\lambda = 1.5406 \text{ \AA}$) generated at 40 kV and 40 mA. Scans were performed at $0.05^\circ \text{ min}^{-1}$ for 2θ values between 10° and 90° . XRD patterns were recorded in the range $10 - 80^\circ (2\theta)$ with a scan step of 0.02° . The average crystallite size ($\langle D \rangle$, A°) was calculated from line broadening analysis using the Debye-Scherrer formula. For this purpose, the (2 0 0) peak of the Pt *fcc* structure around $2\theta = 70^\circ$ was selected as well as to calculate the lattice parameter (a_{fcc}) values for all the Pt-Sn/C catalysts and is shown in Equation (1) and Equation (2). The *Debye-Scherrer* equation was used as shown in Equation (1) to estimate the crystallite size from the XRD data [2].

$$d = \frac{0.9\lambda}{\beta \cos \theta} \quad (3.1)$$

$$a_{fcc} = \frac{\sqrt{2}\lambda_{K\alpha 1}}{\sin \theta} \quad (3.2)$$

where d is the crystal size, 0.9 is the shape factor, λ is the x-ray wavelength, β is the peak width at half peak height (FWHM) and θ is the angle of reflection.

3.2.3 Energy dispersion spectroscopic analysis (EDS) in transmission electron microscope

Energy dispersive X-Ray spectroscopy (EDS or EDX) was used to determine the atomic ratios of Pt and Sn in the electrocatalysts synthesized and also to confirm the presence of Pt and Sn on the catalyst support. EDS analysis was performed on a HRTEM Technai G2 F20 X-Twin MAT. The incident electron energies were kept constant at 20 keV for all the samples.

3.2.4 Inductively coupled plasma – atomic emission spectroscopy

A Thermo ICap 6300 ICP-AES spectrometer was used to measure the concentrations of Pt and Sn in solutions using the general ICP conditions listed in Table 3.1. For the determination of metal loadings 40-50 mg of all the catalysts were decomposed by Aqua regia (3HCl:1HNO₃) and diluted with water to a total volume of 50 mL. After filtration of the residual carbon black support, the samples were analyzed by ICP-AES. Standards (traceable to NIST) were matrix matched to acid concentrations of the samples. After calibration and quality check analysis to verify accuracy of standards, samples were analyzed, without dilution.

Table 3.2. ICP-AES operating conditions for the determination of Pt and Sn in electrocatalysts.

Parameter	Setting
Generator power	1300 W
View mode	Radial
View height	15mm
Plasma	Argon
Shear gas	Argon
Gas flow: plasma	15 ml min ⁻¹
Gas flow: auxillary	1.5 ml min ⁻¹
Gas flow: nebulizer	1.5 ml min ⁻¹
Sample aspiration\rate	2 ml min ⁻¹
Detector	PMT
Emission line: Pt	214.423 nm
Emission line: Sn	284.009 nm
Rinse delay	15 s
Read	Peak area
Replicate read time	2 s
Number of replicates	3

3.3 Electrochemical Characterization

3.3.1 Glassy carbon (GC) preparation

A glassy carbon (GC) electrode (5 mm diameter, $A_g = 0.196 \text{ cm}^2$) was polished to a mirror like image with different grades of alumina suspension, then washed with distilled water and sonicated for 5 min to remove any residual alumina. This cleaning procedure was done before each experiment. Typically 10 mg of catalyst was ultrasonicated (45 min) in a mixture consisting of 2.3 ml of water, 200 μl isopropanol and 20 μl of 5 wt. % Nafion solution until a homogeneous ink was formed. A known volume of the catalyst ink was then transferred *via* a syringe onto a freshly polished (mirror finish) GC electrode to give the desired Pt loading of 20 $\mu\text{g}_{\text{Pt}} \text{ cm}^{-2}$ as required. After the solvents were evaporated in a vacuum oven at 30°C the prepared electrode served as the working electrode.

3.3.2 Cyclic Voltammetry (CV)

Cyclic voltammetry (CV) is a versatile electroanalytical technique for the study of electroactive species. CV monitors the behaviour of chemically active species within a wide potential range. In CV a potential is applied to the system and the faradaic current response is measured (a faradaic current is the current due to a redox reaction). The current at the working electrode is monitored as a triangular excitation potential. The resulting voltammogram can be analyzed for fundamental information regarding the redox reaction at the electrode. It also provides information about the rate of electron transfer between the electrode and analyte and also the stability on the analyte in the oxidation states. For electrocatalysts, CV is typically used to characterize electrocatalytic activity in more detail. Fig 3.1 shows a typical CV plot of the standard Pt/C catalyst in 0.5 M H₂SO₄.

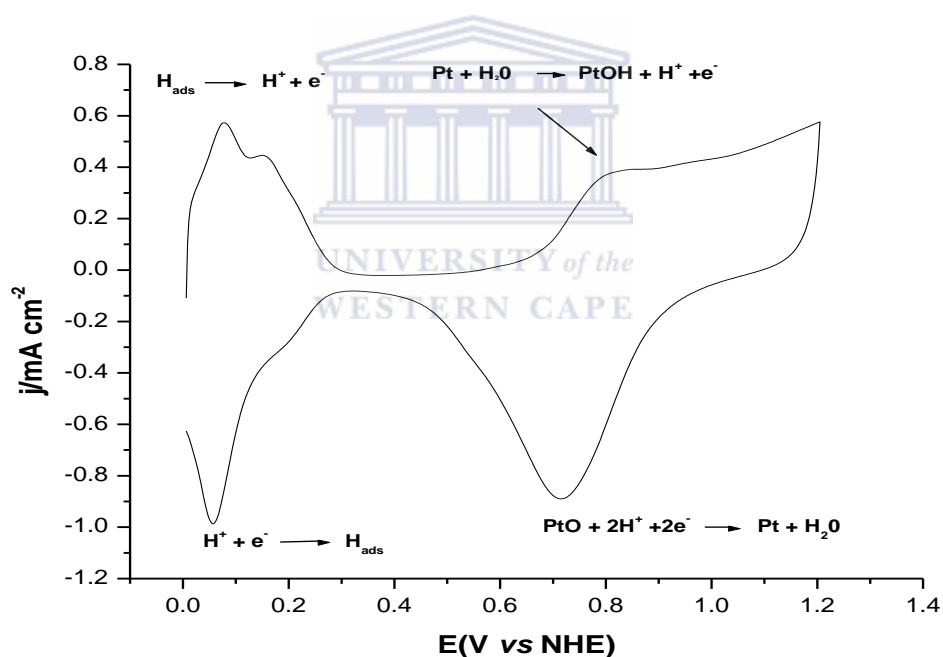


Fig. 3.1 Cyclic voltammogram of Pt/C (Alfa Aesar) in N₂ saturated 0.5 M H₂SO₄ at 20 mV s⁻¹.

The current response below +0.3 V vs NHE is due to the adsorption/desorption of hydrogen and the current response above +0.4 V vs NHE is due to hydroxide and oxide reduction/formation. The hydrogen adsorption/desorption region plays an important role in calculating the electrochemical surface area (ECSA) for Pt and Pt-alloys. The ECSA is an

important property which needs to be determined in order to compare current densities of different catalyst to each other.

The ECSA is an indication of the surface area available for electron transfer and can be calculated by using equation 3 below:

$$ECSA(m^2 g_{Pt}^{-1}) = [Q_H/210 \cdot L \cdot A_g]10^5 \quad (3.3)$$

where $Q_H = (Q' + Q'')/2$ is the average of the integrated areas of the hydrogen desorption/adsorption peak which gives the total charge passed during H^+ adsorption, $210 \mu C cm^{-2}$ is the required charge for the formation of a monolayer of H_2 on a smooth platinum surface, L is the loading of catalyst in $mg_{Pt} cm^{-2}$ and A_g the geometric surface area of the electrode (5 mm in diameter, $A_g = 0.196 cm^2$) [5]. On polycrystalline Pt surfaces, hydrogen desorption/adsorption occurs at different potentials on the (1 0 0), (1 1 0) and (1 1 1) vertices. This leads to the characteristic voltammogram as depicted above which is indicative of surface cleanliness [5-7]. In this study electrochemical measurements were performed using an Autolab PGSTAT 30 potentiostat/galvanostat and a conventional three-electrode electrochemical cell. A platinum foil and a Ag/AgCl (3 M KCl) electrodes served as the counter and the reference electrodes respectively. The electrolyte used for the half-cell measurements was either 0.5 M H_2SO_4 or 0.5 M methanol + 0.5 M H_2SO_4 . Before electrochemical testing commenced the electrodes were cycled 25 times at a scan rate of $20 mV s^{-1}$ between 0 V and +1.2 V vs. NHE until reproducible cyclic voltammograms were obtained in order to remove any impurities. For the MOR experiments the CV scans were carried out in the potential range of +0.2 V to +1.4 V vs. NHE at a scan rate of $20 mV s^{-1}$. Unless otherwise stated, all half-cell tests were performed at room temperature. During the electrochemical measurements a blanket of oxygen or nitrogen was maintained above the surface. All potentials were recorded vs. Ag/AgCl reference electrode but were referred to the normal hydrogen electrode (NHE) in this study.

3.3.3 Rotating disc electrode (RDE) experiments

Rotating disc electrode studies are a hydrodynamic technique commonly used for the quantitative evaluation of an electrocatalyst. The working electrode is rotated to induce forced convection and obtain a diffusion limited current (i_d) [5]. On a RDE the overall current

density (i) is related to the diffusion limited current density (i_d) and the true kinetic current density (i_k), is determined by the mass transport properties of the RDE in a relationship described by the Koutecky-Levich equation (Equation 4):

$$\frac{1}{i} = \frac{1}{i_k} + \frac{1}{i_d} \quad (3.4)$$

For an RDE the Levich equation (Equation 4) relates the diffusion limited current i_d to the rotation rate, ω

$$i_d = 0.62nFAD_0^{2/3}\omega^{1/2}\nu^{-1/6}C \quad (3.5)$$

by substituting equation 4 into 5, it gives a more useful form of the Koutecky-Levich equation for RDE:

$$\frac{1}{i} = \frac{1}{i_k} + \frac{1}{0.62nFD_0^{2/3}\omega^{1/2}\nu^{-1/6}C_0} = \frac{1}{i_k} + B \frac{1}{\sqrt{\omega}} \quad (3.6)$$

where i_k is the kinetic current density, B is the Levich slope, n the number of electrons involved in the ORR per oxygen molecule, C is the saturation concentration for oxygen in the electrolyte ($1.26 \times 10^{-3} \text{ mol l}^{-1}$), F is the Faraday constant (96485 C/mol). D is the diffusion coefficient ($1.93 \times 10^{-5} \text{ cm}^2 \text{ s}^{-1}$), ν the kinematic viscosity of the solution ($1.009 \times 10^{-2} \text{ cm}^2 \text{ s}^{-1}$) and ω is the rotation speed in rpm. The number of electrons involved in the ORR can be calculated using the *Koutecky–Levich* equation, which relates the current density i to the rotation rate of the electrode, ω and a plot of $i^{-1} \nu s \omega^{-1/2}$ should give parallel straight lines in the mixed kinetic-diffusion controlled region(s) with intercepts equal to $1/i_k$ [5].

In this study, RDE experiments were conducted with the catalyst coated on a GC RDE in oxygen saturated 0.5 M H_2SO_4 solution. The polarization curves were recorded at different rotating speed rates from +0.2 to +1.0 V vs NHE at a scan rate of 5 mV s^{-1} .

3.3.4 Brief theory of electrochemical kinetics

One of the objectives of this thesis is to characterize the Pt-Sn/C catalyst for their electrochemical performance of the oxygen reduction reaction. An electrode (Pt) in contact with an electrolyte (ion conductor) saturated with reactant (oxygen) develops an equilibrium potential difference between the electrode (electron conducting) and electrolyte (ion conducting) phases when no net current flows. For conditions of net current flow and under conditions where no mass transport and ohmic losses exist, the electrode-electrolyte potential difference is altered from the equilibrium potential by a certain amount called the ‘activation overpotential’. The activation overpotential is the difference above the equilibrium value required to produce a current. A generalized relationship between current and overpotential is given by the Butler-Volmer equation:

$$I = A \cdot i_0 \left[\exp \left\{ \frac{(1-\alpha)n \cdot F}{R \cdot T} (E - E_{eq}) \right\} - \exp \left\{ \frac{-\alpha \cdot n \cdot F}{R \cdot T} + (E - E_{eq}) \right\} \right] \quad (3.7)$$

where, I is the electrode current, A is the active surface area of the electrode, i_0 is the exchange current density, E is the electrode potential, E_{eq} is the equilibrium potential, α is the symmetry factor, F is the Faraday constant (96485 C/mol); R is the universal gas constant, T is the system temperature, and n is the number of electrons involved in the reaction. At higher overpotential, the second term on the RHS becomes insignificant compared to the first term, under such conditions, the so-called Tafel approximation can be applied and the resulting equation can be rearranged the following equation, commonly referred to as the Tafel equation:

$$\eta_{act} = B \ln \left(\frac{i}{i_0} \right) \quad (3.8)$$

where, η_{act} is the activation overpotential (in Volts), B is the Tafel Slope, and i is the current density (in $A \text{ cm}^{-2}$). The exchange current density, i_0 , is the equilibrium current which describes the rate at which both oxidized and reduce species react at the electrode. It can be thought of as the electrochemical reaction rate constant. A larger exchange current density indicates that the reaction catalyst surface is more active and a current is likely to flow in the

forward reaction direction. Since this exchange current density is controlling the rate of the sluggish ORR and ultimately the fuel cell performance it is important to make it as high as possible. The constant B (also known as the Tafel slope) is given by:

$$B = \frac{RT}{2\alpha F} \quad (3.9)$$

In the above equation the charge transfer coefficient, α , depends on the reaction that is occurring. When examining the exchange current density in the region limited by the kinetics, the ORR can be examined. For oxygen reduction the kinetic current for the mixed activation-diffusion controlled area, where the current is a product of both kinetic and diffusion contributions can be calculated as follows:

$$\frac{1}{i} = \frac{1}{i_k} + \frac{1}{i_L}$$

Rearranging the Koutecky-Levich equation for i_k gives:

$$\frac{1}{i_k} = \frac{i \cdot i_L}{i_L - i} \quad (3.10)$$

The diffusion limited current can be found from the polarization curve and used to convert the total current to kinetic current for the kinetically controlled region of the curve as seen below in Fig. 3.2. This kinetic current can then be used in the Tafel equation to create a plot of $\log(i_k)$ vs. potential. From the Tafel equation the exchange current and Tafel slopes can then be determined to evaluate the kinetics of the catalyst being examined [5,7,8].



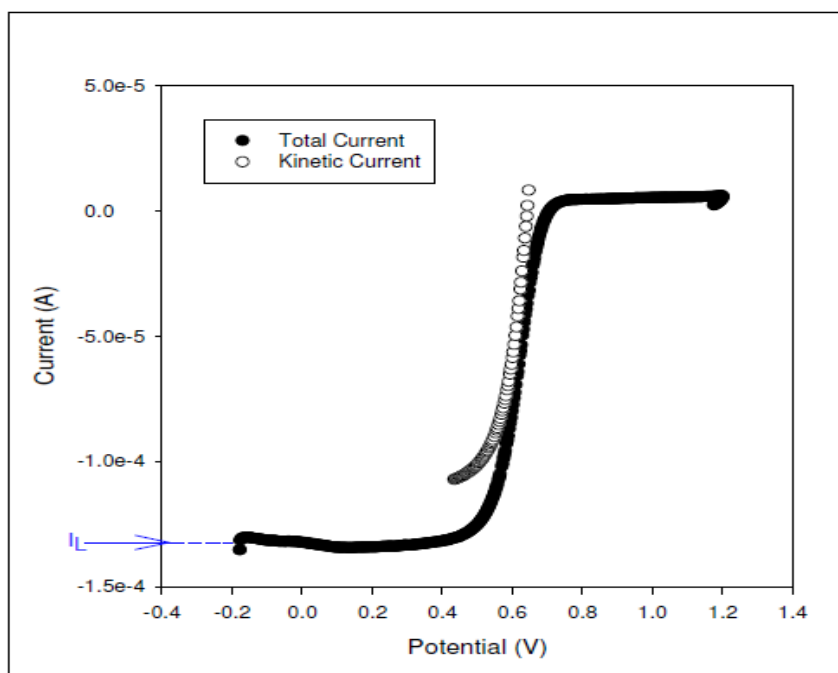
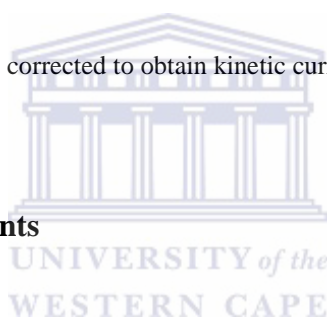


Fig. 3.2 illustration of polarization curve corrected to obtain kinetic current in activation controlled region [6].



3.4 Single Cell DMFC experiments

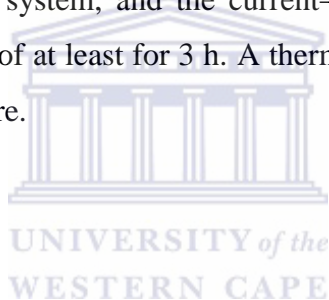
3.4.1 MEA preparation

Two types of proton exchange membranes (PEMs): Nafion 115 membrane (thickness ~ 127 μm , Du Pont, USA), and Nafion 212 membrane (thickness ~ 50 μm , Du Pont, USA), were used as the polymer electrolyte membrane for MEA preparation. Before use, the membranes were pre-treated in hydrogen peroxide solution (5 wt.%) at 80 $^{\circ}\text{C}$ for approximately 1 h; then thoroughly rinsed with deionized water, then transferred into a 0.5 M sulfuric acid solution and boiled at 80 $^{\circ}\text{C}$ for an additional 1 h and finally washed with deionized water. The catalyst inks were prepared by dispersing catalyst powders into a mixture of isopropanol and Nafion solution. The catalyst used for the anode was, Pt-Ru/C (20 wt. % Pt and 10 wt. % Ru, Johnson Matthey) and cathode layers were HiSpec Pt/C (20 wt.% Pt, 40 wt.% Pt, Johnson Matthey), and Pt-Sn/C in-house catalyst respectively; 5% Nafion solution was purchased from Sigma Aldrich. The mixture was ultrasonically dispersed for 30 min before being used. The prepared catalyst ink was machine sprayed (Nordson ASYMTEK, USA) onto the top of a commercial gas diffusion layer (Freudenberg, Germany) followed by drying under infra red lamps. Thereafter, 40 mg 5 wt. % Nafion was sprayed additionally for better

adhesion between the membrane and the catalyst-coated gas diffusion layer. Unless specified, the catalyst loadings for all the cathodes and the anodes were 0.5 mg cm^{-2} of Pt for DMFC test. The active area of the prepared MEAs was 5 cm^2 .

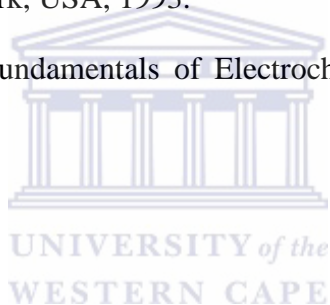
3.4.2 Single cell testing

The prepared MEAs with an active area of 5 cm^2 were assembled with 3-channel serpentine flow fields (Poco graphite blocks) and gold-coated current collectors and then tested in a Fuel cell station (FuelCon Evaluator C-70189, Germany). A 1 M methanol solution was fed to the anode at a flow rate of 50.0 ml min^{-1} from a methanol container with a pump and preheated to the operating temperature which was $70 \text{ }^\circ\text{C}$ for all the fuel cell testing. O_2 was humidified (100%) by passing through the humidifier built in the test station and then fed to the cathode at the flow rate of 5 ml min^{-1} without backpressure. The performance of the fuel cell was monitored by a data acquisition system, and the current–voltage polarization curves were recorded only after the operation of at least for 3 h. A thermocouple was used to monitor and control the desired cell temperature.



REFERENCES

1. H. P. Klug, L. E. Alexander, *X-Ray Diffraction Procedures for Polycrystalline and Amorphous Materials*, Wiley, New York, 1974.
2. http://en.wikipedia.org/wiki/Energy-dispersive_X-ray_spectroscopy
3. http://astronomy.nmsu.edu/jlevans/seminarSpr07/transmission_electron_microscope.png
4. R. Woods, in: A. J. Bard (Ed.), *Electroanalytical Chemistry*, Marcel Dekker, New York, 1976.
5. A.J. Bard, L.R. Faulkner, *Electrochemical Methods: Fundamentals and Applications*, John Wiley, New York, 2001.
6. <http://www.wikipedia.org/levich/equation/> (June 2011)
7. C.M.A. Brett, A.M.O. Brett, *Electrochemistry, Principles, Methods, and Applications*, Oxford University Press, New York, USA, 1993.
8. K.B. Oldhan, J.C. Myland, *Fundamentals of Electrochemical Science*, Academic Press Inc., San Diego, USA, 1994.



Chapter 4

Results and Discussion I

Synthesis of Pt-Sn/C catalysts via the polyol reduction method

4.1 INTRODUCTION

As noted earlier, the polyol reduction method was chosen to prepare the Pt catalyst series due to the fact that this was one of the criteria for this project and also since it appeared to be the most convenient method for our laboratory setup. Presented here are the synthetic protocols of the Pt-Sn/C catalysts by a modified polyol reduction process, followed by heat treatment at various temperatures. The synthesized Pt-Sn alloys were all characterized by XRD, EDX, TEM and metal loading by ICP-AES.

4.2 Experimental

4.2.1 Synthesis

The experimental procedure as reported by Jeyabharathiet. *al.*, [1] for the synthesis of their Pt-Sn/C catalysts was repeated in our laboratory. The procedure was as follows:

Pt-Sn (70%:30%)/C nanoparticles samples were prepared by a polyol reduction process. In this process, to a mixture of 9.28 mg of $H_2PtCl_6 \cdot 6H_2O$, 28.51 mg of $SnCl_2 \cdot 2H_2O$ and 125 mg of Vulcan XC72R carbon, 40 mL of ethylene glycol was added and stirred well to obtain a homogeneous mixture. This was then heated at $85^\circ C$ for 4 h and set aside to cool to room temperature after which the black residue was centrifuged and washed three times with Millipore water. The residue was kept under vacuum for drying at room temperature. The carbon-supported metal nanoparticles were then subjected to heat-treatment in an argon atmosphere at various temperatures, viz., 250, 500, 600 and $800^\circ C$ separately for 4 h in a tubular furnace. The above procedure was repeated several times and the results are given in Fig.4.1. From the XRD data only the Pt (100) peak at around $41^\circ \theta$ was visible and so one would expect a catalyst having very poor performance and bad catalytic activity. No alloying with tin was observed in the XRD pattern. The CVs obtained also showed very poor activity in the hydrogen adsorption/desorption region. The TEM images showed very poor particle loading and a very broad particle size distribution was found. The average particle size was found to be 7-9 nm which is not sufficient to be used as an electrocatalyst for DMFC

application. Using the exact amount of starting material as describe above the Pt loading on the catalyst was calculated and was found to be 5 wt.%. From these results it was clear that this synthetic procedure had several flaws and that drastic changes needed to be implemented to prepare far better catalysts with an improved performance.

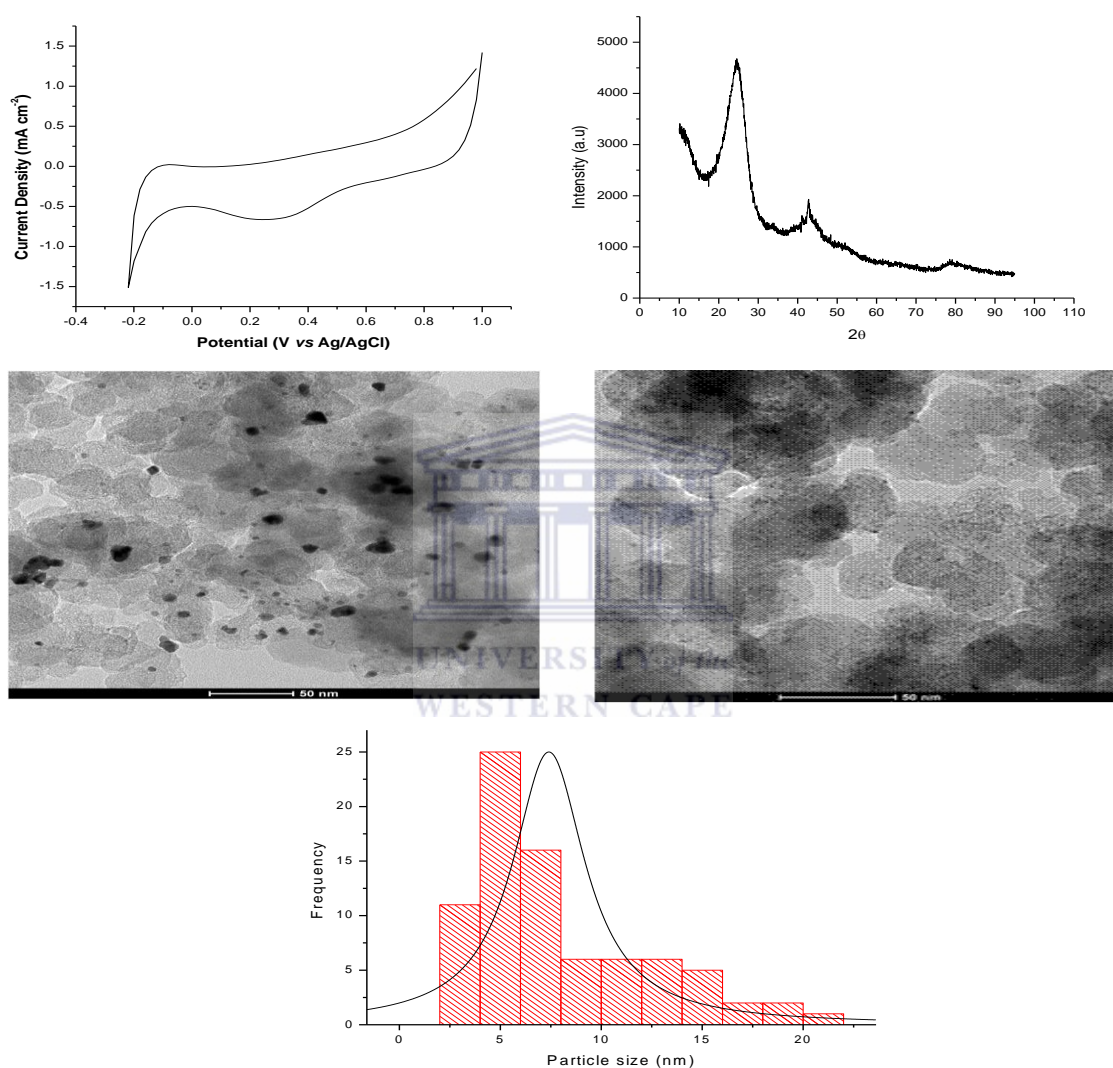


Fig. 4.1 Preliminary results of Pt-Sn/C catalyst synthesis.

The first parameter which was changed involved the temperature which at which the reduction was performed and this was increased from 85 to 130 °C and later to 150 °C under a nitrogen atmosphere. Ethylene glycol (EG) has a boiling point of 198 °C and thus increasing the temperature was a viable option to pursue seeing that we were still operating well below the boiling point of EG and there was no obvious reason to reflux the reaction

mixture. The temperature was increased to in turn, increase the oxidation rate of EG which in turn would reduce the metal precursors in better ways since EG acts as both solvent and reducing agent. The temperature in our view not only plays an important role in the reduction potential of EG but also determines the rate of the reaction. The second parameter which was changed was the pH of the reaction and this was adjusted to above 12 with 1 M NaOH before the carbon black was added to the EG solution in which the metal precursors were dissolved. When both metal precursors were dissolved in the EG the pH was measured as being 5.6. Thus on average between 1-2 ml of NaOH was added to adjust the pH to the desired value of 12-13. Several other groups have also reported on the advantages of changing the pH at this stage as it plays an important role in controlling the growth and particle size of the nanoparticles that are formed during the reduction phase [2]. The final changes effected were that after all the above changes were implemented, the EG suspension was sonicated for 30 – 60 min before the suspension was heated and after the reaction was heated for 4 hours, the reaction mixture was stirred overnight. The results, after these changes were implemented in the modified polyol method, are presented in Fig. 4.2. In all the cases there were significant improvements found in the activity of the catalyst. It was interesting to note that stirring the reaction mixture overnight and adjusting the pH with NaOH was found to have had the biggest improvement on the catalyst as noted from Fig. 4.2a The XRD pattern shows two new low intensity peaks which can be attributed to different phases of SnO₂ which were not visible before the method was modified. The Pt (2 0 0) peak is also visible in the modified polyol method. Also the effect of the operating temperature on the electrochemical activity of the catalyst can be seen in graph (b) where (a), is 150 °C and (b) 130 °C and (c) 85 °C. Higher temperatures viz., >150 °C were also investigated but no real improvement was found and thus the temperature chosen for all catalyst synthesis was kept at 150 °C. From the TEM images, graph (c), it is clear that there was a big improvement on the metal loading and nanoparticle size distribution on the carbon support. EDX, graph (d), also confirmed the presence of only Pt and Sn metal on the carbon support. The presence of Cu is due to the Cu-grid used and is thus not surprising. After these preliminary tests, our modified standard method for the preparation of Pt-Sn/C catalysts was established. The polyol STD method is shown schematically below. The STD method was used as the benchmark method for the synthesis of the Pt-Sn/C catalyst and all new changes made to the polyol method were performed using the STD method as the basic protocol.

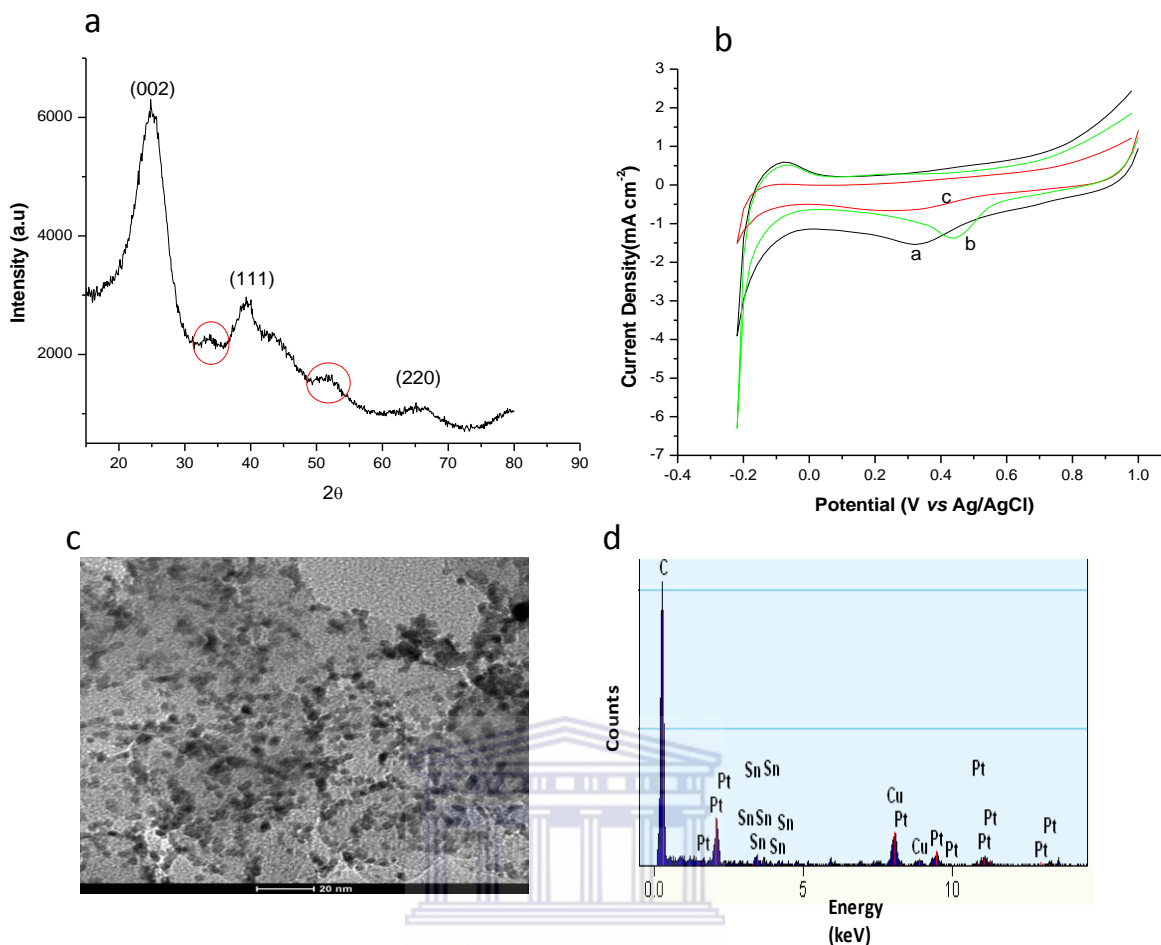
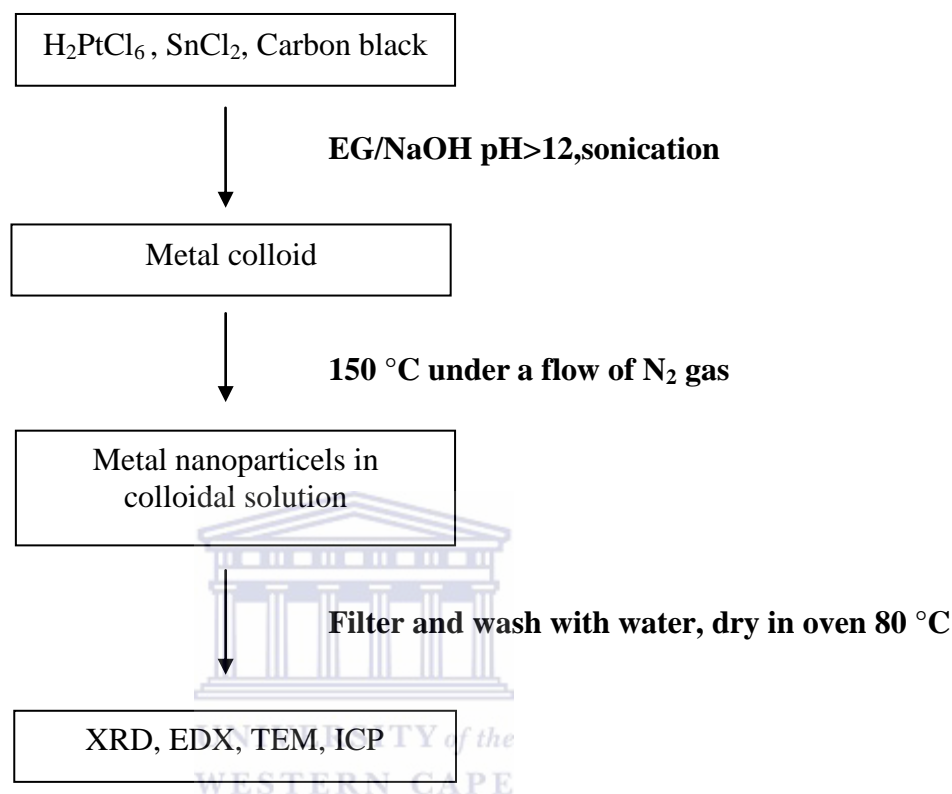


Fig. 4.2 Preliminary results of polyol method after changes were made.

The STD method may be described as follows:

To a mixture of $\text{H}_2\text{PtCl}_6 \cdot 6\text{H}_2\text{O}$ (66 mg, 0.161 mol) a calculated amount of $\text{SnCl}_2 \cdot 2\text{H}_2\text{O}$ and Vulcan XC-72R carbon (125 mg) was suspended in 100 ml ethylene glycol in a Shlenck tube. The pH value of the solution was adjusted to about 13 by addition of 1 M NaOH solution followed by stirring and purging with N_2 . The solution was then heated at 150°C for 4 hours with stirring and set aside to cool to room temperature while being stirred overnight. The catalyst was filtered and the filter cake thoroughly washed with ultra pure water and dried in a vacuum oven at 80°C overnight. The nominal Pt loading was 20 wt% and the nominal atomic ratio of Pt to Sn was 3:1. The STD method was also repeated several times before being scaled up to give the desired Pt loading of 20 wt.%. Although there was a vast improvement in the catalyst performance after the method was modified, there were still several worrying factors when the Pt-Sn/C catalyst was compared to the commercial 20% Pt/C catalyst regarding performance and particle size. The problem manifested itself by the

fact that although our Polyol STD method yielded excellent Pt-Sn/C nanoparticles, the desired Pt loading was not achieved. ICP studies showed that the Pt loading using the STD method was less than 10 wt.%.



During the filtration stage after the reaction, it was observed that the filtrate had a bright yellow colour indicating that there was Pt remaining in the EG solution. This implied that the STD method had to be again altered in such a manner so as to improve the metal loading problem. The fact that not all of the Pt and Sn introduced in the beginning of the reaction was reduced and deposited onto the carbon support which meant that the remainder of the metals were either not fully reduced or if reduced, still suspended in solution. Therefore, the following modifications were incorporated into the STD method to overcome this problem.

4.2.2 Acid Method

After the reaction mixture was cooled down to room temperature the pH of the colloidal suspension was adjusted to either 3 or 5 with 32% HCl or 65% HNO_3 and then stirred overnight. In this instance, the acid acted as a sedimentation promoter and improved the

overall metal loading of the catalyst. After preliminary testing, HCl was chosen as the better sedimentation promoter.

4.2.3 Slurry Sonication Method

In this variation the carbon was added in a slurry form. Carbon Black was dissolved in either 20 ml ethylene glycol or a mixture of EG and water with different ratios, sonicated (ultrasonic bath) for 30 minutes then added to the reaction mixture and sonicated further for 1 hour before the reaction started.

4.2.4 Metals Boiled Method (HA Method)

In this variation the metal precursors were boiled for 1 hour in EG after which the carbon was added either as is or as a slurry, heated for a further 3 hours after which the pH was adjusted to 3 or 5 and stirred overnight.

4.3 Standard acid dropped method (STD)

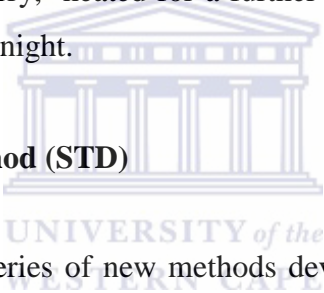


Fig 4.3 illustrates the first of a series of new methods developed for the preparation of Pt-Sn/C nanoparticles. The 3 different catalysts synthesized with this method are annotated as STD, STD pH5 and STD pH3 respectively. The diffraction peak at around 25° is attributed to diffraction at the (0 0 2) plane of the hexagonal structure of Vulcan XC-72R carbon. The diffraction peaks at around 39° , 46° , 68° and 81° are due to diffraction at the Pt (1 1 1), (2 0 0), (2 2 0) and (3 1 1) planes, respectively. These diffraction peaks represent the typical character of a crystalline Pt face, that is face centred cubic or fcc. This indicates that the in-house supported Pt-Sn/C catalysts has the Pt (fcc) crystal structure [3,4]. In addition, some other peaks at around 34° , and 52° , were also observed, which can be related to SnO_2 (1 0 1) and SnO_2 (2 1 1) diffraction peaks. The 2θ of all the Pt-Sn/C STD catalyst shifted slightly to lower values indicating that alloying has occurred. The mean Pt particle diameters of the Pt-Sn/C catalysts were calculated from the Pt (2 2 0) diffraction peak via the Scherrer equation, assuming spherical metal particles. The results are listed in Table 4.1. This result agrees well with recent reports [5,6]. Fig 4.4 presents the low- and high magnification TEM images of the as prepared Pt-Sn/C catalyst using the STD method. A good distribution of mostly spherical

shaped Pt-alloy particles on the carbon support with a narrow particle size distribution was observed.

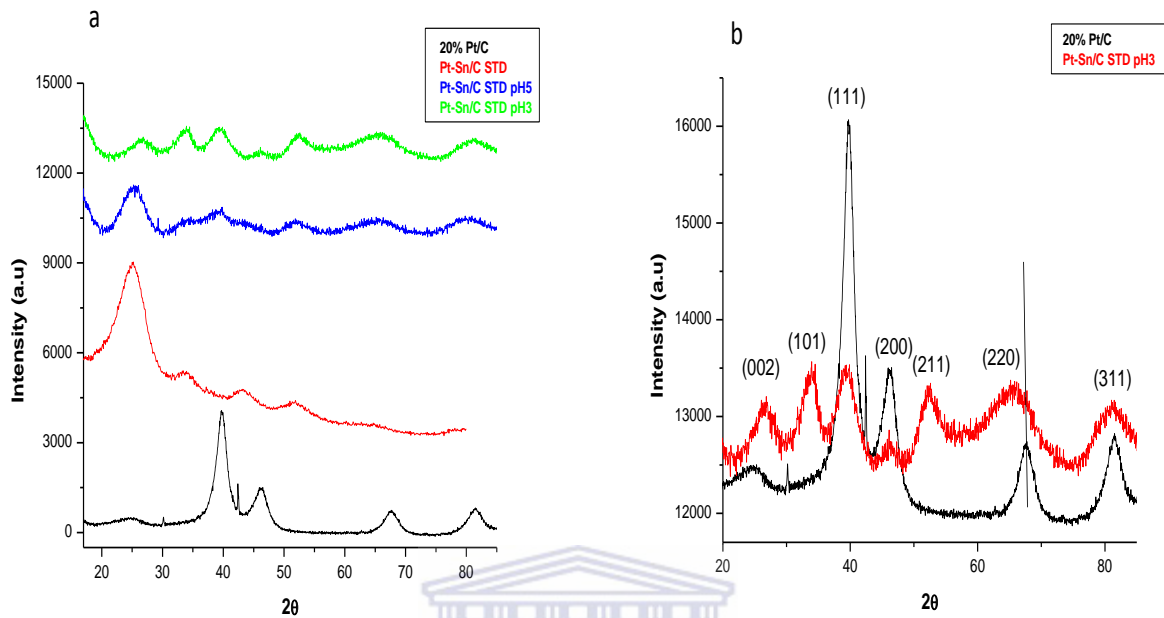


Fig 4.3 XRD patterns of Pt-Sn/C synthesized with STD method, b) comparison of Pt-Sn/C STD pH3 with 20% Pt/C.

For the Pt-Sn/C STD pH3 catalyst the average particle size was found to be 3.77 nm ±0.74 which was the lowest of the 3 catalyst synthesized with the STD method. Fig 4.5 shows the particle size distribution histograms of the Pt-Sn/C STD method catalyst. These histograms are based on the observation of 150 particles. The mean particle diameter (d) is calculated according to equation 4.1.

$$d = \frac{\sum_i n_i d_i}{n} \quad (4.1)$$

Where n_i is the frequency of occurrence particles of the size d_i

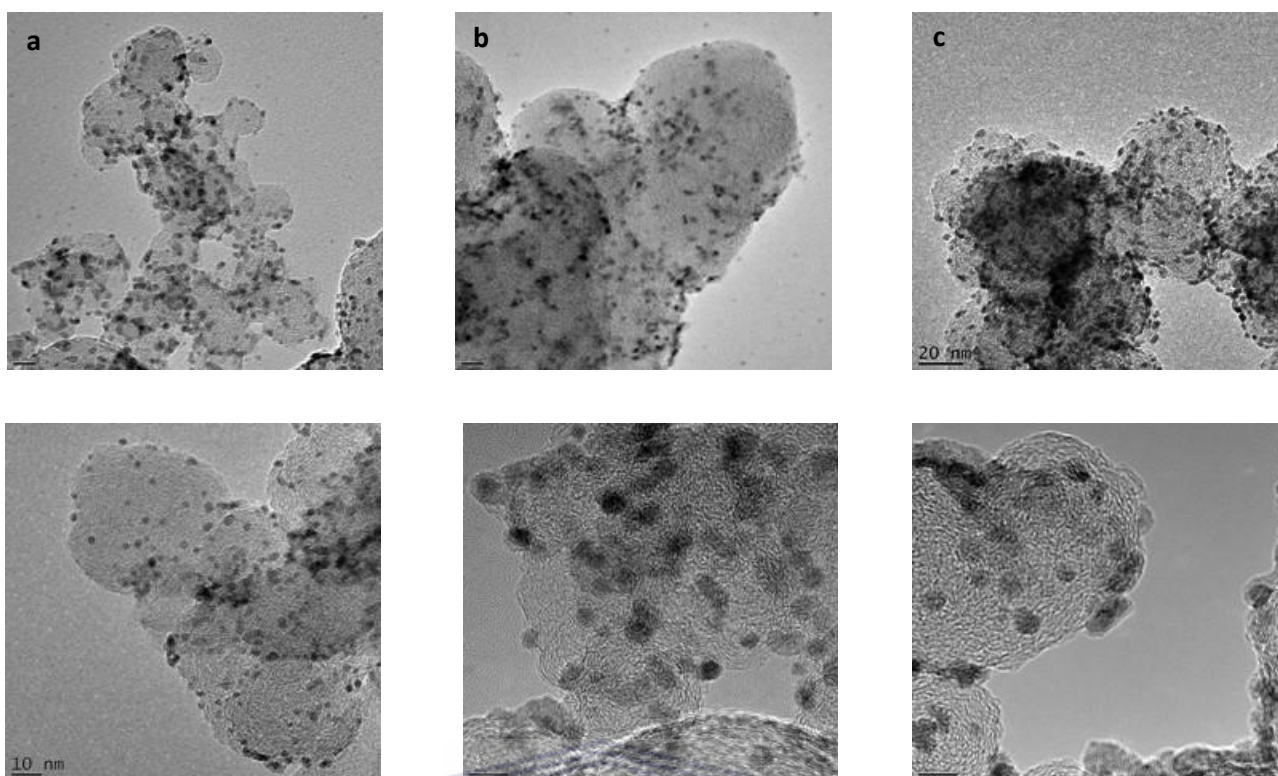


Fig. 4.4 TEM images of high and low magnification of a) Pt-Sn/C STD pH3, b) Pt-Sn/C STD pH5 and c) Pt-Sn/C STD.

The average particle size for all the 3 prepared catalysts using the STD method was found to be very close to each other despite adding the sedimentation promoter. It can therefore be concluded that adding HCl as sedimentation promoter is more beneficial towards the overall metal loading and that the average particle size is less effected by the addition of HCl. Several studies were also performed where the pH was adjusted to 2, 1 and even less than 1 with HCl. However, no improvement in either the metal loading or particle size of the catalyst was found. Therefore we conclude that pH 3 is the optimum pH to prepare the best possible catalyst for the STD method system. During the filtration step after completion of the reaction, it was observed that the Pt-Sn/C STD pH5 catalyst filtrate still had a slight yellowish colour indicating the presence of Pt-Sn colloids in the filtrate. The metal particles which thus were not deposited on the carbon, remained in solution and thus be considered to be a huge waste since Pt is a precious and very expensive metal.

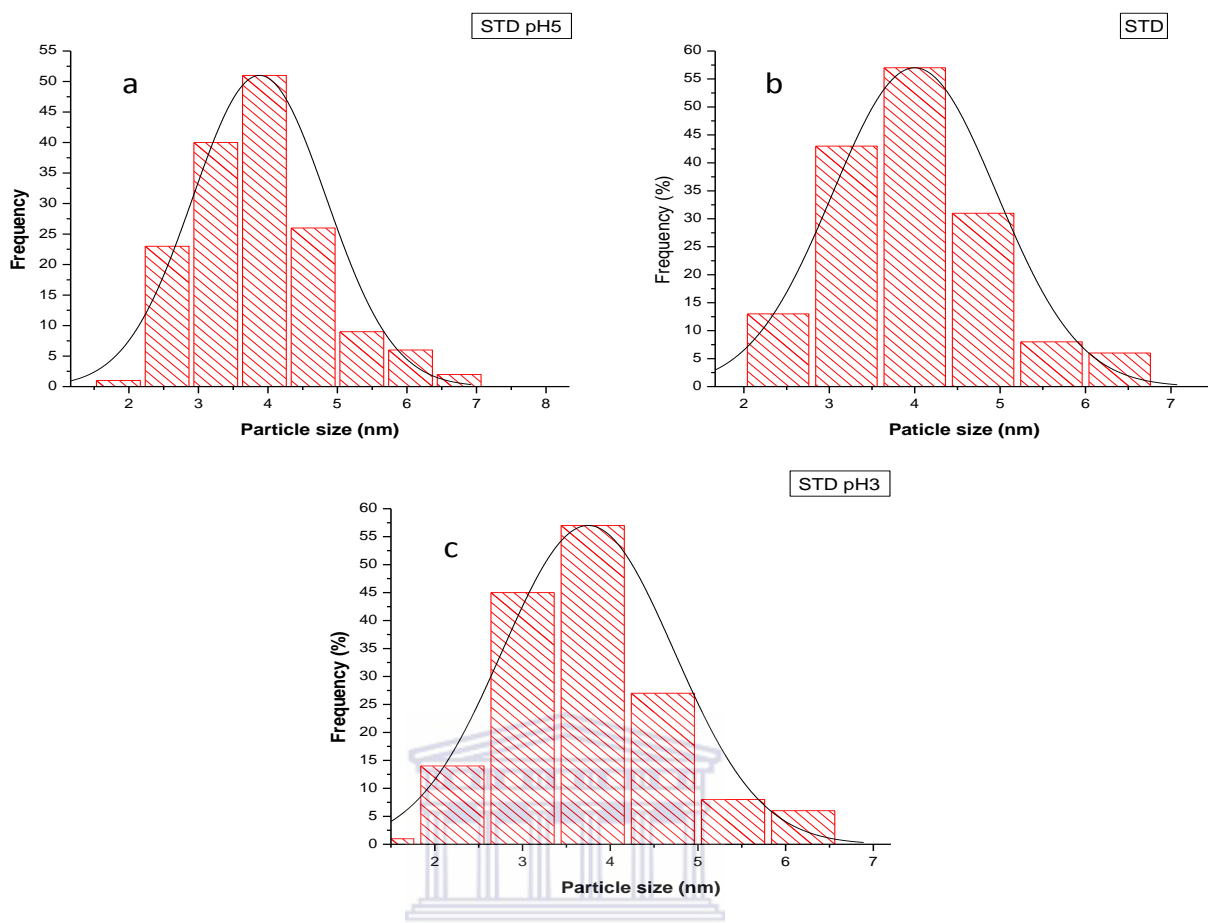


Fig. 4.5 Histogram of Pt-Sn/C STD method catalyst particle size distribution, (a) STD pH5, (b) STD and (c) STD pH3.

When the Pt-Sn/C STD pH3 catalyst was filtered, the filtrate was clear which suggested that all or most of the Pt and Sn salts used in the beginning were reduced and deposited onto the carbon support. By using concentrated HCl as the sedimentation promoter, formation of smaller particles as well as a narrower particle size distribution was observed when the pH was adjusted to between 3-5 and stirring continued overnight. This finding was confirmed by the work done by Oh *et al.*, for their Pt/C system and who explained these phenomena in terms of the Zeta potential [7]. Zeta potential may be defined as the potential difference measured in a liquid, between the shear plane and the bulk of the liquid beyond the limits of the electrical double layer. The magnitude of the Zeta potential gives an indication of the potential stability of the colloidal solution [7-9]. In our preliminary Zeta potential studies it was found that in alkaline solutions both the carbon support and Pt-Sn colloids possessed strong negative surface charge which resulted in an electrostatic repulsive force. During the

polyol reaction, the surface charge originates from the adsorption of a hydroxide ion and glycolate anion due to the oxidation of EG. Therefore the concentration of both ions was found to be dependent on the pH of the solution as seen in Fig. 4.6 and is based on Zeta potential studies. The surface charge of the carbon and the Pt-Sn colloid were measured individually as a function of pH in the polyol process.

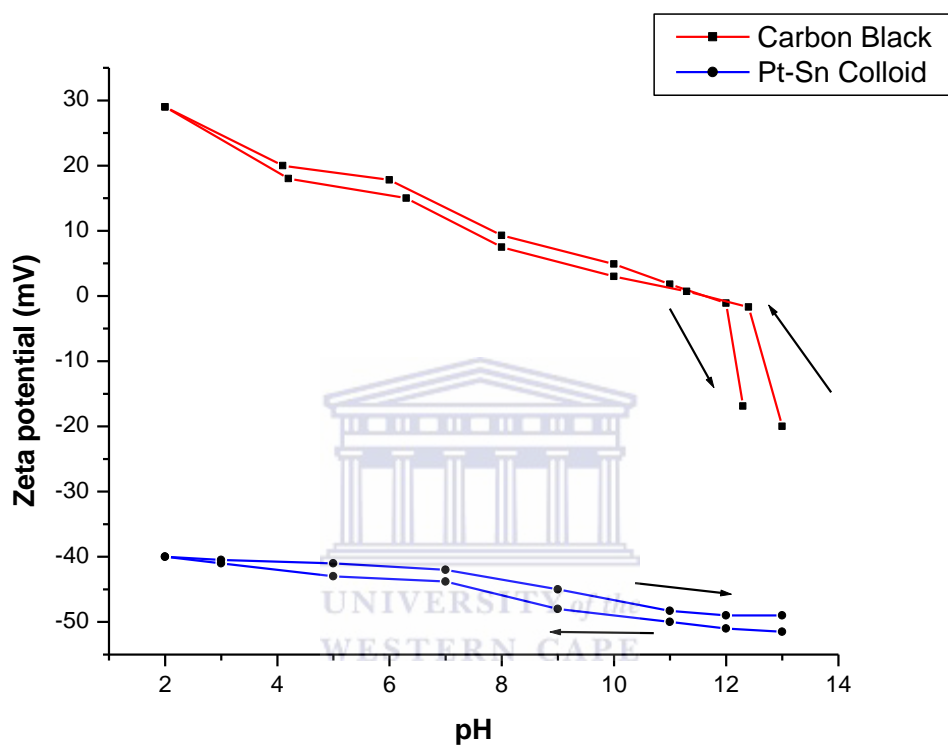


Fig. 4.6 Change in zeta potential of Pt-Sn colloid and carbon support on changing the pH from acidic to alkaline and vice versa.

For the initial stage of the reaction the pH was adjusted to 13 and once the reaction was completed the pH was varied by either adding HCl or NaOH. For carbon the zeta potential moved from an initial positive to a negative value when the pH was changed from 2 to 12. When the pH was reversed, the zeta potential changed to a positive value again. However, for Pt-Sn colloid no significant change in the zeta potential was observed when the pH was changed from alkaline to acidic and vice versa, which implies that the glycolate anions are adsorbed on the surface of Pt-Sn colloid more strongly than that of the carbon support. After completion of the polyol reaction at pH 13, the glycolate anions are at a saturation

concentration. If the pH is then adjusted to either 5 or 3 it should provide the carbon surface with a positive charge. During this stage, the stabilized Pt-Sn colloid which also possesses a negatively charged surface remains constant. The reason being, that after complete reduction of the metal salts, the nanoparticles are suspended in solution by the glycolate anions which act like a chelating type complex and thus hinder the nanoparticles from being deposited onto the carbon support. By adding HCl, the glycolate concentration will be reduced by neutralisation and consequently freeing the nanoparticles suspended in solution and making them available for deposition onto the support. This therefore implied that the adsorption of Pt onto the carbon support would be higher at a lower pH due to the increased electrostatic attraction between carbon and the Pt-Sn colloid thereby resulting in a higher metal loading without concomitantly increasing the particle size. Fig 4.7 shows the difference in solution colour providing further evidence that the suspended Pt-Sn colloidal particles concentration in solution decreases as the solution became more acidic and therefore the metal loading was increased in the process.



Fig. 4.7 Filtered solution of polyol reaction (a) without pH adjustment (b) with pH adjustment to pH5 and (c) with pH adjustment to pH3.

The effect on the as-prepared catalyst by adding HCl to adjust the pH was further confirmed by ICP studies which showed an increase in metal loading for Pt and Sn as more HCl was added to the reaction. Thus addition of HCl affected a big and positive difference in the metal loading for the 3 catalysts. However, the particle size remained relatively constant and thus no real big difference was observed for this aspect of catalyst synthesis. The particle size appears to be constant throughout the pH adjustment stage which may be explained by the

fact that the surface charge of Pt-Sn nanoparticles was not affected by the pH adjustment step as illustrated in the zeta potential experiment. Consequently, the electrostatic repulsive forces existing between Pt-Sn particles prevent any aggregation. The Zeta potential experiment therefore explains why the metal loading for the Pt-Sn/C STD catalyst is so low and why there was a big improvement in the metal loading for the Pt-Sn/C STD pH3 catalyst. Table 4.1 summarizes the findings of the polyol STD method. The particle size estimated by XRD is in all cases lower than that estimated by TEM. There are several reasons for this observation. To begin with, one is only able to detect the crystal lattice structures from XRD and it is therefore possible that some of the Pt present is deposited as larger particles with crystal imperfections making them undetectable by XRD and thus leading to lower particle size than what is actually present. Furthermore, with XRD the actual crystal size is estimated and it is therefore possible for some of the crystals to agglomerate forming bigger particles which in turn will manifest themselves as larger particles in TEM observations. Secondly, when preparing the samples for TEM a solvent (MeOH, EtOH) is used to make a suspension. Although the solvent is left to evaporate, the particles could swell and therefore appear bigger when analyzed with TEM. Thus there is a type of solvent effect caused by the solvent used that might well influence the particle size while in the case for XRD this factor is not an issue.

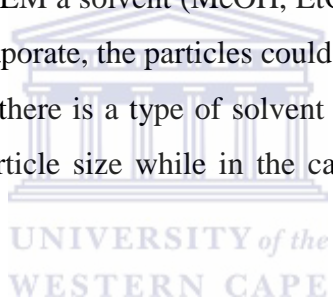


Table 4.1. Values of lattice parameters and particle size for Pt-Sn/C catalyst.

Catalyst	Crystallite				
	Pt ₇₅ Sn ₂₅ phase	Size	Particle Size	Sn loading	Pt loading
	Lattice parameter (nm)	XRD (nm)	TEM (nm)	(wt.%)	(wt.%)
20 % Pt/C (JM)	0.3923	3.56	3.88		20.43
PtSn\C (STD pH3)	0.3927	3.64	3.77 ± 0.74	8.32	17.63
PtSn\C (STD pH5)	0.3929	3.79	3.86. ± 0.78	8.24	13.85
PtSn\C (STD)	0.3933	3.87	3.99 ± 0.96	7.81	10.06

The compositions of the Pt-Sn/C catalysts were evaluated by EDX analysis. Fig. 4.8 shows the typical EDX spectrum. It was found that there were no foreign elements apart from for Pt,

Sn, C, and Cu (due to the grid). In our study EDX confirms the presence of Pt and Sn in all the catalysts prepared by the STD method.

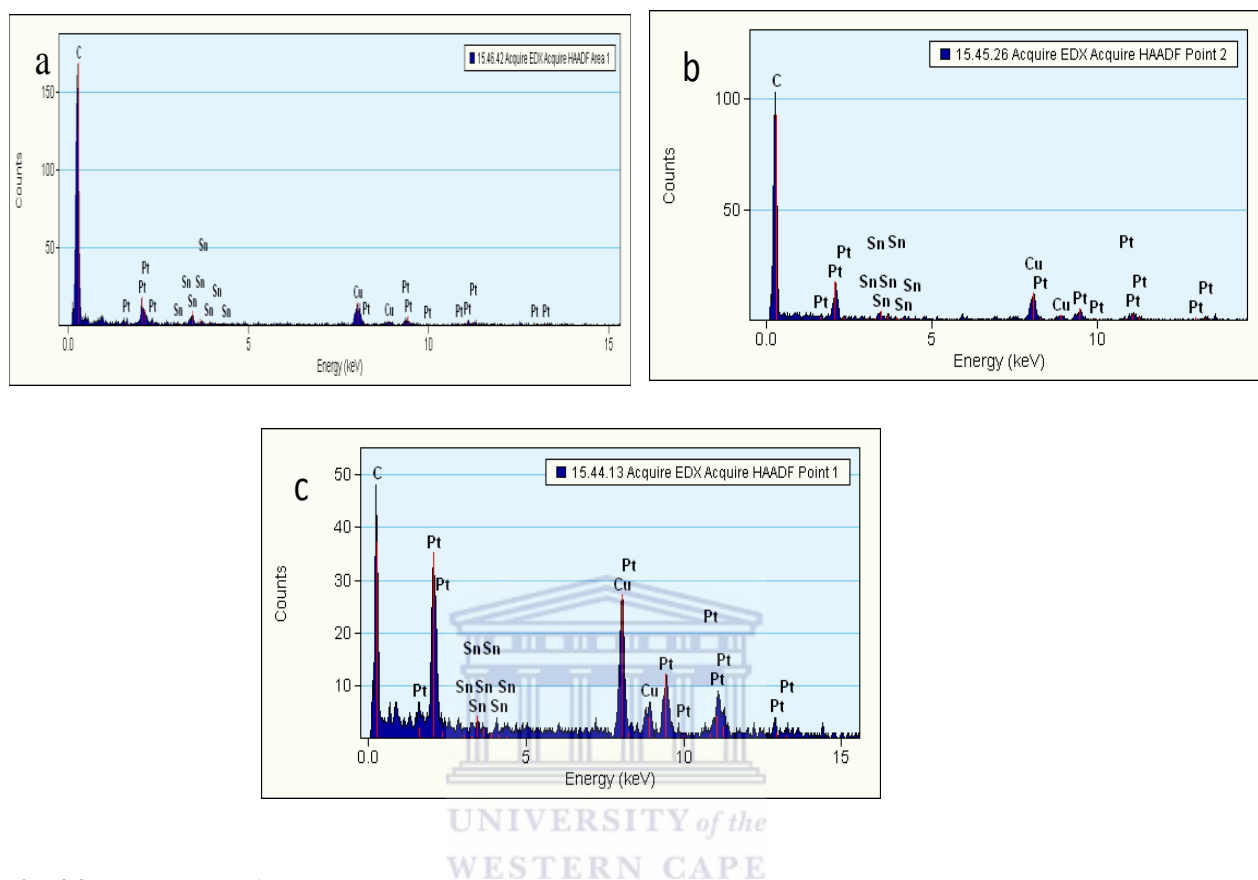


Fig. 4.8 EDX spectra of as prepared Pt-Sn/C catalyst, a) STD, b) STD pH5, c) STD pH3.

4.4 Slurry method

With this variation on the polyol method we were investigating what effect sonication and addition of the carbon support would have on the particle size, distribution and metal loading. Carbon black was added to EG to form a suspension and then sonicated for 30 min. To this suspension was added the EG solution containing the metal precursors and sonication was applied to the mixture for a further 30 min. After this pre-treatment the STD method procedure was followed. Solvent mixtures of water:EG (1:1), (1:2) and (1:4) were also investigated and used as solvent systems for the formation of the carbon slurry or to dissolve the metal precursors. In the polyol process water is believed to act as a stabilizer which in turn would assist to control the growth of nanoparticles [6]. The water:EG mixtures of (1:1) and (1:2) gave very poor results when used for the slurry formation and metal precursors

solution. The water:EG (1:4) mixture was found to give results comparable to those of pure EG when used for both systems. For our systems studied, it was found that including too much water into the synthetic protocol apart from decreasing the relative amount of EG also decreased the catalyst performance. The H₂O:EG (1:4) solvent results were better due to relatively less water being used and therefore more EG was readily available to reduce the metal precursors. Reports in literature regarding improvements to the protocol all described adding water but most of these catalyst studied were single systems and not bi-metal systems as in our case and in most of the reported studies the water composition was between 10-20% [6,7]. Another reason for the decrease in performance when adding too much water could be due to the addition of aqueous NaOH when adjusting the pH. Addition of NaOH is known to act as a stabilizer too, playing an important role in particle growth. The stabilizing effect of NaOH in our system could be greater than that of water and therefore there is little or no improvement when water is used. The role of water was not further investigated in this study and thus all the catalysts reported were synthesized by mixing the carbon black in EG to only obtain a carbon slurry. The catalysts synthesized using this variation was noted as Slurry STD, Slurry pH5 and Slurry pH3. The corresponding XRD patterns are shown in Fig. 4.9.

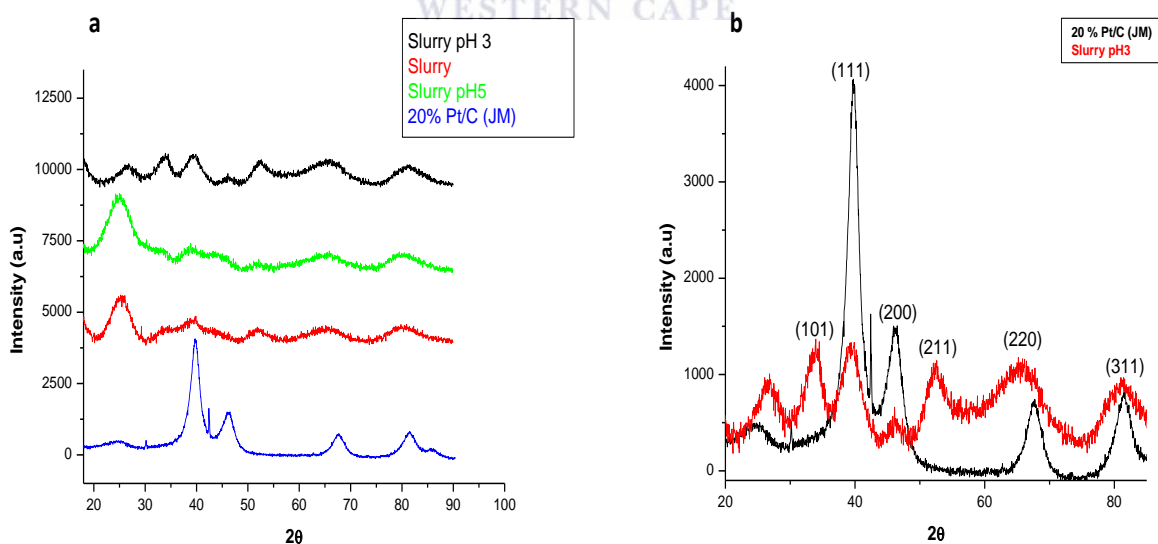


Fig 4.9 XRD patterns of Pt-Sn/C synthesized with Slurry method, b) comparison of Pt-Sn/C Slurry pH3 with 20% Pt/C.

All 3 catalysts show peaks at 2θ values around 39° , 46° , 66° and 79° corresponding to the (1 1 1), (2 0 0), (2 2 0) and (3 1 1) planes of face centred cubic (*fcc*) structures of Pt. The broad peaks indicate that the particles are in the nanocrystalline range. As seen previously the diffraction peak at 2θ value of 25° correspond to the (0 0 2) plane of the carbon structure. TEM images and EDX spectrum of the Slurry method catalyst are shown in Figs 4.10 and 4.11. For this variation a very narrow distribution of metallic nanoparticles of average size 3-4.5 nm on the carbon support can be seen from the TEM images. When compared to the STD method the particles are smaller. Elemental analysis performed by EDX confirms the presence of respective elements Pt, Sn and very small quantity of oxygen. The calculated metal loading (wt. %) of all the catalysts are given in Table 4.2. It was observed that the Pt loading increased from Slurry STD to Slurry pH3.

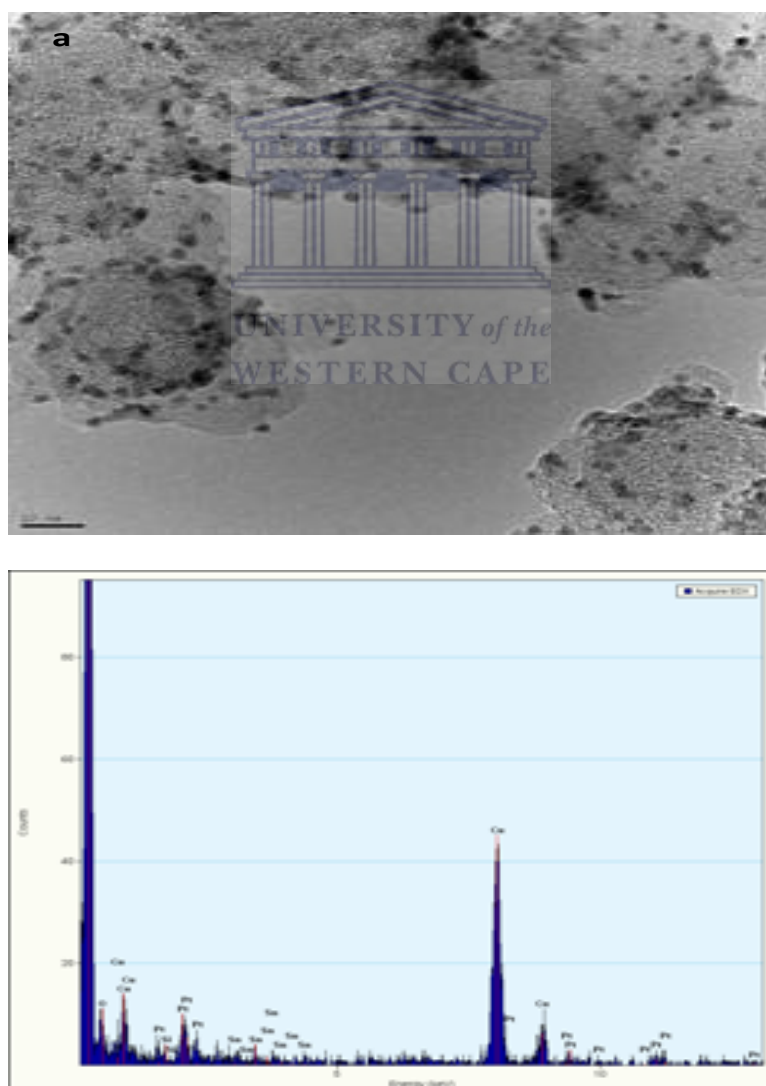


Fig. 4.10 TEM image and EDX spectrum of Pt-Sn/C Slurry STD.

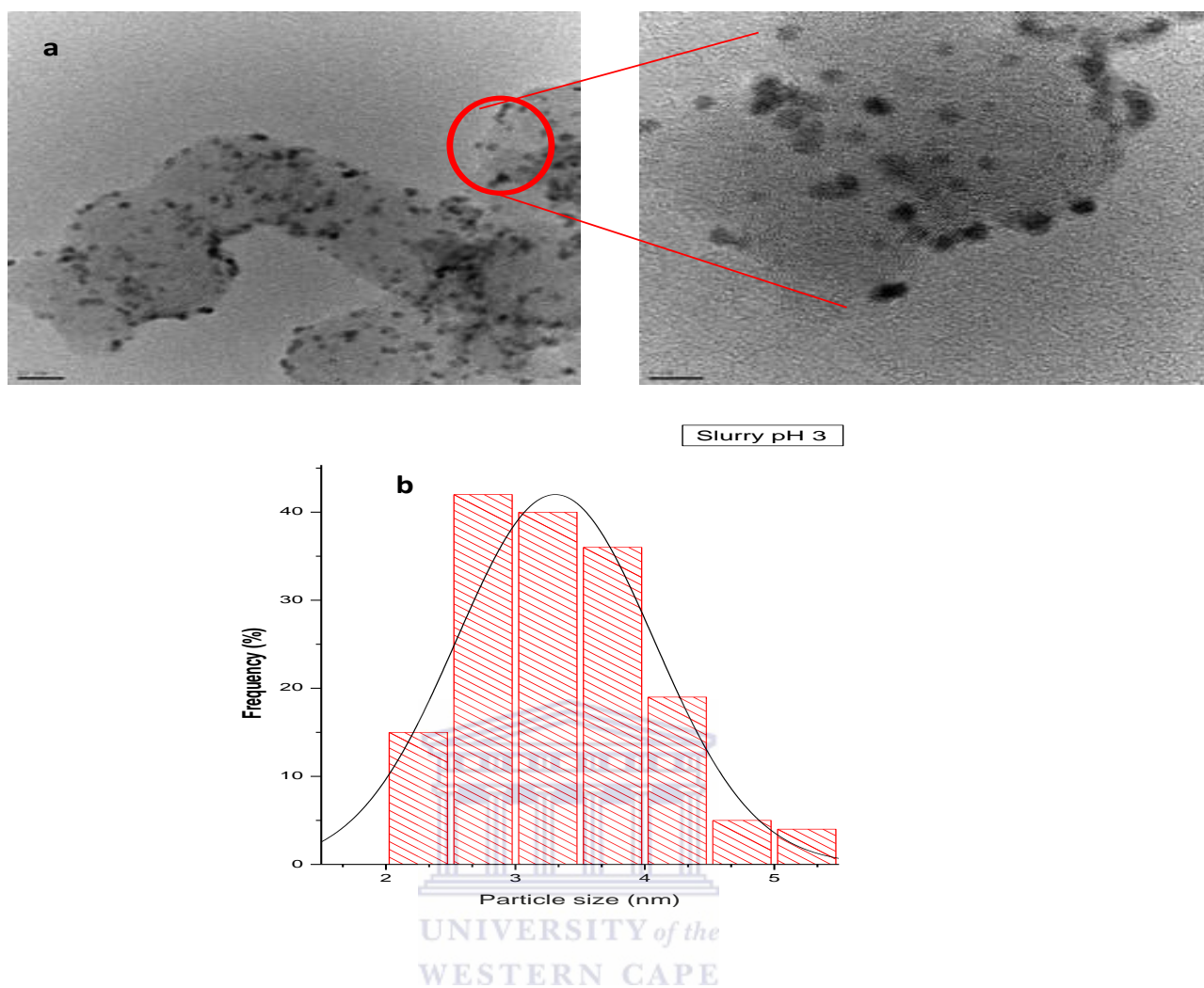


Fig 4.11 (a) Low and high magnification TEM images of Pt-Sn/C Slurry pH3, (b) histogram of particle size distribution of Pt-Sn/C Slurry pH3 catalyst.

Table 4.2 Values of lattice parameters, metal loading and particle size for Pt-Sn/C Slurry catalyst.

Catalyst	Crystallite				
	Pt ₇₅ Sn ₂₅ phase	Size	Particle Size	Sn loading	Pt loading
	Lattice parameter (nm)	XRD (nm)	TEM (nm)	(wt.%)	(wt.%)
20 % Pt/C (JM)	0.3923	3.56	3.88		20.43
PtSn\C (Slurry pH3)	0.3931	3.23	3.32 ± 0.57	8.45	18.17
PtSn\C (Slurry pH5)	0.3924	3.52	3.86. ± 0.74	8.13	12.53
PtSn\C (Slurry STD)	0.3930	3.77	3.88 ± 0.87	7.28	10.43

4.5 Metals heated first (HA Method)

In the HA method the aim was to investigate what the effect on the catalyst activity would be if the metal precursors were heated first (together or first heating the SnCl_2 and then adding the Pt salt) and then adding the carbon black after an hour. In a typical experiment the normal STD method procedure was followed but the metal precursors were firstly dissolved in EG and heated at $190\text{ }^\circ\text{C}$ for 30 -60 min under constant stirring, cooled down to room temperature while stirring before the carbon black was added and then reheated at $150\text{ }^\circ\text{C}$ for another 3 hours under nitrogen. We found that the color of the mixture changed from a slight yellowish to slight brown-blue. When SnCl_2 was heated alone first the solution turned blue indicative of colloidal tin hydroxide formation after 20 min. The slight blue color of the colloid may be due to the very small particles of tin hydroxide in the colloid. It is believed that the particles reflect different colors when the particle sizes decrease to nanometer scale. The preferred variation used for the HA method was that both metal precursors be heated together for all future syntheses. The catalysts synthesized using this variation were designated as Pt-Sn/C HA STD, HA pH5 and HA pH3 respectively.

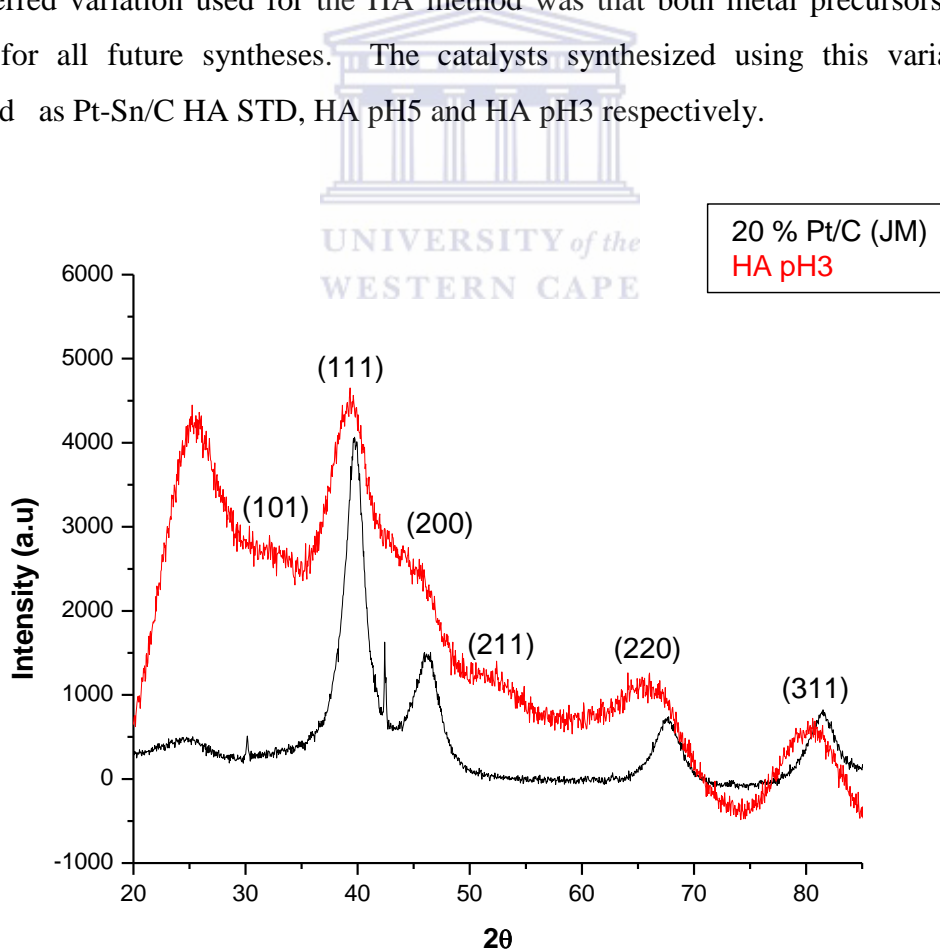


Fig. 4.12 XRD patterns of Pt-Sn/C HA pH3 compared to commercial 20% Pt/C (JM).

The XRD pattern of the as-prepared Pt-Sn/C HA pH3 catalyst was collected and is illustrated in Fig. 4.12. For the as-prepared Pt-Sn/C catalyst the diffraction peaks at around 39° , 44° , 66° - and 79° correspond to the Pt (1 1 1), (2 0 0), (2 2 0) and (3 1 1) planes respectively. Compared with the 40% Pt/C catalyst the 2θ values shift to slightly lower values confirming that the alloying process of Pt with Sn occurred, since Sn enters the *fcc* lattice of Pt. In addition, the low intensity peaks around 34° and 52° respectively can be attributed to that of the SnO₂ (1 0 1) and SnO₂ (2 1 1) diffraction peaks. These peaks are observed to be much lower in intensity than the previous catalyst (STD and Slurry method) and a reason for this could be due to the preparation method used for the nanoparticles

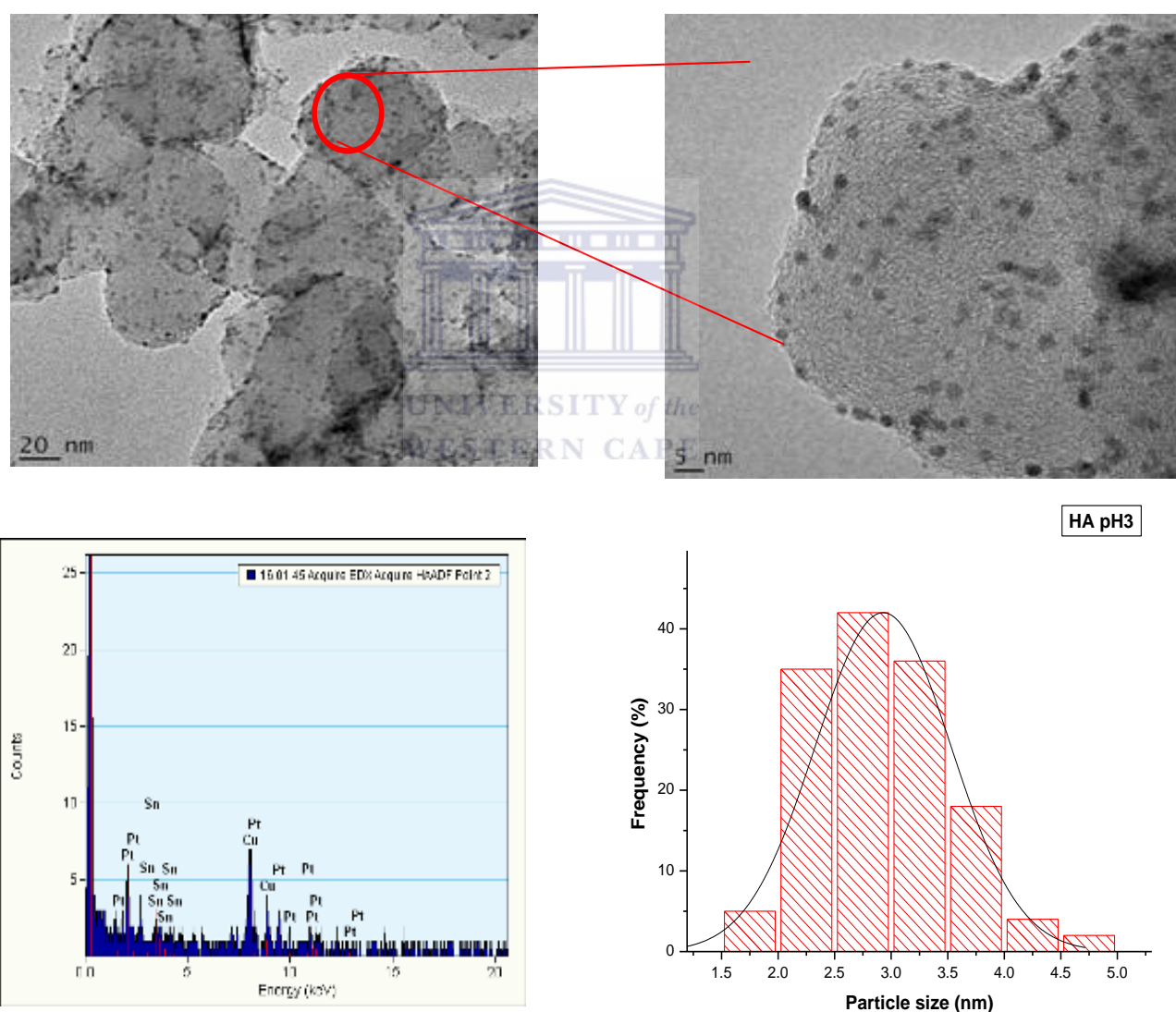


Fig. 4.13 TEM, EDX and particle size histogram of Pt-Sn/C HA pH3 catalyst.

The intensity and broad peak shapes point to a relatively close Pt-Pt distance and thus very small particle size. The primary crystallite size calculated by the Sherrer formula for Pt-Sn/C HA pH3 was about 2.9 nm. Fig 4.13 illustrates the comparison between the TEM images, the corresponding particle size distribution and EDX spectra of the as-prepared Pt-Sn/C HA pH3 catalyst. As may be noted, the nanoparticles demonstrate spherical morphology with a uniform dispersion on carbon. The Pt-Sn/C HA pH3 has a particle size of 3.02 nm \pm 0.37 with a narrow particle size distribution. The particle sizes obtained by using the HA method is summarized in Table 4.3. It was found that for the catalysts synthesized using the HA method the TEM data are satisfactorily consistent with the crystallite size obtained from the XRD data.

Table 4.3 Values of lattice parameters, metal loading and particle size for Pt-Sn/C Slurry catalysts.

Catalyst	Crystallite		Particle Size	Sn loading	Pt loading
	Pt ₇₅ Sn ₂₅ phase	Size			
	Lattice parameter (nm)	XRD (nm)			
20 % Pt/C (JM)	0.3923	3.56	3.88		20.43
PtSn\C (HA pH3)	0.3930	2.90	3.02 \pm 0.57	8.75	18.86
PtSn\C (HA pH5)	0.3927	3.25	3.39. \pm 0.43	8.13	12.22
PtSn\C (HA STD)	0.3932	3.42	3.55 \pm 0.47	7.05	9.41

4.6 Metal heated first and then carbon added in slurry form (HA Slurry method)

In this variation a combination of the Slurry and HA method was used. Both these methods showed improvements on the STD polyol method and thus it was of interest to investigate how the catalyst would perform after using these methods in their syntheses. The HA method was followed as described earlier but after an hour the carbon was added in slurry form. The advantage of using this method is that essentially the best of both worlds regarding the properties would be incorporated into the new catalysts. The catalysts synthesized using this

variation were designated as Pt-Sn/C HA Slurry STD, HA Slurry pH5 and HA Slurry pH3 respectively. The X-ray diffractograms of the Pt-Sn/C HA Slurry catalysts are shown in Fig. 4.14. As seen previously in all the other Pt-Sn/C catalysts the electro catalyst showed peaks at approximately $2\theta = 40^\circ, 47^\circ, 67^\circ$ and 81° , which are associated with the (1 1 1), (2 0 0), (2 2 0) and (3 1 1) planes respectively of the *fcc* structure of platinum and platinum alloys. The peaks associated with the SnO₂ phases were only present in the HA Slurry STD and HA Slurry pH5 catalyst and then only in low intensities. . When compared to commercial Pt/C there was a clear shift of the *fcc* peaks to lower angles for the Pt-Sn/C catalyst and this therefore implies the alloying of tin with platinum. The *fcc* lattice parameters were evaluated from the angular position of the (2 0 0) peaks and the calculated value for Pt-Sn/C HA Slurry pH3 (0.3935 nm) was larger than the one obtained for pure Pt (0.3923 nm). This is due to a lattice expansion after alloying, indicating that part of the Sn was incorporated in the *fcc* structure of Pt therefore indicating interacting between Sn and Pt. The XRD analysis implies that Pt alloyed with Sn in the Pt-Sn/C HA Slurry pH3 catalyst, while separate Pt and SnO₂ phases exist in the Pt-Sn/C HA Slurry STD and HA Slurry pH5 catalyst.

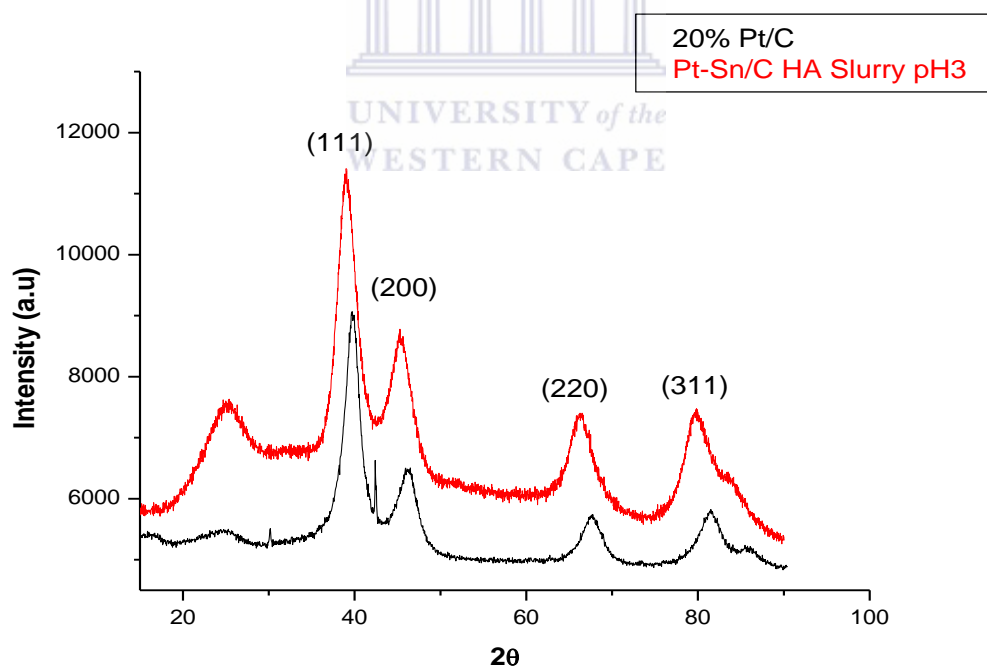


Fig. 4.14 XRD patterns of Pt-Sn/C HA pH3 compared to commercial 20% Pt/C (JM).

Table 4.4 summarizes all the physical characterization data of the as prepared Pt-Sn/C HA Slurry catalysts. The TEM photographs of Pt-Sn/C HA Slurry pH3 electro catalyst are shown in Fig. 4.15, in which the morphology and dispersion of Pt and Sn over the carbon support is

clearly illustrated. Most of the metal particles were found to be less than 3.5 nm and the nanoparticles show homogeneous dispersion with similar particle sizes. Most of the nanoparticles had a spherical shape of approximately 1.5 – 3.5 nm in size with a very sharp size distribution, which is in good agreement with the XRD results.

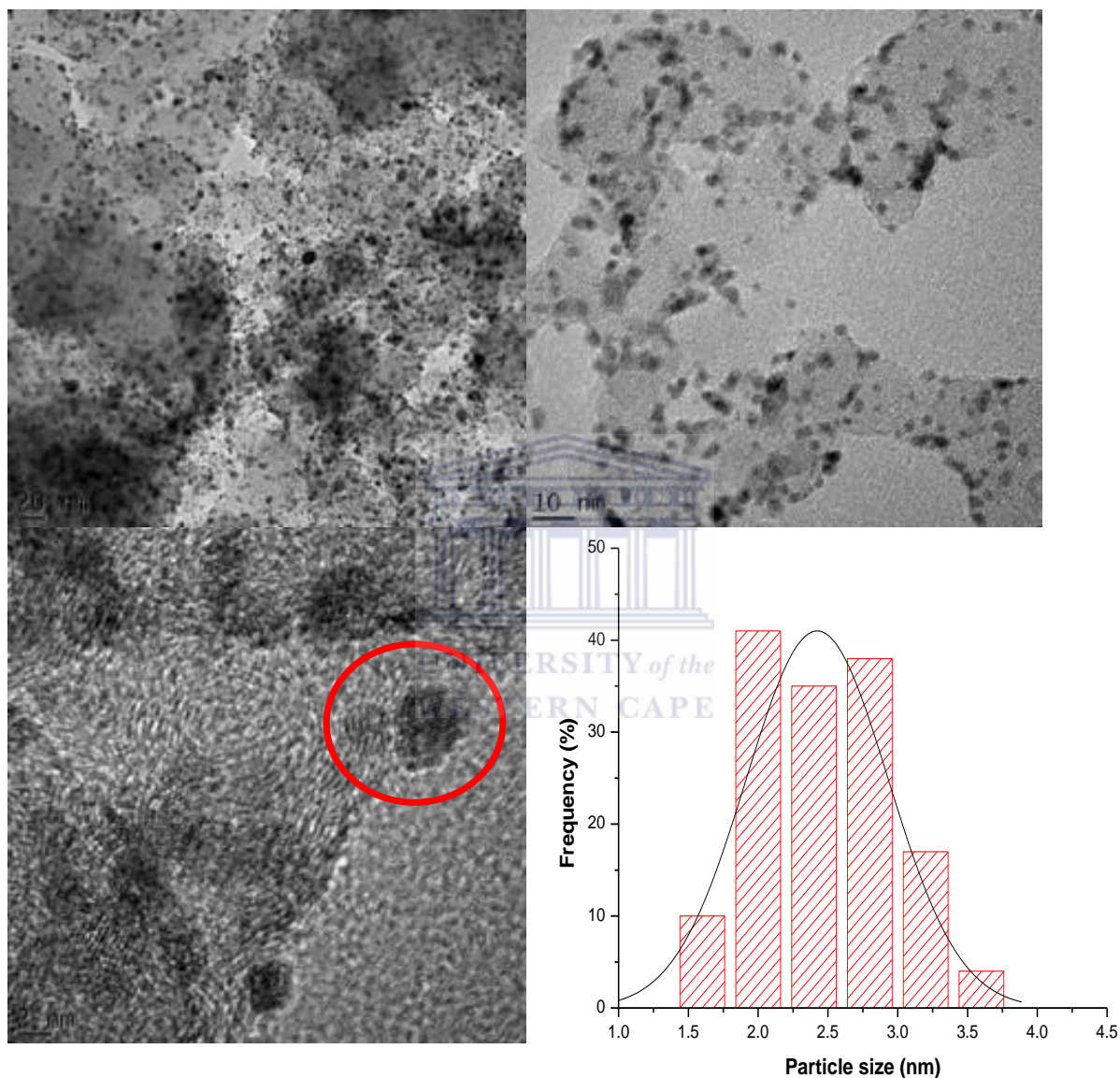


Fig. 4.15 Low and high TEM images of Pt-Sn/C HA Slurry pH3

A STEM micrograph of the as prepared Pt-Sn/C HA Slurry pH3 catalyst is displayed in Fig. 4.16a. Platinum and Sn signals were detected for a single nanoparticle in spot O₂. This means that in the as prepared catalysts, Sn and Pt nanoparticles are not separated from each other. They are alloyed but importantly, do not form a core shell structure. In STEM images Sn particles appear darker and deviate often from the spherical shape.

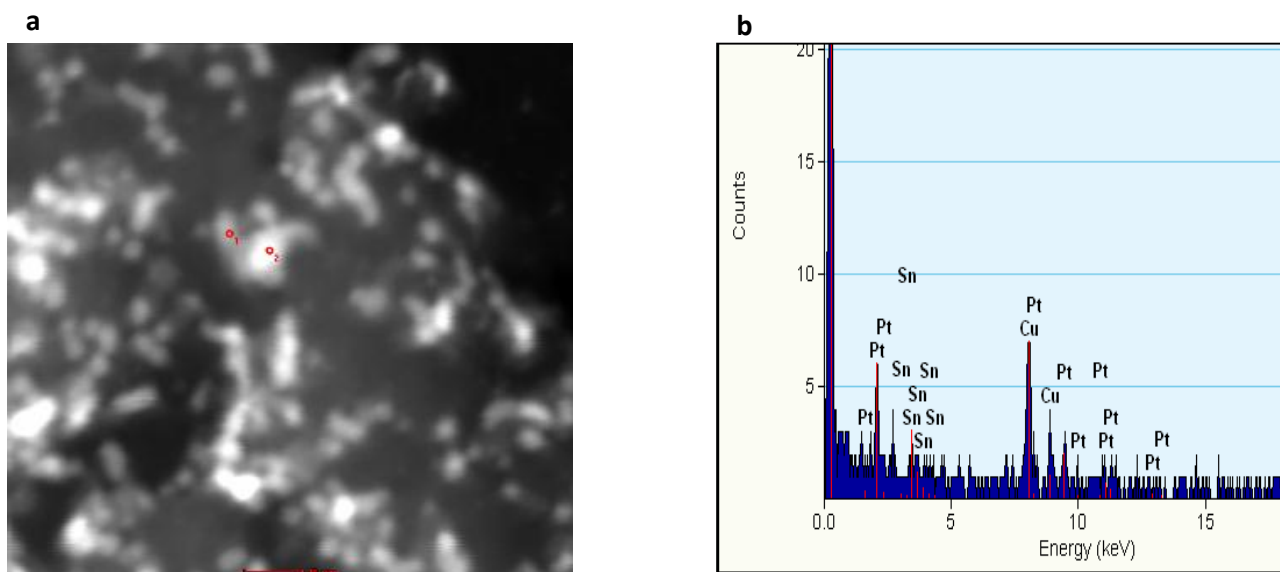


Fig. 4.16 a) HAADF-STEM image of Pt-Sn/C HA Slurry pH3 b) corresponding EDX spectra of area O₂ analyzed with STEM.

On the other hand, Pt nanoparticles appear brighter and are on average smaller than Sn particles. Finally XRD and TEM results jointly indicate that the catalysts investigated with the HA Slurry method are alloyed, have similar mean particle sizes with good dispersion and thereby demonstrating the suitability of the HA Slurry method to prepare nanometer catalysts having a high metal loading.

Table 4.4 Values of lattice parameters, metal loading and particle size for Pt-Sn/C HA Slurry catalysts

Catalyst	Crystallite			Pt	
	Pt ₇₅ Sn ₂₅ phase	Size	Particle Size	Sn loading	loading
	Lattice parameter (nm)	XRD (nm)	TEM (nm)	(wt.%)	(wt.%)
20 % Pt/C (JM)	0.3923	3.56	3.88		20.43
PtSn\C (HA Slurry pH3)	0.3938	2.30	2.49 ± 0.47	9.07	19.35
PtSn\C (HA Slurry pH5)	0.3947	2.98	3.29 ± 0.65	8.97	14.04
PtSn\C (HA Slurry STD)	0.3932	3.37	3.48 ± 0.79	7.55	10.54

4.7 Heat-treatment of Pt-Sn/C HA Slurry pH3 catalyst.

The Pt-Sn/C HA Slurry pH3 catalyst was identified as the best as prepared catalyst synthesized and was therefore chosen to undergo heat-treatment at various temperatures. It is well known that the catalyst performance strongly depends on the preparation procedure, the addition of metal precursors, the type of support as well as the heat-treatment strategy followed. Heat-treatment has been recognized as an important and necessary step for catalytic improvements of especially the cathode catalyst used to promote the ORR. Several heat-treatment techniques exist such as oven/furnace heating [10] plasma thermal heating [11] and microwave heat-treatment [12] have all been applied to prepare PEM/DMFC fuel cell electro catalysts. The most widely used of the curing techniques still remains the oven/furnace heating technique where the catalyst is heated under an inert atmosphere (Ar, He, N₂) or reducing (H₂) atmosphere in the temperature range of 100 – 900 °C for 1-4 h [13]. Heat-treatment for Pt based electro catalysts has been found to be a necessary step, which has a significant impact on the surface morphology, particle size and distribution and metal dispersion on the support. The advantages of heat-treatment are to remove any impurities resulting during the early preparation stages and to allow a uniform dispersion and stable distribution of metal on the support, and therefore, improve the electro catalytic activity [11-15]. Thus the Pt-Sn/C HA Slurry pH3 catalyst was treated at different temperatures (250 -600 °C) under an Ar atmosphere. An alumina boat was thus loaded with 50 -100 mg of catalyst and inserted into the center of a quartz tube. The tube was pre-purged with Ar for 30 min to remove any oxygen that might cause possible surface oxidation of Pt-Sn particles. The quartz tube was placed into the tube furnace which was heated to the desired temperature. Samples were heated for 4 hours under Argon and after the elapsed time were left to cool down under Ar. Fig 4.17 (a-d) shows XRD spectra of Pt-Sn/C HA Slurry pH3 heated at different temperatures. All the heat-treated catalysts showed the characteristic diffraction peaks of (1 1 1), (2 0 0), (2 2 0) and (3 1 1) associated with the *fcc* structure of Pt. The Pt-Sn alloy samples after heat-treatment were slightly shifted to higher angles with increasing temperature when compared to that of the as prepared Pt-Sn/C catalyst, hence indicating a contraction of the lattice and an insertion of smaller Sn for larger Pt particles which further supported alloy formation. The degree of angle shifting increases with increasing temperature, suggesting an increasing degree of alloying between Sn with Pt. In addition it is noticeable that the degree of crystallinity increases with increasing temperature. However, when the heat-treated catalysts were compared to that of the commercial Pt/C catalyst there

was a shift to lower 2θ angles for the heat-treated catalysts. No peaks corresponding to Sn or its oxides were observed. For the 500 and 600 °C heated catalyst several new peaks were observed as shown in Fig. 4.18. These new peaks can be attributed to the formation of the cubic $Pt_{75}Sn_{25}$ alloy phase along with hexagonal $Pt_{50}Sn_{50}$ alloy formation [1]. The average crystallite size calculated from the (2 0 0) peak showed an increase with temperature.

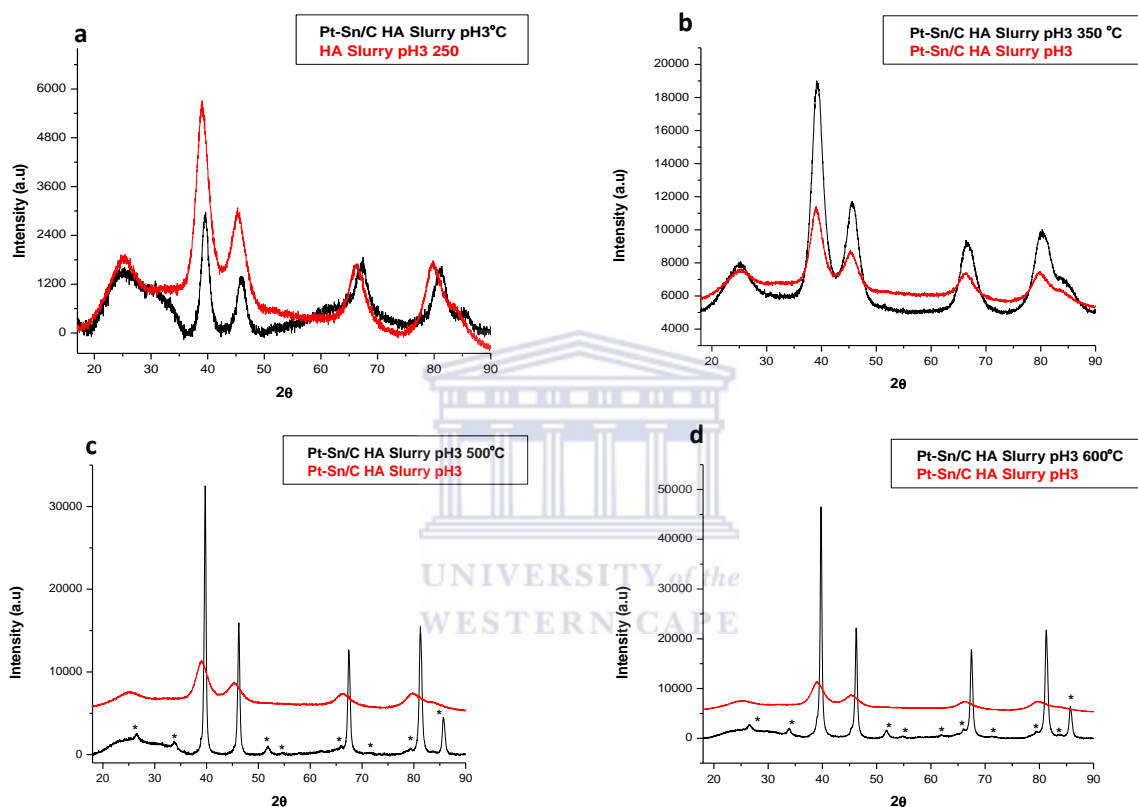


Fig 4.17 (a-d) XRD patterns of Pt-Sn/C HA Slurry pH3 showing the effect of heat treatment at different temperatures on the catalyst crystalline character.

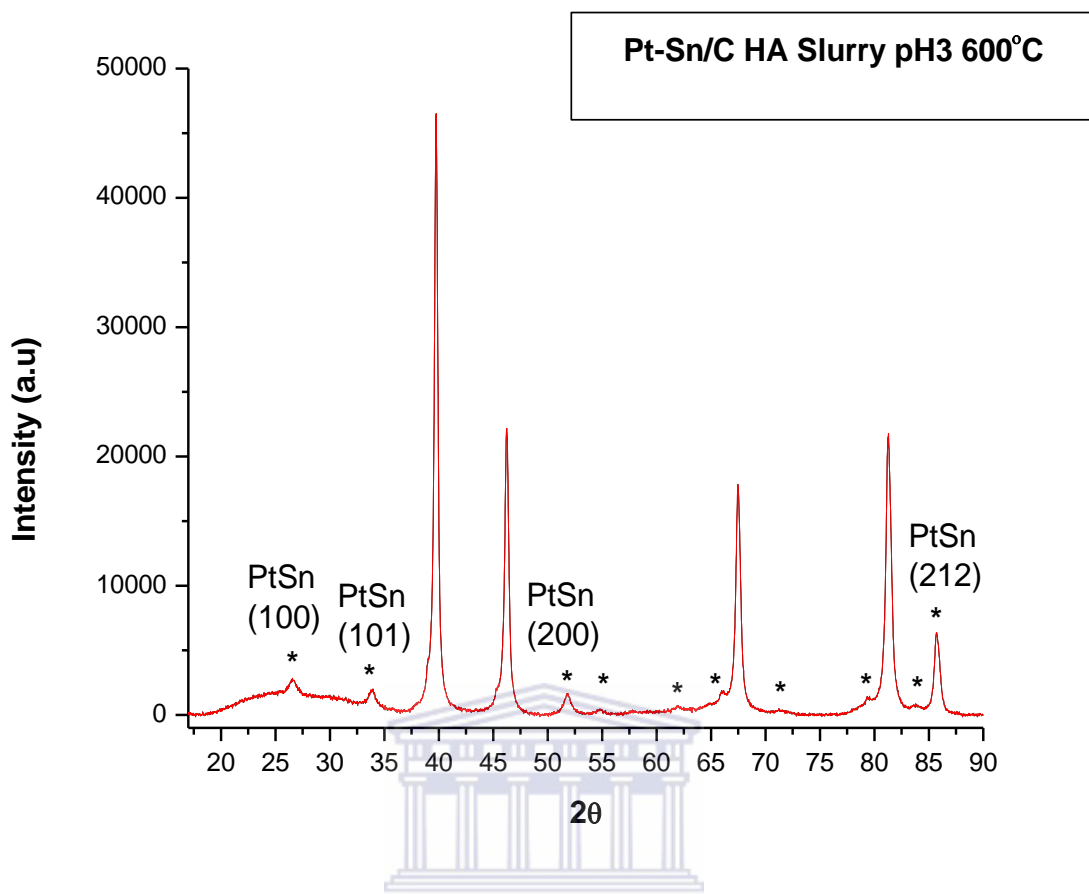


Fig. 4.18 XRD pattern of Pt-Sn/C HA Slurry pH3 heated at 600 °C indicating some of the new peaks formed due to heat-treatment.

Fig. 4.19 presents the TEM images of the heat treated Pt-Sn/C catalysts at 250 and 350 °C. Spherical shaped Pt-Sn nanoparticles on the carbon support with uneven particle sizes can be seen for both catalysts. The particle sizes obtained by TEM are given in Table 4.5. Heat treatment has a big effect on the particle size and particle size distribution. For the Pt-Sn/C 250 °C the particles were generally between 2.3 to 10 nm with an average particle size of ca. 5.2 nm. When compared to the particle size for the as-prepared Pt-Sn/C HA Slurry pH3 (which was 2.5 nm), an increase in particle size of over 50% was found for the Pt-Sn/C catalyst heated at 250 °C. When heat treating catalysts at high temperatures the particles tend to agglomerate. For both catalysts only small portions of agglomeration were visible. However, it was observed that heat-treatment had no negative impact on the overall metal loading on all the catalysts as seen in Table 4.5.

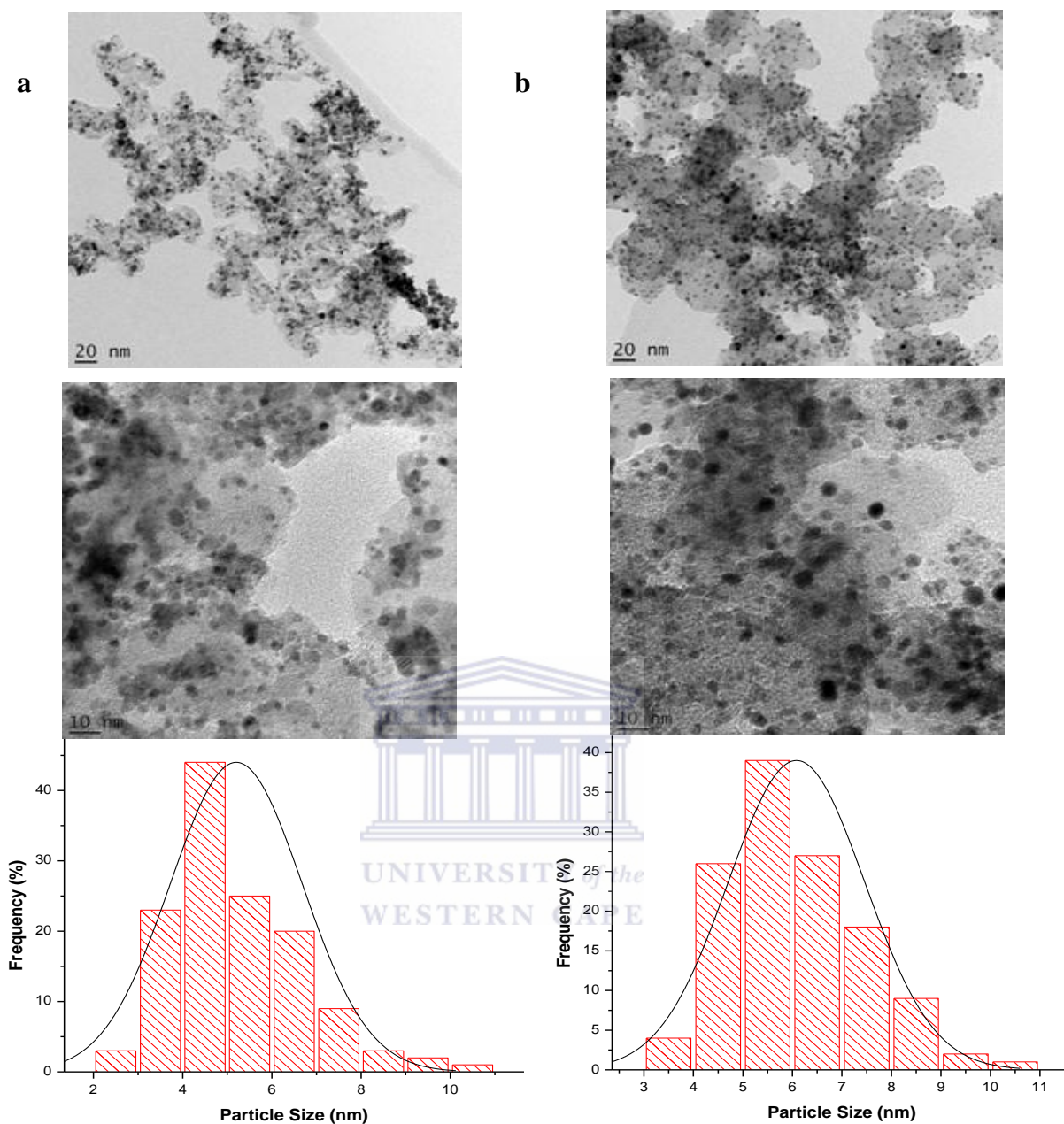


Fig. 4.19.(a) Low and high TEM images of Pt-Sn/C HA Slurry pH3 250 °C and corresponding particle size distribution histogram (b) Low and high TEM images of Pt-Sn/C HA Slurry pH3 350 °C and corresponding particle size distribution histogram.

The catalysts heated at 500 °C led to particle agglomeration and an increase in particle size when compared to catalysts heated at lower temperature as seen in Fig. 4.20.

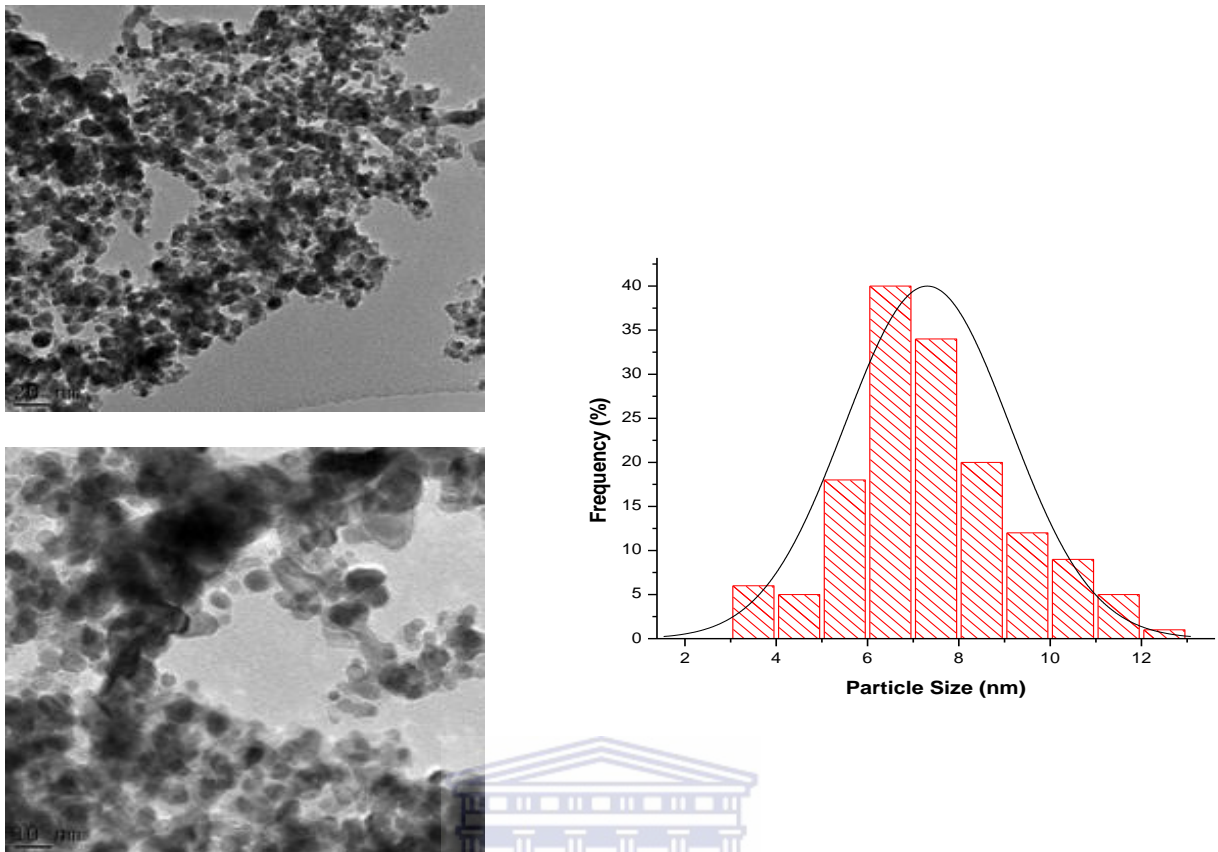


Fig 4.20. Low and high TEM images of Pt-Sn/C HA Slurry pH3 500 °C and corresponding particle size distribution histogram.

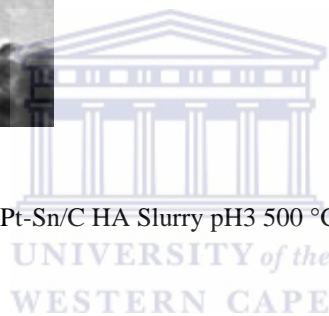


Fig 4.21 illustrates the Pt-Sn/C HA Slurry pH 3 600 °C catalyst. The nanoparticles are uniformly dispersed on the carbon support with very little particle agglomeration found. The catalyst had a very wide particle size distribution and a average particle size of ca. 8.68 nm. The catalysts heated at 600 °C shows the crystal lattice fringes of the Pt-Sn nanoparticles marked. It was observed that with increasing temperature the amount of particles showing the crystal lattice fringes increased when studied under high magnification with TEM. As the temperature increased the crystal lattice fringes of the Pt-Sn nanoparticles became visible at lower magnification indicating an increase in crystallinity of the catalysts. From the TEM images we can conclude that the degree of crystallinity increases with increasing temperature and this data corresponds well with the XRD where the intensity of the diffraction peaks of the different Pt phases increased with increasing temperature.

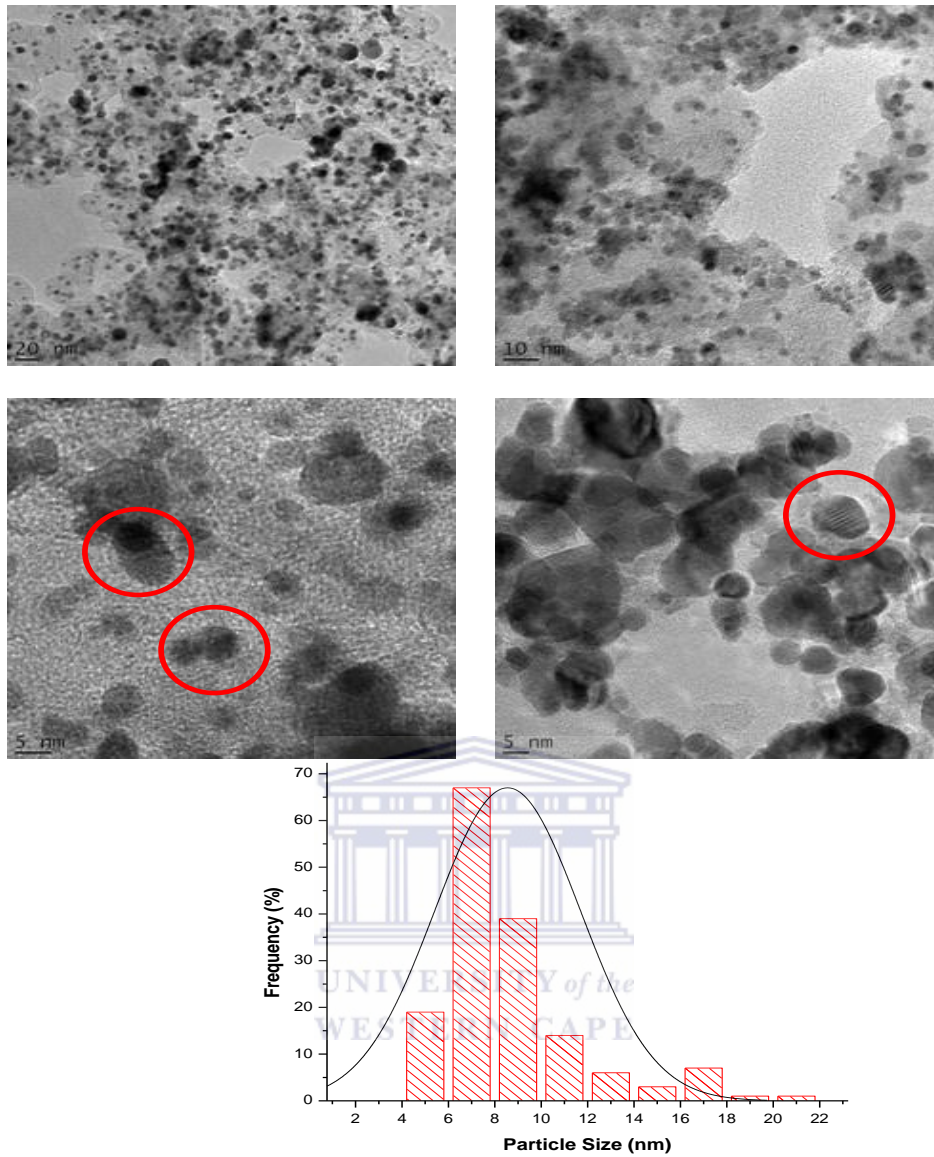


Fig. 4.21 Low and high TEM images of Pt-Sn/C HA Slurry pH3 600 °C indicating crystal lattice fringes and corresponding particle size distribution histogram.

Table 4.5 Values of lattice parameters, metal loading and particle size for Pt-Sn/C HA Slurry catalysts heated at different temperatures.

Catalyst	Crystallite			Sn loading (wt.%)	Pt loading (wt.%)
	Pt ₇₅ Sn ₂₅ phase	Size	Particle Size		
	Lattice parameter (nm)	XRD (nm)	TEM (nm)		
20 % Pt/C (JM)	0.3923	3.56	3.88		20.43
PtSn\C (HA Slurry pH3)	0.3938	2.30	2.49 ± 0.47	9.07	19.35
PtSn\C (250 °C)	0.3959	5.06	5.2 ± 1.44	9.32	18.87
PtSn\C (350 °C)	0.3950	6.02	6.08 ± 1.86	9.02	19.24
PtSn\C (500 °C)	0.3947	7.74	7.34 ± 2.64	8.78	19.22
PtSn\C (600 °C)	0.3941	9.05	8.68 ± 3.59	8.65	19.03

4.8 Comparison of Pt-Sn/C with other Pt-Sn/C catalysts used as cathode catalyst.

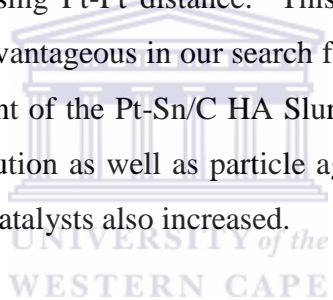
As mentioned earlier, the literature has many reports where Pt-Sn/C catalysts have been used as anode catalysts for MOR or EOR applications. However, only a few reports are available where the Pt-Sn/C or Pt-SnO_x/C systems have been used as cathode catalysts or where SnO_x has been used as support as an electrocatalyst for the cathode electrode. Table 4.6 shows data for these findings compared with the data of our in-house Pt-Sn/C catalysts. Comparison of our in-house catalysts on the basis of physical characterization to those synthesized by the group of Jeyabharathi [1] revealed that our in-house Pt-Sn/C catalysts were superior in many ways. In the first place our catalysts all had a smaller particle size, demonstrated small portions of agglomeration and had a narrower particle size distribution. Furthermore, our catalysts were comparable to those synthesized for DEFC applications which indicate that our modified polyol method is quite suitable for the synthesis of Pt-Sn nanoparticles with small particle sizes. A comparison of the electrochemical properties of the different Pt-Sn/C catalysts will be reported in the following chapter.

Table 4.6 Comparison of different Pt-Sn/C catalyst physical properties used for fuel cell applications

Catalyst	Method of preparation	Crystallite size (nm)	Particle size (nm)	Reference
Pt-Sn/C	Polyol	5.79	6 ± 0.6	Jeyabharathi <i>et. al.</i> , 2008
Pt-Sn/C 250 °C	Polyol	5.63	5 ± 0.7	Jeyabharathi <i>et. al.</i> , 2008
Pt-Sn/C 500 °C	Polyol	16.68	6. ± 0.9	Jeyabharathi <i>et. al.</i> , 2008
Pt-Sn/C 600 °C	Polyol	20.73	-	Jeyabharathi <i>et. al.</i> , 2008
Pt-Sb- SnO ₂	Polyol	3.5	2.5	You <i>et.al.</i> , 2009
Pt-SnO _x /C	NaBH ₄ Reduction	-	-	Parrondo <i>et. al.</i> ,2010
Pt-Sn/C (3:1)	Carbonyl complex route	2.4	3.1± 1.6	Boucher <i>et. al.</i> ,2003 used in DEFC
Pt-Sn/C (4:1)	Polyol	1.6	2.2 ± 0.6	Jiang <i>et.al.</i> , 2007 used in DEFC
Pt-Sn/C (3:1)	Polyol	2.0	2.6 ± 0.5	Jiang <i>et.al.</i> , 2007 used in DEFC
Pt-Sn/C	Polyol	2.3	2.49 ±0.47	This work
Pt-Sn/C 250°C	Polyol	5.06	5.20 ±1.44	This work
Pt-Sn/C 350°C	Polyol	6.02	6.08 ±1.86	This work
Pt-Sn/C 500 °C	Polyol	7.74	7.34 ±2.64	This work
Pt-Sn/C 600 °C	Polyol	9.05	8.68 ±3.59	This work

4.9 Conclusions

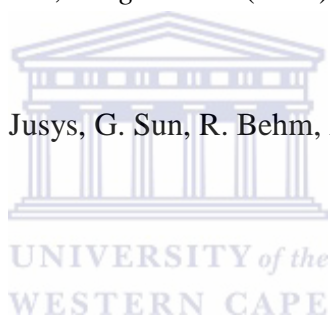
Pt-Sn/C catalysts were synthesized using a modified polyol reduction method employing sonication and using HCl as sedimentation promoter. The average particle size distributions were found to be in the range of 2.3 – 4 nm for the different *as*-prepared catalysts from HR-TEM results. 2θ values shifted to lower angle values in the XRD confirming that the alloying process between Sn and Pt had indeed occurred. Of the twelve catalysts studied the Pt-Sn/C HA Slurry pH3 was identified as the best *as*-prepared catalyst. The pH adjustment step had the benefit of an increase in metal loading of 30-45% and importantly, without affecting the particle size. This result is attributed to a change of electrostatic forces. Pt-Sn/C HA Slurry pH3 catalysts were subjected to curing by heat-treatment in order to study the changes on the morphology and physical properties of the catalyst. The lattice parameter value of the heat-treated catalysts increased with increasing temperature when compared to that of Pt/C ($a_0 = 0.3923$ nm) indicating an increasing Pt-Pt distance. This increased Pt-Pt distance for the heat-treated catalysts could be advantageous in our search for a methanol tolerant catalyst for DFMC application. Heat treatment of the Pt-Sn/C HA Slurry pH3 led to increase in particle size, broader particle size distribution as well as particle agglomeration. As the temperature increased the crystallinity of the catalysts also increased.



REFERENCES

1. C. Jeyabharathia, P. Venkateshkumarb, J. Mathiyarasua, K.L.N. Phania, *Electrochim. Acta* 54 (2008) 448
2. B. He, Y. Chen, H. Liu, Y. Liu, *J. Nanosci. Nanotechno.* 5 (2005) 266
3. R.W. Pekala, S.T. Alviso, X. Lu, J. Gross, J. Fricke, *J. Non-Cryst. Solids* 188 (1995) 34
4. Y. Takasu, T. Kawaguchi, W. Sugimoto, Y. Murakami, *Electrochim. Acta* 48 (2003) 3861
5. W. Li, W. Zhou, Li. H, Z. Zhou, B. Zhou, G. Sun, Q. Xin, *Electrochim. Acta* 49 (2004)
6. C. Lim and C.Y. Wang, *J. Power Sources* 113 (2003) 145
7. H.S. Oh, J.G. Oh, Y.G. Hong, H. Kim, *Electrochim. Acta* 52 (2007) 7278–7285.
8. R.J Hunter, *Zeta potential in Colloid Science*, Academic Press, UK, 1981
9. J. Zhao, W. Chen, Y. Zheng, X. Li, Z. Xu, *J Mater Sci* 41 (2006) 5514–5518
10. L. Jiang, G. Sun, Z. Zhou, S. Sun, Q. Wang, S. Yan, H. Li, Q. Xin, *J. Phys. Chem. B* 109 (2005) 8774
11. G. Yu, Weixiang, J. Zhao, J. Qiulin, *J Appl. Electrochem.* 36 (2006) 1021
12. S.J Mujerkee, *App. Electrochem.* 20 (1990) 537

13. H. Liu, C. Song, Y. Thang, J. Zhang, *ElectrochimicaActa* 52 (2007) 4532
14. M. Nie, P.K Shen, M. Wu, Z. Meng, *J. Power Sources* 162 (2006) 173
15. C. Bezerra, L. Zhang, H. Liu, K.Lee, A.L Marques. H.Wang, J. Zhang, *J. Power Sources* 173 (2007) 891
16. J. Parronhoa, F. Mijangos, B. Rambabu,*J Power Sources* 195 (2010) 3977
17. D. You, K. Kwon, H. Pak, *Catal. Today* 146 (2009) 15
18. A.C Boucher, N. Alonso-Vante, *Langmuir* 19 (2003) 10885
19. L. Jiang, L. Colmenares, Z. Jusys, G. Sun, R. Behm, *Electrochim. Acta* 53 (2007) 377



Chapter 5

Results and Discussions II

Electrochemical Characterization of Pt-Sn/C electrocatalysts

5.1 Introduction

The structural and physical properties of the Pt-Sn/C catalysts were presented in Chapter 4. The electrochemical characterization of prospective methanol tolerant Pt-Sn/C catalysts and their comparison to the commercial Pt/C (*HiSPEC3000*, *HiSPEC4000* JM and TEC10V50E form TKK) is presented in this Chapter. The Pt-Sn/C electrocatalysts prepared as mentioned in the previous chapter were electrochemically characterized in a half-cell configuration using different electrolytes to determine their electrochemical surface areas, measure their catalytic activity towards the ORR, investigate their resistance towards MOR and their durability for possible use in a DMFC. The subsequent electrochemical properties can be correlated to the physical properties of the catalysts established in the previous chapter.

5.2 Test protocol for the electrocatalyst

Prior to electrochemical characterization of commercial and in-house prepared catalysts, it was important to design the appropriate electrochemical experiments needed to attain relevant results of the catalysts that were both reproducible and accurate. For this reason different parameters such as electrode preparation, catalyst loading and experimental setup were investigated before electrochemical characterization commenced. For EC characterization two methods were used for the preparation of the electrode. The first approach was to specially design an EC cell that could accommodate the fabricated electrode. The cell had to accommodate purging by various gasses, be completely sealed from external contaminants which could negatively influence the results and also be temperature controlled if necessary. The electrode for this cell was not the conventional GC electrode which is normally used for CV studies but rather an electrode fabricated from highly conductive carbon paper, similar to the carbon paper used in a fuel cell for the MEA. The catalyst ink was prepared by dissolving 25 mg catalyst in 10 ml isopropanol, 100 mg water and sonicated for 45 minutes. To the ink 75 mg 5 wt.% Nafion was added sonicated for a further 30 minutes

before a specific amount of catalyst was sprayed onto the carbon paper with a hand spray gun. A round hole counter (10 mm in diameter, $A_g = 0.786 \text{ cm}^2$) was then used to press out the working electrode. The advantage of using the in-house EC cell is that the working electrode was always fixed at the same position and the counter and reference electrode were inserted in a special fitting for the B14 opening to ensure that the electrodes were kept intact at the same position for every experiment. Figure 5.1 shows a picture of the in-house EC cell as well as the electrodes prepared from the carbon paper. Another advantage of the in-house EC cell setup was that when doing RDE on a GC where O_2 is supplied to the electrode surface through rotation of the electrolyte ensuring fresh reactants reach the electrode surface, the in-house EC cell allows for the O_2 to be fed directly to the surface of the electrode through its unique design. The Teflon holder of the electrode has a special stainless steel tube fitted from the fabricated electrode.

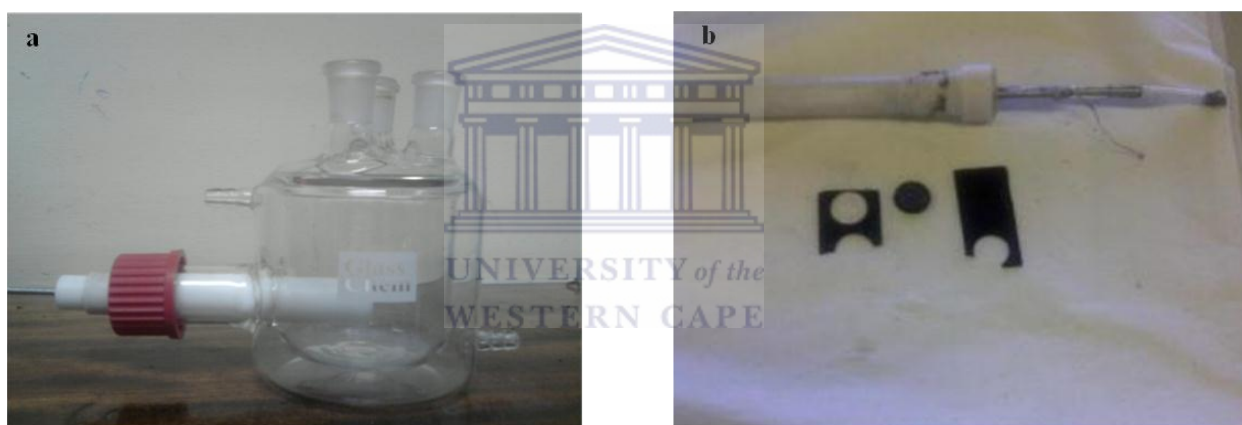


Fig. 5.1(a) In-house EC cell (b) electrodes fabricated for the EC cell by spraying on Torai carbon paper.

This allows for “true” ORR results obtained due to the fact that the EC cell resembles conditions the actual catalysts would be exposed to in a fuel cell when a MEA is tested. However, upon further investigations a problem arose when the catalysts activity towards oxygen needed to be investigated. In our EC cell the carbon sprayed working electrode was kept fixed in a stationary position so the EC cell was not fitted for an electrode rotation feature needed to extract important catalyst activity information. Therefore with our EC cell it was not possible to gain kinetic information regarding KL-plots, number of electrons transferred in ORR and Tafel data which is important information regarding catalyst activity which would be otherwise possible if a RDE was used. Although the in-house EC cell gave satisfactory results for CVs (Fig. 5.2) to calculate ECSA values and MOR data, the EC cell

had limitations when compared to the GC RDE. The catalysts in this study were characterized (for CVs, MOR and ORR) by using a GC electrode by drop-casting the catalyst ink on the electrode surface to achieve a homogeneous film that covers the entire electrode area as explained previously in chapter 3.

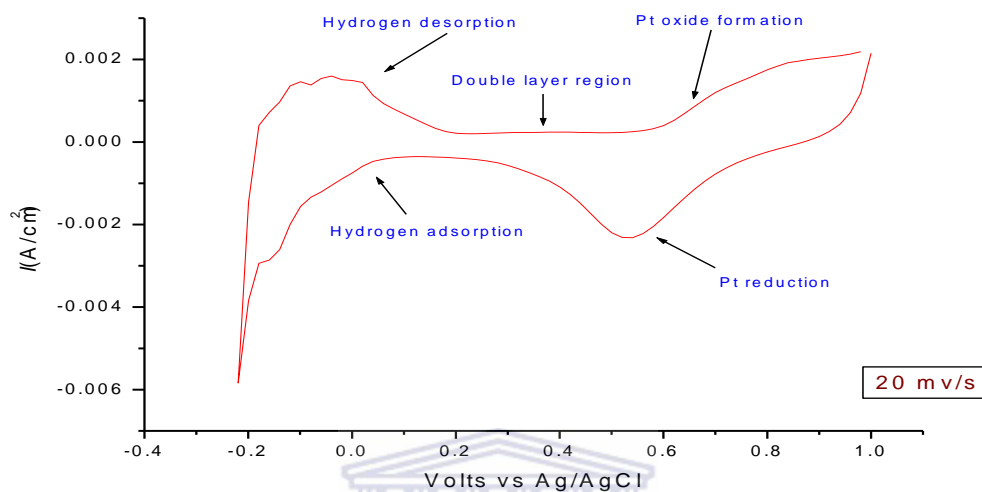


Fig. 5.2 CV of Pt/C using the EC cell and modified Teflon electrode for catalyst testing [1]

5.3.1 Electrochemical method validation of Pt disc.

Prior to conducting experiments with supported Pt catalysts, the CV, MOR and RDE methods were validated using a polycrystalline Pt disc. A 3 mm Pt disc electrode ($A_g = 0.07 \text{ cm}^2$) was polished to a mirror finish with different grades of alumina. It was further washed with ultra pure water and sonicated for 2 minutes to remove any residual alumina.

5.3.2 Electrochemical Surface Area (ECSA)

A typical CV scan recorded in the anodic direction at a polycrystalline Pt surface in acid medium is shown in Figure 5.3. The peaks in this picture are labeled in their order of appearance with increasing potential. At cathodic potentials (0 - 0.3 V), reversible H_a peaks due to the adsorption and desorption of hydrogen on different crystallographic planes of the Pt surface are observed (region 1). The following flat plateau can be attributed to the double layer region during which water is adsorbed on Pt (region 2). Increasing anodic potentials

results in the formation of O_A peaks indicative for the formation of different Pt oxides (region 3). In the reverse scan Pt oxides are reduced during a unique and irreversible process [2,3].

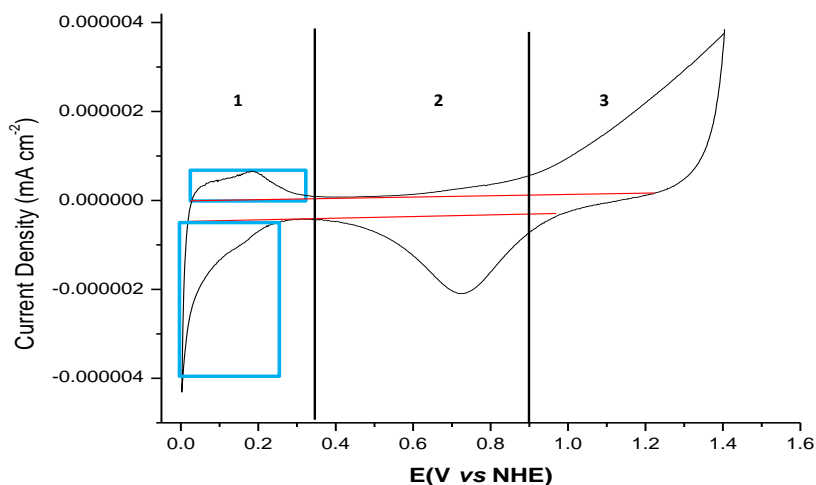


Fig. 5.3 Typical CV for a Pt electrode showing H desorption/adsorption region. The red lines are baselines set so as to eliminate contributions to current from charge/discharge of the electrochemical double layer (Coulombic current).

The ECSA was measured by integrating the shaded area found on the CV shown in Fig.5.3 by using equation 3.3 For the 3 mm Pt disc, the ECSA measured was $0.043 \pm 0.002 \text{ cm}^2$.

5.3.3 Methanol oxidation reaction (MOR)

A typical CV for methanol electro-oxidation on Pt is shown in Figure 5.4 ; its unusual shape can be explained when looking at the different surface transitions that occur at Pt (see above), and from which it can be concluded with some simplification that methanol oxidation only occurs on Pt^0 surfaces when water is activated [4]. Data describing the electrocatalytic properties of Pt and Pt-based surfaces, such as the maximum oxidation current density or the onset of oxidation, were extracted from these experiments. For the 3 mm Pt electrode the oxidation current density was 0.103 mA cm^{-2} at $+0.83 \text{ V vs NHE}$.

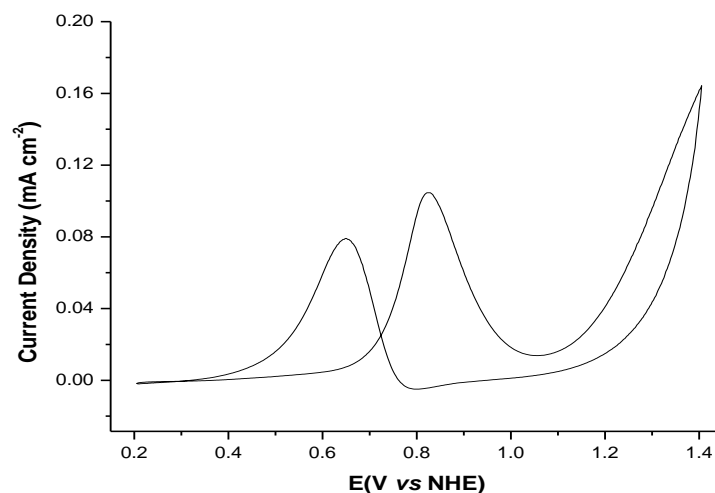


Fig. 5.4 CV for methanol oxidation at Pt electrode in 0.5 M H₂SO₄ + 0.5 M MeOH at 20 mV s⁻¹.

5.3.4 Oxygen reduction reaction (ORR)

In the measurement of electrocatalyst activity our aim was to obtain a value for the synthesized Pt catalyst activity that is as free as possible from mass-transport effects. To obtain an accurate value of the catalyst's activity it was important to measure the current in a regime where ORR kinetics dominate and any other factors present (mass-transport) can be calculated and used to make corrections to obtain the precise kinetic current i_k . Fig. 5.5 shows the methodology used for measuring and analyzing the ORR activity of Pt-based catalysts. This method involves acquiring linear sweep voltammograms (LSVs) under O₂ at different rotation speeds. The scan rate selected for all ORR experiments was 5 mV s⁻¹. A background scan using N₂ purged electrolyte instead of O₂ was carried out before ORR experiments were performed and subtracted from O₂ I-V curves to eliminate and correct for the effect of pseudo-capacitive currents. The current is measured during an anodic scan rate (0 to +1.0 V vs NHE) at various rotation speeds. The direction of the sweep is important since during a cathodic scan (+1.0 - 0.V) the Pt surface is covered in adsorbed oxide species which decrease the ORR rate [5-7].

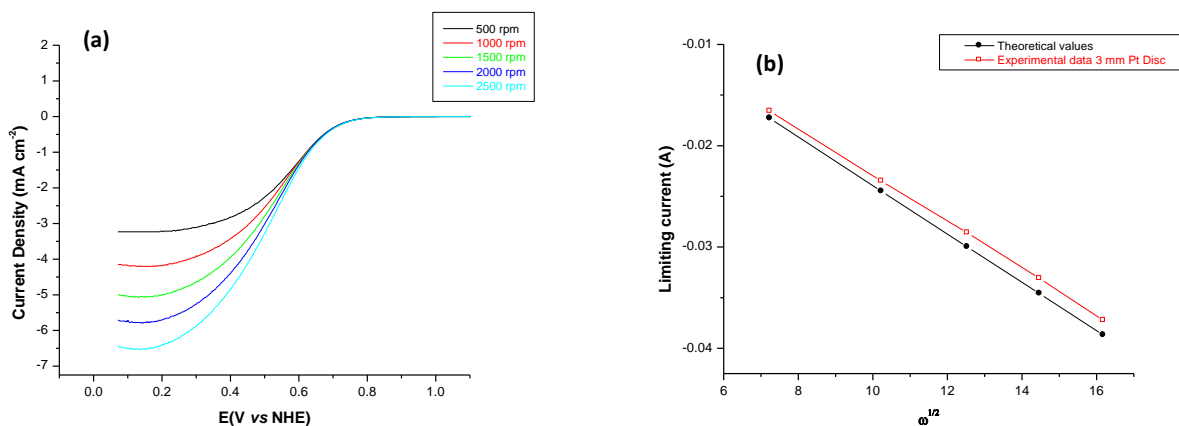


Fig. 5.5 (a) Polarization curves recorded in O₂ saturated electrolyte on Pt electrode (b) Levich plot demonstrating linear dependence of limiting current on and theoretical values for i_{lim}

The Levich plot in Fig. 5.5 (b) shows a linear relationship between the limiting current for the Pt electrode measured at ca.+0.1 V vs NHE and the square root of the rotation rate $\omega^{1/2}$ as predicted by the Levich equation. The experimental data correspond well with the theoretical values. Using the slope, the O₂ diffusion coefficient was calculated experimentally by using the values in Table 5.1 [2,7]. The experimental O₂ Diffusion coefficient calculated for the Pt electrode was $1.25 \times 10^{-5} \text{ cm}^2 \text{ s}^{-1}$, which is in reasonable agreement with the accepted value of $1.4 \times 10^{-5} \text{ cm}^2 \text{ s}^{-1}$ [5]

Table 5.1 Parameters in the Levich equation.

Levich Equation	$I_{lim} = 0.62nFCD^{2/3}v^{-1/6}\omega^{1/2}$
Faraday Constant F	94685 C mol^{-1}
Concentration O ₂	$1.1 \times 10^{-6} \text{ mol cm}^{-3}$
Kinematic viscosity ν H ₂ O	$0.01 \text{ cm}^2 \text{ s}^{-1}$
O ₂ Diffusion coefficient D for 0.5 M H ₂ SO ₄ (25°C)	$1.4 \times 10^{-5} \text{ cm}^2 \text{ s}^{-1}$
Number of electrons n	4

The small difference is probably due to the cell not being fully sealed off from the atmosphere. On completion of the CVs, I-Vs and background experiments we plot i^{-1} vs $\omega^{-1/2}$ (Koutecky-Levich or K-LPlot) as shown in Fig 5.6. The intercept extrapolated to infinite rotation speed is then extracted and finally a plot of $\log i_k$ vs V , known as the Tafel plot, is derived.

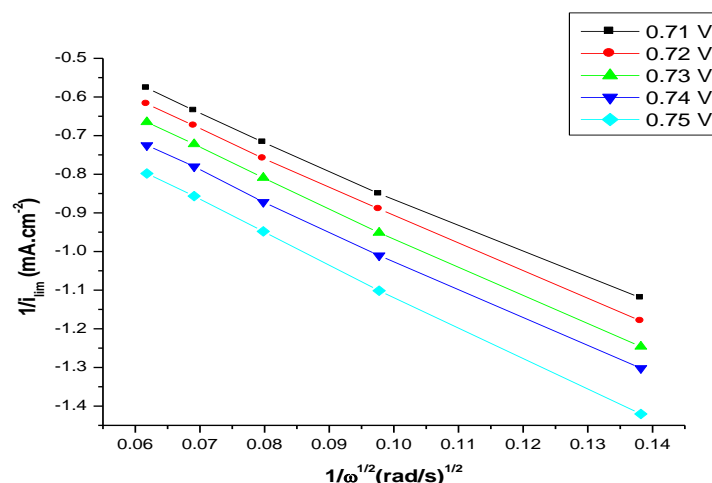


Fig. 5.6 K-L Plots used to calculate i_k from intercept and number of electrons from the slope.

The K-L Plots shown are linear over the range of rotation rates used indicating mixed kinetic–diffusion control with a very slow electron transfer. From the slopes of the K-L plots the number of electron was calculated [2,5]. The values for n were constant over the potential range of 0.65 – 0.75 V with $n = 3.82$. The Tafel slope was found to be around -60 mV dec^{-1} and -120 mV dec^{-1} for lower potentials. These values are in good agreement with previous work done [7]. However, there are still several controversies regarding reporting the Tafel slope in the high current density regime which researchers refer to as the “double Tafel regime.” From the Tafel graphs the exchange current densities (i_0) are the most fundamental intrinsic kinetic parameter and these values can only be obtained by extrapolating the measured currents over *ca.* four orders of magnitude, which may result in large errors on the obtained values [7].

Table 5.2 Electrochemical parameters found for crystalline Pt electrode.

3 mm Pt electrode	
ECSA	0.043 cm ²
MOR	0.103 mA cm ⁻² @ +0.82 V vs NHE.
Tafel slopes	-60 /-120 mV dec ⁻¹
SA@ 0.75 V	9.14μA cm _{Pt} ⁻²
Number of electrons	3.82

It has therefore become something of a convention to report specific activities i_s (SAs) and the mass activities i_m (MA) for Pt/C catalysts from ORR activity at +0.85 or +0.9V vs NHE instead of the exchange current densities (i_0) [5-7]. By doing so the data can be measured and reported with no extrapolation required. Table 5.2 summarizes all the kinetic data for the 3 mm Pt electrode obtained during the method validation test. We can therefore conclude the validity of the RDE method used on the Pt disc and will be used when performing RDE studies on thin-films.

5.4 Electrochemistry studies of commercial Pt/C thin-films

For this study different commercial Pt/C catalysts supplied by Johnson Matthey UK and Tanaka Kikinzoku Kogyo (TKK Japan) were used as benchmark. Numerous reports are available were the catalytic activities of these state of the art Pt/C were tested, many of which are in good mutual agreement [7]. However there are still several controversies regarding certain data published in literature by different groups and it was therefore important to validate the commercial Pt/C using our method and then to compare the synthesized Pt-Sn/C catalysts against it. All electrodes prepared in this study were done by using the drop-casting method followed by drying under an infra red lamp for 1 hour or in a vacuum oven at max 35 °C for 30 min. However the films produced by this method were found to vary in their performance as the quality of the film was dependant on several factors such as Pt dispersion, ink formulation, drying conditions and GC surface [6]. It was also observed that when dropping the required amount of catalyst ink on the electrode, better results were achieved when all the ink was deposited on the electrodes at once and left to dry rather than dropping the ink on the electrode bit by bit and then left to dry in between. A small ink quantity (10 μ l) was chosen to achieve a uniform disperse film with a Pt loading of 20 μ g_{Pt} cm⁻². It's been reported that when larger quantities of ink are used it leads to complications when doing calculations, thereby producing incorrect data. This was also done to avoid excessive mass-transport losses in overlay thick catalysts agglomerates deposited on the RDE [6,7]. Each experiment was carried out in triplicate with a new electrode to eliminate bad results due to bad films. A difference of up to 25% in ECSA values were found for a bad film compared with a good film prepared for an experiment with the same catalyst ink. The ECSA for 20% Pt/C (JM) was 53.98 m²g_{Pt}⁻¹, for 40% Pt/C 56.08 m² g_{Pt}⁻¹ and 68.21 m² g_{Pt}⁻¹ for TKK. Figure 5.7 shows the CVs of the 3 mm Pt electrode and the GC modified thin -film electrode for commercial 20% Pt/C. It is evident that by modifying the GC electrode with Pt/C catalyst an

increase in ECSA was observed when compared to the blank Pt electrode which indicates that Pt/C might be a very active electrocatalyst.

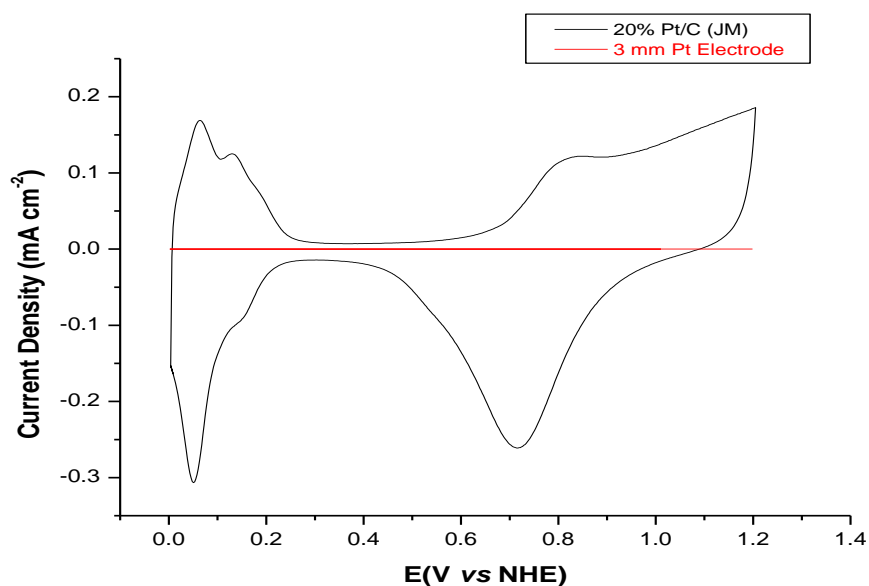


Fig. 5.7 CV for 3 mm Pt electrode 20 wt.% Pt/C commercial catalysts showing the difference in ECSA.

For high quality ORR measurements a uniform thin film was required that covers the entire surface area of the GC electrode. ORR measurements for Pt/C thin-films were carried out using a RDE in 0.5 M H₂SO₄ saturated with O₂ as described in chapter 3. However, when doing RDE studies on thin-films the measurement of the solution resistance was found to be an important factor when reporting accurate data [8-10]. Therefore, for all RDE experiments conducted the raw ORR RDE data was corrected for background currents by subtracting a LSV scan performed under N₂ atmosphere at 5 mV s⁻¹ with no rotation. The solution resistance was then measured by measuring the high-frequency impedance at operating conditions. In ORR studies the electrolyte concentration usually is 0.1 M or higher so the Ohmic resistance is not expected to change during measurement [7]. The solution resistance was then measured and the solution resistance was found to be an important factor when reporting accurate data [8-10]. The mean potential was chosen to be within the diffusion limiting regime for the ORR in an oxygen saturated solution to include any resistance induced by the measurement of the ORR. The potential amplitude was chosen as 5 mV s⁻¹ with frequencies starting at 10 kHz and ending with 1 Hz on a logarithmic scale. The *IR*- drop was calculated by using $\Delta E = IR$ where *I* is the current at each data point and *R* is the ohmic resistance between the working and the reference electrode, determined by Electrochemical

Impedance Spectroscopy (EIS) at 10 kHz. Fig. 5.8a shows the effect of the background corrections on the measured data. The raw RDE data shows a positive current above +1.10 V vs NHE which is due to Pt oxide formation. However, by subtracting the background scan the increase in current disappears. By doing the IR-drop correction, the curve in the mixed controlled region is shifted towards more positive potentials (Fig 5.8b). The shift seems to be very subtle but is of great importance to measure accurate data [10].

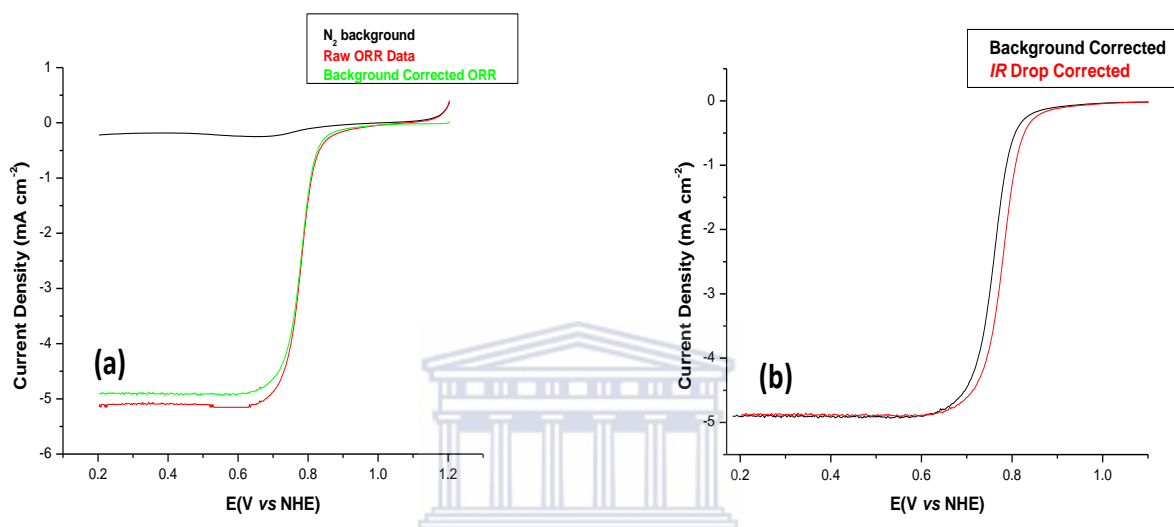


Fig 5.8 (a) Linear sweep voltammograms under N₂ showing the effect of subtracting background scan for 20% Pt/C (b) polarization curve of 20% Pt/C showing the effect of IR drop corrections on RDE.

After correcting all the ORR data the limiting current densities at each rotation speed were obtained and a Levich plot (limiting current vs $\omega^{1/2}$) based on the ORR values were created. The limiting current observed for all the Pt/C thin films were found to be close to the theoretical value as predicted by the Levich equation for a 5 mm diameter RDE in O₂ saturated solutions [2,5-7]. The limiting current at 1500 rpm should be ca. -5.4 mA cm⁻² and the experimental values were -5.12 mA cm⁻² for 20% Pt/C, -5.32 mA cm⁻² for 40% Pt/C and -5.35 mA cm⁻² for TKK which are within 10% of the theoretical value. From the slope of the Levich plots in Fig 5.9, the diffusion coefficients (D_0) for the commercial 20% Pt/C catalyst was found to be $1.29 \times 10^{-5} \text{ cm}^2 \text{ s}^{-1}$. A summary of the data collected during RDE experiments for the 3 commercial catalysts is presented in Fig. 5.10.

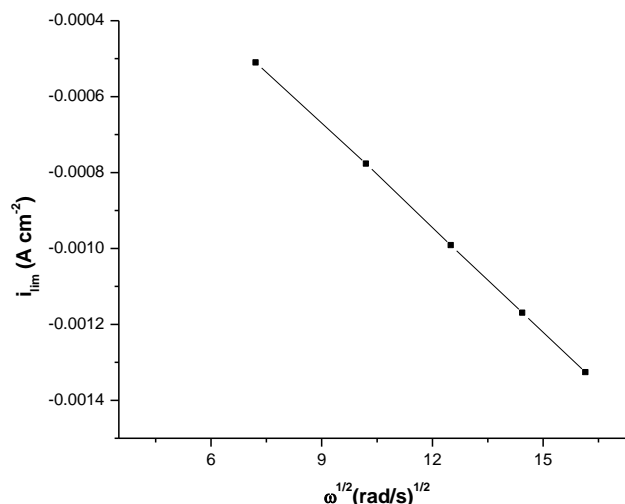


Fig 5.9 Levich plot for thin film 20% Pt/C RDE showing linear relationship between limiting current and $\omega^{1/2}$.

The kinetic current i_k can be calculated by using Equation 5.1

$$i_k(\text{A}) = \frac{i_{lim}(\text{A}) \cdot I(\text{A})}{(i_{lim} - I)} \quad (5.1)$$

Where i_k is the kinetic current (A) and i_{lim} is the measured limiting current (A). After correcting the ORR polarization curves then, i is the value of the curve at $E = +0.85 \text{ V vs NHE}$ and i_{lim} is that $E = \text{ca. } +0.2 \text{ V vs NHE}$ or, alternatively, the kinetic current may also be calculated using the ORR polarization curves for at least five different rotation speeds (500 – 3000 rpm) by which the current at infinite speed can be determined by extrapolating from the K-L Plots shown in Fig 5.10. This method of calculating i_k is more rigorous but time consuming. After establishing that the ORR of the Pt/C thin-film catalysts obeyed first order kinetics, Tafel plots for mass transport corrected mass-specific current densities for O_2 reduction were obtained at 1500 rpm. The Tafel slopes were fitted at low and high overpotential regions in order to facilitate the comparison with literature data [11]. The resulting Tafel slopes for the commercial Pt/C catalysts are summarized in Table 5.3. They are in good agreement with Tafel slopes for polycrystalline Pt electrodes and other carbon supported Pt catalyst [7,11], with values around -60 mV dec^{-1} at low overpotentials ($E > +0.85 \text{ V vs NHE}$) and values of -120 mV dec^{-1} for high overpotentials ($E < +0.8 \text{ V vs NHE}$).

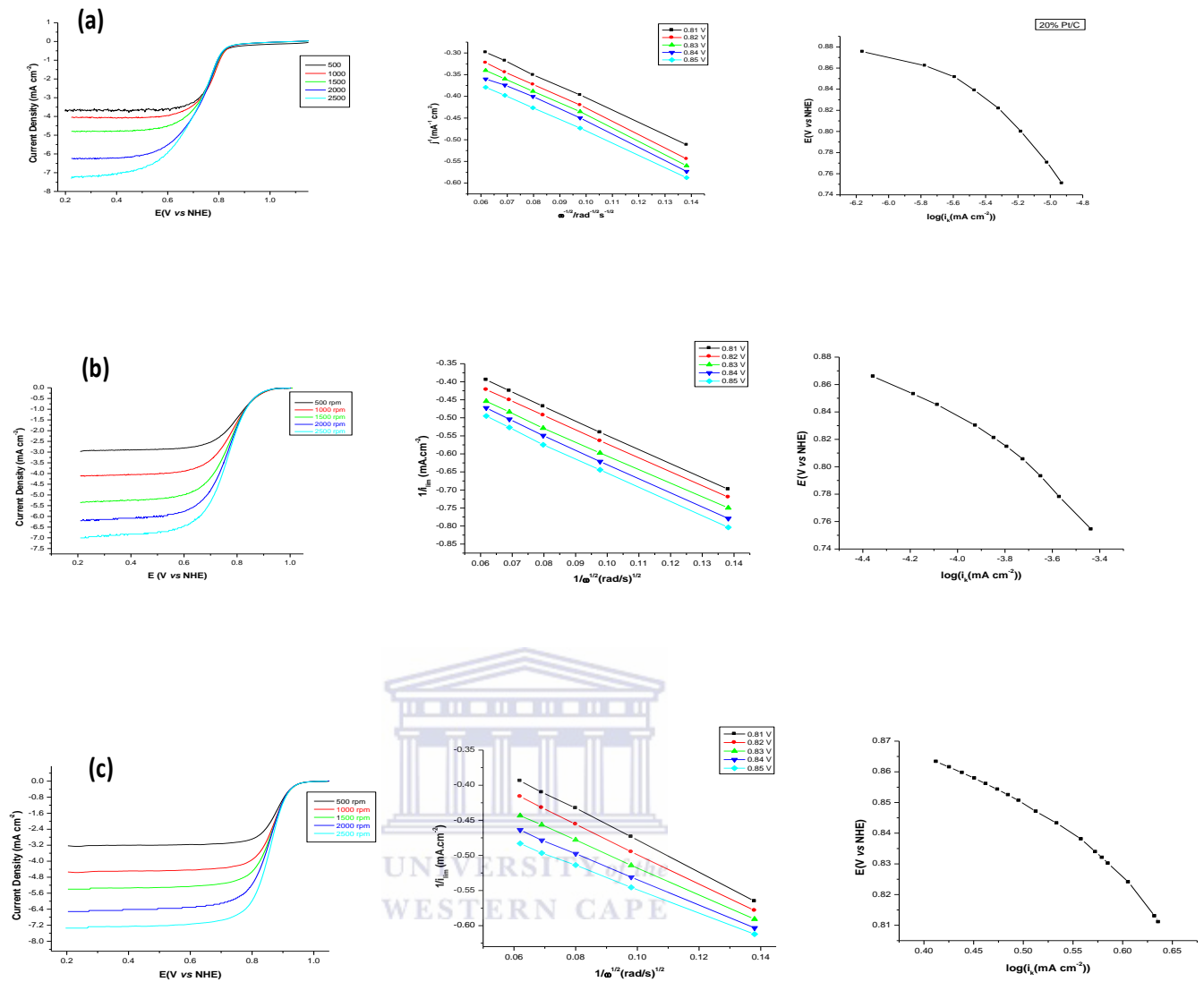


Fig 5.10 (left) iR corrected background subtracted RDE data at various rotation speeds for commercial Pt/C (a) 20% JM, (b) 40% JM and c) 46% TKK, (centre) K-L Plots;(right) mass-transported corrected Tafel plots in O_2 saturated 0.5 M H_2SO_4 .

To compare different catalysts activities the kinetically controlled current densities were taken and compared at +0.85V vs NHE. This potential was chosen as the influences of mass transport are negligible at this region. At this potential the Pt specific area (SA) were estimated by the calculation of i_k and normalizing to the Pt electrochemical surface at +0.85 V vs NHE using Equation 5.2

$$I_s(\text{Am}_{\text{Pt}}^{-2}) = \frac{I_k(A)}{ECSA} \quad 5.2$$

and the Pt mass specific activities (MA) were estimated at +0.85 V vs NHE by Equation 5.3

$$I_m(\text{A g}_{\text{Pt}}^{-1}) = \frac{I_k(\text{A})}{\text{Pt loading (mg)}} \quad 5.3$$

Another important value to report when comparing different catalysts activities is the half wave potential $E_{1/2}$. This term is defined as the potential at which the current due to the reduction/oxidation of a substance is equal to one half of the diffusion current (i_d). The $E_{1/2}$ permits to assess further information regarding the different catalysts electro-activity towards the ORR [2,4]. All the kinetic data for the Pt/C commercial catalysts are summarized in Table 5.3. The thin-film RDE method for the electrochemical characterization of Pt/C catalysts proved to be a valid method as the experimental results obtained were found to be in good agreement with previous studies [5-7]. Therefore the thin-film method was used to characterize the Pt-Sn/C catalysts synthesized via the polyol method. All parameters used for Pt-Sn/C analysis were the same as when we established the electrochemical testing protocol for Pt/C catalyst.

Table 5.3 Electrochemical properties of commercial Pt/C catalyst.

Catalyst	Particle size (nm)	ECSA ($\text{m}^2 \text{g}_{\text{Pt}}^{-1}$)	D ($10^{-5} \text{cm}^2 \text{s}^{-1}$)	$E_{1/2}$ (V)	SA @ 0.85V ($\text{A m}_{\text{Pt}}^{-2}$)	MA @ 0.85V ($\text{A g}_{\text{Pt}}^{-1}$)	Tafel Slope /mV dec ⁻¹
20% Pt/C	3.94	53.98	1.29	0.79	3.87	289	-59/-119
40 % Pt/C	3.80	56.08	1.23	0.80	3.92	297	-60/-121
46% TKK	2.97	64.35	1.27	0.86	5.06	421	-62/-121

5.5 Electrochemical characterization of Pt-Sn/C STD catalysts

Figure 5.11 shows the cyclic voltammograms obtained in 0.5 M H_2SO_4 . CV plots of Pt/C catalyst is typical of unalloyed Pt with clearly defined and resolved hydrogen adsorption/desorption peaks in the region of 0 – +0.30 V vs NHE. The CV of the Pt-Sn/C catalysts showed no well resolved hydrogen desorption/adsorption peaks as seen in the case for the Pt/C catalyst. Colmati et al., tested their Pt-Sn/C catalyst in similar conditions (0.5 M

H₂SO₄ at a scan rate of 50 mV s⁻¹ at RM) They found that the well alloyed Pt₇₅Sn₂₅ sample had no well defined hydrogen adsorption/desorption peaks and double layer behavior [12]. Therefore, this implied that our Pt-Sn/C simply demonstrated a low degree of alloying with Sn, the presence of a high portion of tin oxide phase and low ECSA [12,13]. This is consistent with the XRD results discussed earlier. By comparing the CVs obtained for pure Pt and bi-metallic Pt-Sn, it was observed that the peak potential corresponding to the reduction of Pt-oxide has shifted towards lower potentials ($\Delta E = -120\text{mV}$). This can be explained by either the strengthening of the Pt-O bond or by the effect of tin on the reaction kinetics of the reaction or to the formation of an alloy. From the CVs it is evident that the incorporation of Sn “blocks” some of the Pt active sites having an effect on the hydrogen adsorption/desorption properties of Pt-Sn/C catalysts as opposed to Pt/C catalysts [14,15].

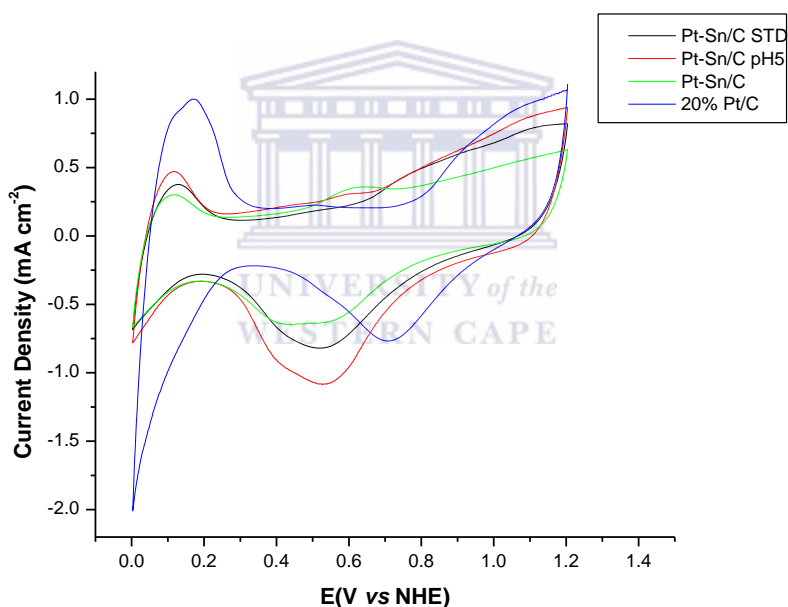


Fig. 5.11 CV of 20% Pt/C and Pt-Sn/C catalysts synthesized with the Polyol STD method recorded in 0.5 M H₂SO₄ at a scan rate of 20 mV s⁻¹ at room temperature.

5.5.2 Methanol Oxidation of Pt-Sn/C STD catalysts

In order to evaluate the *as-prepared* Pt-Sn/C catalyst for MOR, all data were compared to 20% Pt/C in solutions of 0.5 M sulfuric acid + 0.5 M methanol as shown in Figure 5.12. The figure shows that the methanol oxidation current at a potential of +0.85 V vs. NHE for Pt-

Sn/C STD catalysts were less than that of the commercial 20% Pt/C which was 8.28 mA cm^{-2} at the same potential. It was observed that all the Pt-Sn/C STD catalysts showed lower methanol oxidation currents indicating that the Pt-Sn/C system do have methanol tolerant capabilities. These results are in good agreement with work recently published by Antolini *et.al.* [18]. They found that alloying Pt with Sn to any extent significantly reduces the MOR activity which was also observed in this study. The Pt-Sn/C catalyst synthesized using the STD method showed the lowest oxidation current indicating that not changing the pH after the reaction is complete has an effect on the MOR activity. However for the Pt-Sn/C STD pH3, that showed a Pt loading of 17.63 wt. %, a corresponding current of 5.8 mA cm^{-2} was observed which is far less than the MOR current observed for 20% Pt/C catalyst indicating that the Pt-Sn/C catalyst has increased methanol tolerance capabilities. Further methanol oxidation studies were performed to investigate how small amounts of methanol may influence the MOR current if methanol cross-over should occur at the cathode which is a huge concern in the development of DMFCs. Data in figure 5.13a for Pt-Sn/C STD pH3 catalyst were obtained after adding aliquots of methanol to the electrochemical cell containing 50 ml of 0.5 M H_2SO_4 .

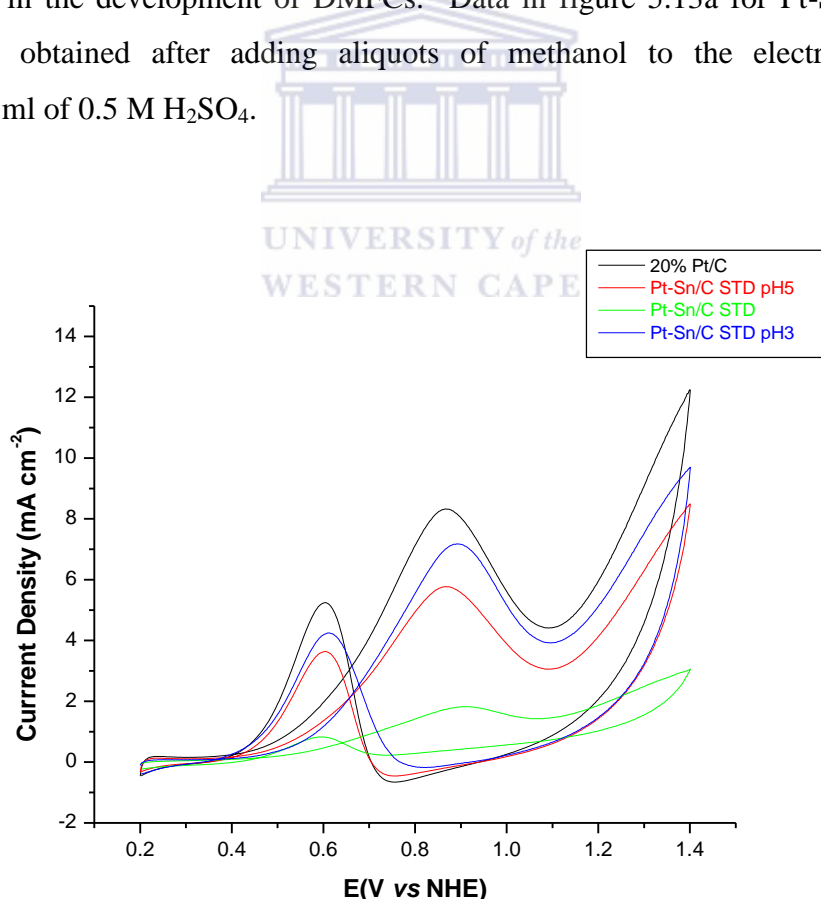


Fig. 5.12 CVs of methanol oxidation obtained on a Pt-Sn/C electrode and compared with that of 20% Pt/C in 0.5 M H_2SO_4 solution containing 0.5 M methanol; scan rate 20 mV s^{-1} , Pt loading $20 \text{ } \mu\text{g cm}^{-2}$.

The amount of methanol was increased with each scan to investigate the ability of the catalyst to show resistance towards methanol oxidation if small amounts of methanol permeate through the membrane. Small changes were observed when the methanol concentration was low. As the amount of methanol increased (Fig 5.13a), so the shape of the CV changed until the expected form for a MOR CV was seen when 100 μl methanol was added. For the 20% Pt/C catalyst a change was immediately visible as soon as the methanol (10 μl) was added to the solution where in the case for the Pt-Sn/C STD pH 3 catalysts, activity towards methanol oxidation was only observed after 30 μl methanol was added.

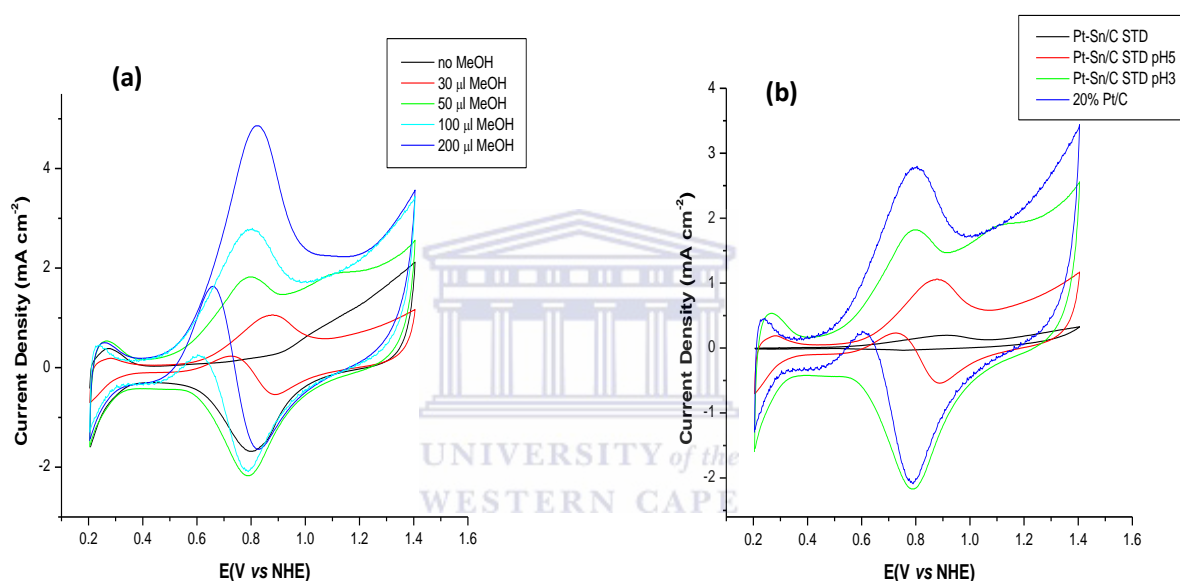


Fig. 5.13 (a) CV of MOR tolerance obtained on a Pt-Sn/C electrode after adding various amounts of methanol (b) CV of MOR tolerance obtained on different Pt-Sn/C electrodes after adding 50 μl methanol and compared to Pt/C in 0.5 M H_2SO_4 solution; scan rate 20 mV s^{-1} .

For the Pt-Sn/C STD catalyst even after adding 500 μl methanol, no methanol oxidation peaks were observed. The results after adding 50 μl methanol to all the Pt-Sn/C catalysts are shown in Fig. 5.13b. All of the synthesized Pt-Sn/C catalysts performed better when compared with Pt/C generating a lower methanol oxidation current at ca. +0.81 V vs. NHE for the same amount of methanol added.

5.5.3 Oxygen Reduction Kinetics of Pt-Sn/C Catalyst

To obtain kinetic information for the various catalysts, rotating disc electrode (RDE) experiments were performed under *steady-state* conditions as mentioned earlier. The LSV was recorded between +0.2 - +1.0 V *vs* NHE at a scan rate of 5 mV s⁻¹. Fig 5.14 shows the LSVs of Pt-Sn/C STD catalysts and 20% Pt/C in O₂ saturated 0.5 M H₂SO₄. It shows that the ORR on all the Pt-Sn/C catalysts is diffusion controlled when the potential is less than +0.50 *vs* NHE and under mixed diffusion control (or surface reaction control region) in the potential region between +0.55 - +0.85 V *vs* NHE. The E_{1/2} for Pt-Sn/C STD was +0.71 V *vs* NHE and for Pt-Sn/C pH3 +0.73 V *vs* NHE. A gradual reduction of half wave potential was observed when going from Pt-Sn/C STD pH 3 to Pt-Sn/C STD. The difference in ORR half wave potentials are caused by differences in the surface activation of the various catalysts, which are related to the size, metal loading and distribution of the metal nanoparticles.

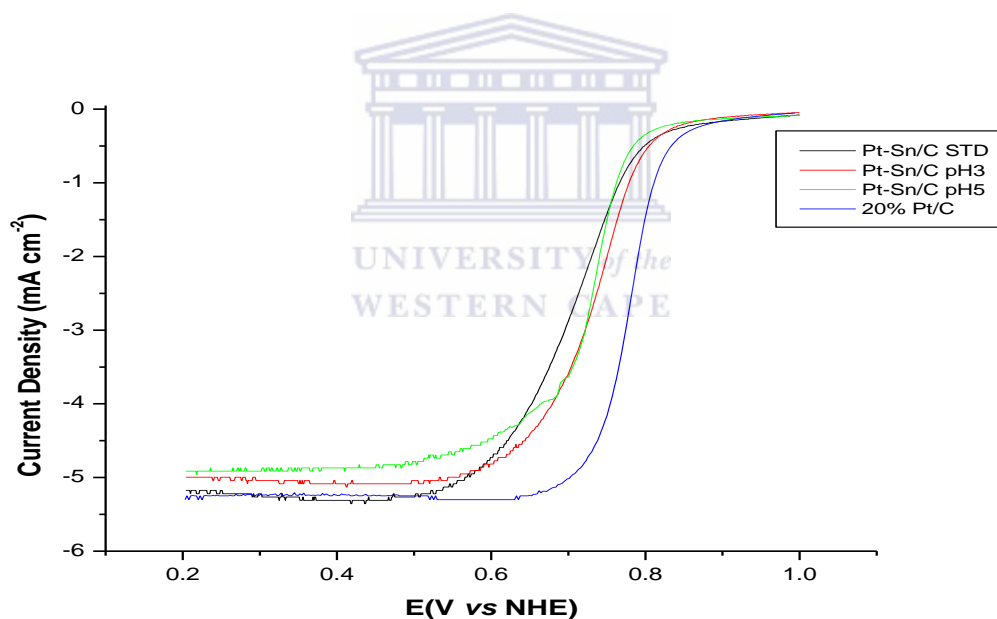


Fig.5.14 Polarization curves obtained with a RDE for O₂ reduction on Pt-Sn/C electrodes and compared with that of Pt/C in 0.5 M H₂SO₄ solution at 1500 rpm; scan rate 5 mV s⁻¹.

Table 5.4 summarizes the electrochemical properties of the Pt-Sn/C STD catalysts. The ORR activity of all the STD Pt-Sn/C catalysts were low when compared to 20% Pt/C catalyst. From the kinetic data of Pt-Sn/C STD catalysts we can conclude that although the STD method produced nanoparticles with very small sizes and relatively even size distribution the poor performance of the catalysts in the kinetic controlled region when compared to commercial Pt/C catalyst makes it insufficient for use in DMFCs. The Pt-Sn/C showed

methanol tolerant properties but performed poorly when promoting the ORR. In order for the STD method to be considered to synthesize Pt-Sn/C nanoparticles for DMFC use, further test needs to be done to improve the ORR capabilities of the catalysts synthesized using this method which was found to be a very quick and easy method of preparing Pt-Sn/C nanoparticles.

Table 5.4 Electrochemical properties of Pt-Sn/C and Pt/C catalysts from ORR data.

Catalyst Pt-Sn/C	Particle Size (nm)	E_{1/2} (V)	ECSA (m² g⁻¹_{Pt})	SA @ 0.85V (Am_{Pt}⁻²)	MA @ 0.85V (A g⁻¹_{Pt})	Tafel Slope (mV dec⁻¹)
STD	3.99± 0.96	+0.705	24.32	0.67	87	-83/-196
STD pH5	3.86± 0.78	+0.726	15.05	0.85	95	-70/-144
STD pH3	3.77± 0.74	+0.735	18.16	1.32	102	-69/133
20% Pt/C	3.42±0.31	+0.79	53.98	3.87	289	-59/-119

5.6 Electrochemical characterization of Pt-Sn/C HA, Slurry and HA Slurry method catalysts.

The electrochemical properties of Pt-Sn/C Slurry, Pt-Sn/C HA and Pt-Sn/C HA Slurry STD and pH5 catalysts are summarized in Table 5.5 based on CVs and MOR results conducted on the various catalysts. There was a gradual increase in ECSA as the metal loading increased and as the particle size decreased on the different catalysts. The Pt-Sn/C Slurry pH3 and Pt-Sn/C HA pH3 catalysts showed well defined hydrogen adsorption/desorption peaks at 0 – +0.25V vs NHE. All of the catalyst samples showed the Pt-oxide formation reduction peaks at around +0.60 – +0.75 V vs. NHE. As seen previously for the Pt-Sn/C STD catalysts, when comparing the CVs for pure Pt and Pt-Sn, it was observed that the peak potential corresponding to the reduction of platinum oxide (PtO) has shifted slightly towards lower potentials. For this series the shift was less as noticed before for the Pt-Sn/C STD catalysts series ($\Delta E = -50\text{mV}$). This slight shift in reduction potential confirms the alloying character of all the Pt-Sn/C catalysts. Improvements in ECSA for this series of catalysts suggest that fewer Pt sites are “blocked” by the incorporation of Sn and that smaller particle sizes are beneficial towards achieving a higher ECSA. For the MOR, all the catalysts showed resistance towards methanol oxidation. When compared to commercial Pt/C (with same metal

loading) the corresponding methanol oxidation currents found were lower for MOR and for the methanol permeation test if small quantities of methanol should cross-over from anode to cathode side.

Table 5.5 Electrochemical properties of Pt-Sn/C Slurry and HA catalysts constructed from CVs and MOR experiments.

Catalyst Pt-Sn/C	Particle Size (nm)	ECSA (m² g⁻¹ Pt)	MOR current @0.85 V(mA cm⁻²)	MOR current after 50 µl methanol @0.85 V(mA cm⁻²)
Slurry STD	3.88	16.23	2.88	1.23
Slurry pH5	3.86	16.90	3.03	1.44
Slurry pH3	3.32	27.43	4.15	1.53
HA STD	3.55	16.88	3.98	1.89
HA pH5	3.39	22.05	3.56	1.96
HA pH3	3.02	31.12	5.05	2.12
HA Slurry STD	3.48	27.77	4.69	1.80
HA Slurry pH5	3.29	24.65	5.13	2.03
20% Pt/C	3.94	53.98	5.98	2.77
40% Pt/C	3.80	56.08	6.87	3.43
46% TKK	2.97	64.35	9.24	4.87

The Pt-Sn/C HA pH3 catalysts (18.86 wt. % Pt) showed that although an increase in ESCA and MOR current was observed even with the catalyst loading close to that of Pt/C (20.43 wt. %), that by alloying the Pt with Sn, this catalyst displays important methanol oxidation tolerant capabilities. Haner and Ross [17] studied the effect of tin atoms on the Pt surface by using single crystal faces of the Pt₃Sn alloy. They found that the non alloy surfaces were more effective catalysts than any pure Pt surface and that alloying Pt with Sn to any extent reduced the activity (as seen in the low ECSA values for our Pt-Sn/C series compared to Pt/C). In their conclusion they found that the effect of Sn is primarily an electronic effect and voltammetry data supported their findings that there is a very strong “ligand effect” on the way methanol adsorbs on the Pt surface due to the alloying with Sn and that this effect is not beneficial towards the catalyst’s MOR activity [17,18]. Summarizing, Pt-Sn/C HA and Slurry alloy catalyst surfaces are not that suitable for the MOR. Alloying Pt with Sn to any extent significantly reduced the MOR activity thus giving the Pt-Sn/C methanol resistant properties

which is be beneficial when Pt-Sn/C catalysts are used as a cathode catalyst. Since the oxygen reduction reaction (cathode reaction) is significantly more sluggish than the methanol oxidation reaction (anode reaction) it was of interest to further investigate the Pt-Sn/C HA and HA Slurry catalysts behavior for ORR seeing that the above catalysts series already fulfilled one of the criteria for a cathode catalyst which is to suppress the MOR. The ORR data for the above Pt-Sn/C catalysts series are summarized in Table 5.6. Fundamentally, the ORR electrochemical kinetics for Pt-Sn/C should be no different than Pt/C catalysts. As discussed in Chapter 3 and above, the two important parameters of interest are exchange current density (i_0) and Tafel slope. A high exchange current density results in faster reaction kinetics which is desirable for the ORR. Therefore this means that a high SA will also imply faster reaction kinetics. The kinetic values obtained for the Pt-Sn/C series catalysts showed mixed results. The HA pH5 and HA pH3 catalysts were the only two catalysts that showed kinetic values close to that of commercial 20% Pt/C. Although there was a big improvement in this series of catalysts synthesized with the different polyol methods as compared to the Pt-Sn/C STD catalysts series (evident by $E_{1/2}$, MA and SA), the kinetic values obtained were not that satisfactory. The Pt-Sn/C showed superior performance for MOR tolerance in comparison to the commercial Pt/C catalysts but, the fundamental reaction for the cathode catalyst is the promotion of the ORR in a fuel cell and in this regard the Pt-Sn/C catalysts performance were not quite up to the desired standard despite showing good resistance towards the MOR.

Table 5.6 Electrochemical properties of Pt-Sn/C and Pt/C catalysts from ORR data.

Catalyst Pt-Sn/C	$E_{1/2}$(V)	SA @ 0.85V (μAcm^{-2})	MA @ 0.85V ($\text{A g}^{-1}_{\text{Pt}}$)	Tafel Slope (mV dec^{-1})
Slurry STD	+0.70	1.19	95	-80/-177
Slurry pH5	+0.71	1.66	127	-73/-160
Slurry pH3	+0.72	1.94	189	-67/-132
HA STD	+0.70	1.35	163	-86/-195
HA pH5	+0.72	2.01	213	-65/-125
HA pH3	+0.73	2.12	225	-63/-126
HA Slurry STD	+0.71	1.46	117	-73/-150
HA Slurry pH5	+0.72	1.80	176	-63/-125
20% Pt/C	+0.79	3.87	289	-59/-119

The Tafel slopes of the Pt-Sn/C HA pH3 and HA pH5 were almost the same to that of commercial Pt/C. This could be explained in terms of the coverage of the electrode surface by adsorbed oxygen which follows a Langmuir isotherm (low coverage) at high overpotential and a Temkin isotherm (high coverage) at lower overpotentials [5-7,11,15]. However, Tafel slope values calculated by ORR for the other Pt-Sn/C catalyst suggest a rather more complex reaction mechanism, indicating that the ORR kinetics was negatively influenced by the addition of tin and that the variation used on these catalysts during synthesis is not suitable for Pt-Sn/C to be used as possible ORR catalysts. A shift to higher positive potentials for $E_{1/2}$ was also observed from Slurry STD to HA pH3 catalyst. This improvement is due to the lessened coverage of oxide/hydroxide on the Pt surface at high potential resulting in a larger number of reaction sites available to promote ORR. However, when compared to the commercial catalyst this series of catalysts also did not perform satisfactory. The activity towards ORR was found to be as follows: Pt-Sn/C (HA pH3), >Pt-Sn/C (HA 5pH), >Pt-Sn/C (Slurry pH3), >Pt-Sn/C (HA Slurry pH5), >Pt-Sn/C (Slurry pH5), > Pt-Sn/C (HA slurry STD), Pt-Sn/C (HA STD) >Pt-Sn/C (Slurry STD).

5.7.1 Electrochemical characterization of Pt-Sn/C HA Slurry pH3 and HA Slurry pH3 heat-treated samples.

From the physical and structural properties investigated in the previous chapter the Pt-Sn/C HA Slurry pH3 catalysts was found to be the best synthesized as prepared catalyst and was subjected to heat-treatment. Electrochemical measurements were performed at room temperatures in 0.5 M H_2SO_4 . Prior to recording experimental data the CV was cycled 25 times at 100 mV s^{-1} between 0 and +1.0 V vs NHE in order to produce a clean electrode surface. The Pt-Sn/C catalysts were first characterized electrochemically by CV. Fig 5.15 shows the CV plots of Pt-Sn/C HA Slurry pH3 series catalysts. During the initial scan (before recording CV) it was observed that the peak current densities for the as-prepared catalyst increases initially with cycle, which could be attributed to surface roughing and removal of contaminants from the catalyst surface. Although the as-prepared sample (Fig. 5.15) showed a large PtO reduction peak ($E = +0.65 \text{ V vs NHE}$ comparable to Pt/C) during the early cycles, the peak current density decreased slightly after 20 cycles, indicating possible instability of the catalyst. For the heat-treated 500 °C and 600 °C catalysts the peak current densities remained the same after the initial surface cleaning stage, indicating much improved stability due to alloying and larger particle size as seen with TEM and XRD data. For the as-prepared

Pt-Sn/C HA Slurry pH3 catalysts well defined hydrogen adsorption/desorption peaks were not observed, suggesting the high dispersion of the catalyst with disordered surface structure [19].

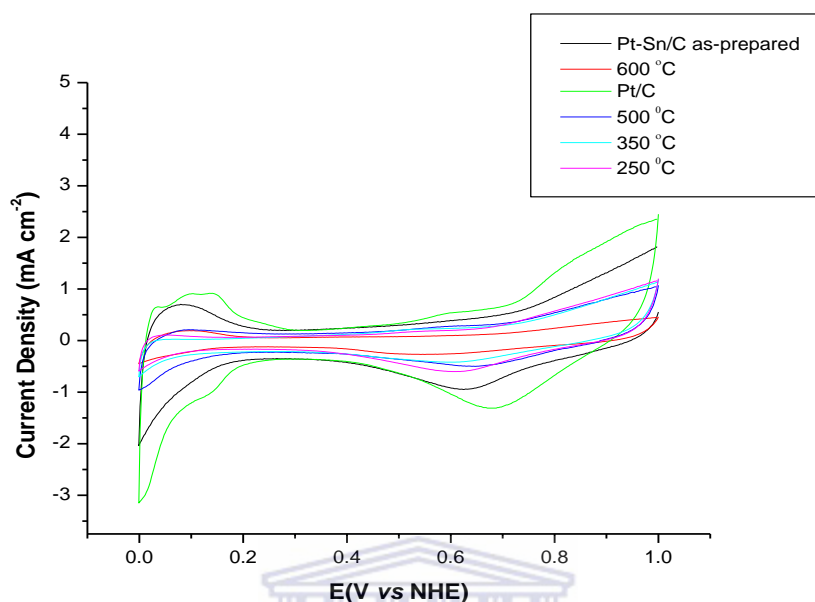


Fig.5.15 Cyclic voltammograms obtained on a Pt-Sn/C HA Slurry pH3 electrode and compared with that of Pt/C 0.5 M H_2SO_4 solution; scan rate of 20 mVs^{-1} .

For the different heat-treated Pt-Sn/C catalysts it was observed from the CVs that the hydrogen adsorption/desorption current decreases with increasing temperature. Therefore, the incorporation of Sn appears to block the active sites affecting the catalyst hydrogen adsorption/desorption properties of the heat-treated Pt-Sn/C catalyst contrary to Pt/C [15]. The decrease in ECSA for the heat-treated catalysts can therefore be attributed to increase in particle size and higher degree of alloying as the temperature increased.

The ORR were performed in O_2 saturated 0.5 M H_2SO_4 solution with a 5 mm GC RDE between +0.2 – 1.0 V vs NHE at a scan rate of 5 mV s^{-1} . Fig. 5.16 shows the LSVs of as-prepared and heat-treated Pt-Sn/C HA Slurry pH3 and commercial Pt/C catalyst. It is evident that the oxygen reduction on the as-prepared Pt-Sn/C, Pt-Sn/C 250 °C and Pt/C catalysts is diffusion controlled when the potential is less than +0.7 V vs NHE and is under mixed diffusion-kinetic in the potential region between +0.7 V – +0.90 V vs NHE. Oxygen reduction activity of the catalysts were calculated by taking the activity at +0.85 V vs NHE after subtracting the background scan and performing the IR-Drop correction are given in Table 5.7. The results of LSV indicated that the as-prepared Pt-Sn/C catalysts exhibited

higher ORR activity than the commercial 20% Pt/C (JM). The increase in ORR activity is attributed to the inhibition of formation of hydroxy species on the Pt surface.

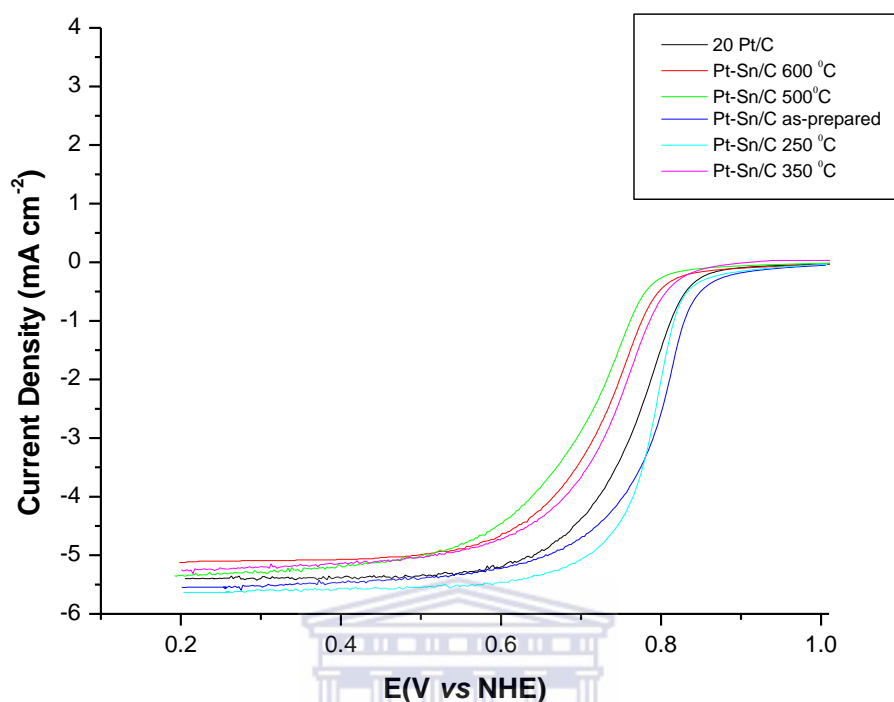


Fig. 5.16 Polarization curves obtained with a RDE for O₂ reduction on a Pt-Sn/C electrode and compared with that of Pt/C in 0.5 M H₂SO₄ solution at 1500 rpm; scan rate 5 mV/s.

Moreover, oxygen reduction proceeded in a relatively positive potential region for the as-prepared Pt-Sn/C catalyst compared to Pt/C. The half wave potential for ORR of the Pt-Sn/C alloy is higher compared to that of the 20% Pt/C catalyst. This could be due to differences in the surface activation which is related to the size and distribution of the metallic nanoparticles. The similar shape of LSVs and high current density of the as-prepared Pt-Sn catalyst to that of the Pt/C catalyst indicates that the oxygen reduction takes place in the same manner with the catalysts but with facile kinetics on the Pt-Sn alloy [19]. For the Pt-Sn/C heat-treated catalysts a decrease in SA was observed going from the as-prepared sample to the 500 °C heat-treated sample and then with an increase for the 600 °C annealed catalyst. This jump can be attributed to the large sections of agglomeration of the nanoparticles found for Pt-Sn/C 500°C catalyst when investigated with TEM. Only the Pt-Sn/C 250 °C showed higher MA and SA values for the heat-treated samples proving that the alloying effect is an important factor affecting the catalytic activity towards ORR and that the temperature of

250 °C is the optimum temperature to achieve the best possible performance for the heat treated Pt-Sn/C catalyst compared to Pt/C. The heat-treated catalysts showed that a bigger particle size and particle distribution does not necessary implies a decrease in ORR activity as seen for the as-prepared catalysts that showed a particle size distribution of 2.49 nm and Pt-Sn/C 250 °C a particle size of 5.08 nm but whose ORR performance was comparable to 20% Pt/C and Pt-Sn/C HA Slurry pH3 catalysts. The relatively higher oxygen reduction activity for the as-prepared and 250°C Pt-Sn/C catalysts compared to 20% Pt/C catalyst, can be correlated to the distribution of nanoparticles and orientation of surface atoms in the crystal planes, altering the redox energy levels as a function of particle size, particle distribution and the metal loading effect. The fact that the Pt-Sn/C 250 °C catalyst showed slightly higher SA than the commercial 20% Pt/C catalyst is encouraging, and showed that the ORR reaction is not inhibited by the alloying with Sn when heat-treated although, the same cannot be said of the other heat-treated Pt-Sn/C catalysts where a decrease was observed as the temperature was increased.

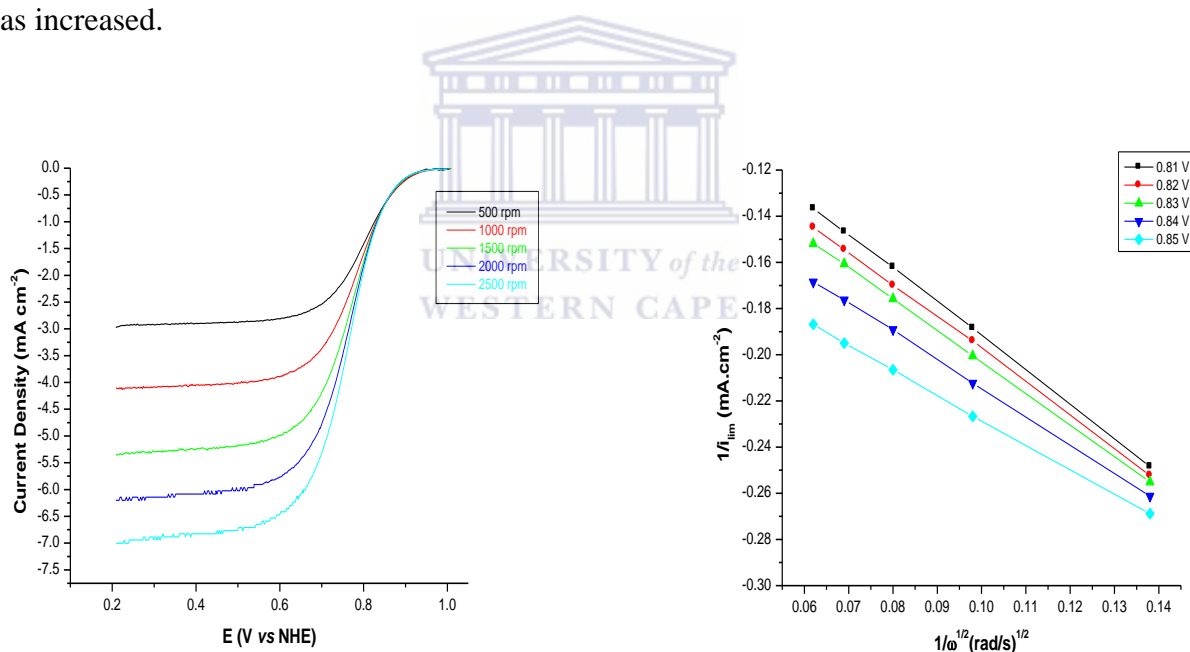


Fig.5.17(left) Polarization curves obtained with a RDE for O_2 reduction on Pt-Sn/C HA Slurry pH3 electrode in 0.5 M H_2SO_4 solution at 1500 rpm; scan rate 5 mV/s, (right) Koutecky – Levich plots prepared from as prepared Pt-Sn/C HA Slurry pH 3 data at different potentials in mixed kinetic-diffusion controlled region.

The higher MA for as-prepared and 250 °C Pt-Sn/C catalysts indicated that these 2 catalysts are possibly suitable for application in DMFC. Further kinetic information regarding the electron transfer reaction was gained when constructing KL-plots for the Pt-Sn/C HA Slurry pH3 shown in Figure 5.17. The K-L Plot (plot of i^{-1} vs. $\omega^{-1/2}$) gave parallel straight lines at

various potentials in the range of +0.8 V – +0.85 V vs NHE in the mixed diffusion controlled region. The K-L plots showed linearity in the selected potential range confirming that the oxygen reduction reaction follows first order kinetics. The number of electrons calculated from the slopes of the KL-Plot for as-prepared Pt-Sn/C HA Slurry pH3 was 3.43. The K-L plots of all the Pt-Sn/C HA Slurry pH3 catalyst series showed linearity confirming that the oxygen reduction reaction follows first order kinetics with respect to molecular oxygen. From the number of electrons calculated for Pt-Sn/C HA Slurry pH3 catalysts series, we can conclude that oxygen reduction on all the Pt-Sn/C catalysts occurred *via* the direct reduction of oxygen to water which is supported by the desired 4e⁻ transfer path for ORR. However, we cannot exclude the notion that a certain percentage of hydrogen peroxide could have been formed during the ORR. Rotating Ring Disc Electrode (RRDE) experiments need to be conducted to evaluate if H₂O₂ is in fact formed during the ORR. For this dissertation, RRDE experiments were not conducted as we did not have the necessary equipment in our laboratory to perform these tests or to perform ORR experiments at elevated temperatures to match DMFC conditions as the reaction kinetics of ORR will differ when performed at higher temperatures used for DMFC operations.

Table 5.7 ORR kinetic properties of Pt-Sn/C HA Slurry pH3 catalysts series.

Catalyst Pt-Sn/C HA Slurry pH3	E_{1/2} (V)	ECSA (m² g⁻¹_{Pt})	Number \bar{n} (n)	SA @ 0.85V ($\mu\text{Acm}_{\text{Pt}}^{-2}$)	MA @ 0.85V (A g⁻¹_{Pt})	Tafel Slope (mV dec⁻¹)
as-prepared	0.81	26.24	3.44	3.84	323	-62/-122
250 °C	0.79	20.98	3.52	3.08	297	-61/-123
350 °C	0.73	16.69	3.34	2.17	225	-59/-121
500 °C	0.71	11.32	3.23	1.18	109	-67/-125
600 °C	0.72	9.84	3.08	1.22	82	-63/-130
20% Pt/C	0.79	53.98	3.58	3.87	289	-59/-119
40 % Pt/C	0.82	56.08	3.43	3.92	327	-60/-121
46% TKK	0.86	64.35	3.54	5.06	421	-62/-121

Furthermore, kinetic information on the electron transfer reaction mediated by the Pt-Sn/C HA Slurry catalysts were compared to Pt/C and is illustrated in Fig. 5.18. This illustrated E

vs log i_k curves or Tafel plots (obtained using Eq. 5.1). Table 5.7 summarizes the data obtained at room temperature in 0.5 M H₂SO₄ saturated with oxygen at 1500 rpm based on an anodic scan from +0.2 V to + 1.0. V *vs* NHE at a scan rate of 5 mV s⁻¹ in the range of ±0.72 < E < ±0.88 V *vs* NHE for Pt/C and Pt-Sn/C. Two Tafel slopes i.e. ca. -62 and -59 mV dec⁻¹ in the low current region and -122 and -119 mV dec⁻¹ for the high current region were observed for Pt/C and the as-prepared Pt-Sn/C HA Slurry pH3 catalysts respectively. For Pt/C the low and high Tafel slopes were in good agreement with values found in the literature [5,7,15]. The Tafel slopes of the Pt-Sn/C HA Slurry pH3 and heat-treated catalysts were almost the same as that of commercial Pt/C. This could be explained in terms of the coverage of the electrode surface by adsorbed oxygen which follows a Langmuir isotherm (low coverage) at high overpotential and a Temkin isotherm (high coverage) at lower overpotentials. This implies that the rate determining step for the ORR is unchanged for Pt-Sn/C HA Slurry pH3 catalysts despite some differences in their electrocatalytic and physical properties [5,15]. The as-prepared Pt-Sn/C HA Slurry pH3 and Pt-Sn/C 250 °C catalysts showed similar catalytic activity towards ORR and gave an indication that the catalytic mechanism for ORR might be the same as that of Pt/C indicating that the ORR kinetics was not negatively influenced by the addition of tin, heat-treatment at 250 °C and difference in particle size for Pt-Sn/C 250°C catalysts. The activity towards ORR was found to be as follows: Pt-Sn/C (HA Slurry pH3) >Pt-Sn/C (HA Slurry pH3) 250 °C >Pt-Sn/C (HA Slurry pH3) 350 °C >Pt-Sn/C (HA Slurry pH3) 600°C >Pt-Sn/C (HA Slurry pH3) 500°C. These findings are in good agreement with work done by Jeyabharathi and co-workers [15] where they also observed that the as-prepared Pt-Sn/C catalyst showed better performance than the different heat-treated Pt-Sn/C catalysts. However, they could not fully explain why their as-prepared catalyst showed better performance than the heat-treated catalysts. They observed a minimal decrease in particle size when moving from the as-prepared catalyst (which was reported as 5.79 nm based on their TEM results) to Pt-Sn/C 250 °C (reported as 5.63 nm). On the other hand, in our case the particle size doubled (from 2.49 nm) when moving from as-prepared to Pt-Sn/C 250 °C (5.08 nm) based on TEM experiments the as-prepared and heat-treated catalyst results were comparable to each other.

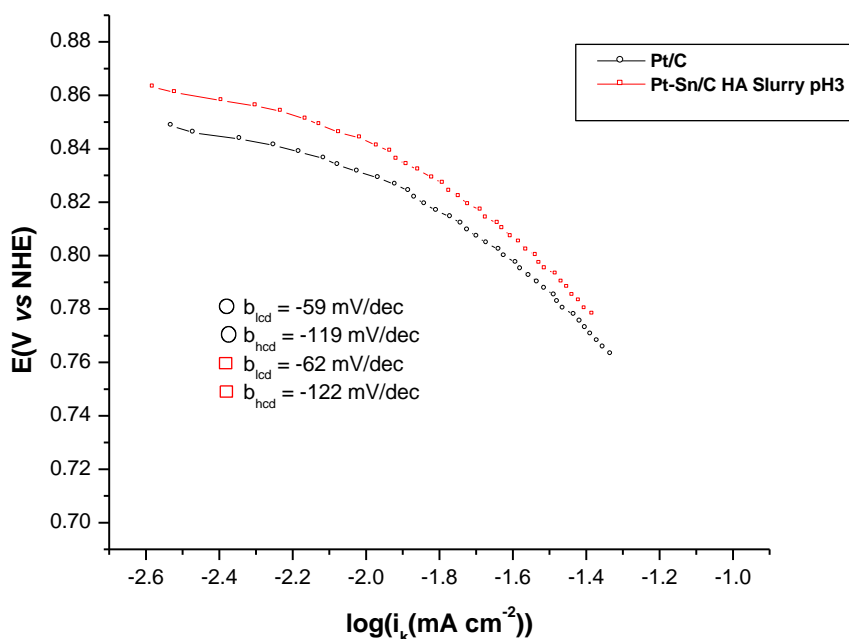


Fig. 5.18 Mass transfer Tafel polarization curves of Pt/C and Pt-Sn/C electrodes for ORR (R.T, 1500 rpm, scan rate of 5 mV s^{-1} in $0.5 \text{ M H}_2\text{SO}_4$ solution saturated in oxygen).

5.7.2 Effect of particle size on ORR for Pt-Sn/C HA Slurry pH3 catalysts

Considering the ORR mechanism (discussed in Chapter 2) the first step would involve oxygen adsorption onto the surface of the Pt. The oxygen can dissociate into oxygen atoms followed by an electron transfer reaction. What is also possible is that the electron transfer can occur with the adsorbed molecular oxygen. Irrespective of the above steps, the final step of the ORR mechanism is the formation of water. The water formed during the ORR must leave the surface and thus a fine balance is required for the strength of the bonding of oxygen to the Pt surface. If the bond is too weak the oxygen will not adsorb and if it's too strong the water produced will not leave the surface of the Pt thus blocking further sites for the reaction to continue and thus in a sense, the oxygen then acts as a poisoning agent in the process. It is therefore believed that the size of the platinum particle may affect this oxygen bond strength and several groups have reported that for maximum ORR performance a particle size of between 3-5 nm is desirable as the SA decreases as the particle size decreases and thus slower reaction kinetics are observed [20-22]. However these claims did not take into account the influence of the capacitive current by subtracting the background scans and performing IR-

drop correction on the raw ORR data when reporting values for SA and MA based on particle sizes. Therefore, findings made during these studies could be considered to be inaccurate. Recently Nesselberger et. al., [23] reported (after subtracting background scans) that there was little variation in SA for Pt particles with sizes ranging from 2-8 nm, and the results obtained for the as-prepared Pt-Sn/C HA Slurry pH3 and Pt-Sn/C 250 °C catalysts are in good agreement with this findings.

5.7 3 Methanol oxidation and methanol tolerant studies of Pt-Sn/C HA Slurry pH3 and HA Slurry pH3 heat-treated samples.

In order to evaluate the Pt-Sn/C catalyst series for MOR, all data were compared to 20% Pt/C in solutions of 0.5 M sulfuric acid + 0.5 M methanol as shown in Figure 5.19. The figure shows that the methanol oxidation current density of 7.11 mA at a potential of +0.86 V vs. NHE for Pt-Sn/C HA Slurry pH3 is less than that of the commercial current density for Pt/C which was 8.25 mA at the same potential. It was observed that the as-prepared Pt-Sn/C catalysts activity was 15% less than that of Pt/C. It was also interesting to note that the methanol oxidation current decreases drastically as the temperature increased from 250 – 600 °C and that the methanol oxidation peak shifted to higher positive potentials. For the Pt-Sn/C 350 -600 °C catalysts, the methanol oxidation peak was observed at ca. +0.9 V vs NHE. This shows (as seen with CV data) that the degree of alloying of Pt with Sn increases as the temperature of the heat-treatment increases. More Pt active sites are blocked thus causing a reduction in the methanol oxidation current. Methanol oxidation permeation studies were also conducted on the Pt-Sn/C HA Slurry pH3 catalysts series. Figure 5.20 shows CVs obtained after adding aliquots of methanol to the electrochemical cell containing 50 ml of 0.5 M H₂SO₄. The amount of methanol was increased with each scan to investigate the ability of the catalyst to show resistance towards methanol oxidation if methanol should cross-over through the membrane during DFMC testing. All the Pt-Sn/C HA Slurry pH3 catalysts showed lower methanol oxidation current densities for the same amount of methanol added. The results after adding 50 and 200 µl methanol to all the Pt-Sn/C catalysts are shown in Table 5.8. All of the synthesized Pt-Sn/C HA Slurry pH3 catalysts performed better when compared with Pt/C generating a lower methanol oxidation current at ca. +0.86 V vs NHE for the same amount of methanol added. Methanol tolerant properties of Pt-Sn/C pH3 catalysts were gained in an electrolyte solution containing 0.5 M H₂SO₄ + 0.5 M methanol using a

polarization technique. The potentials were scanned from +0.2 - +1.0 V vs NHE at a scan rate of 5 mV s^{-1} under an oxygen atmosphere and the polarization curves are shown in Fig. 5.21.

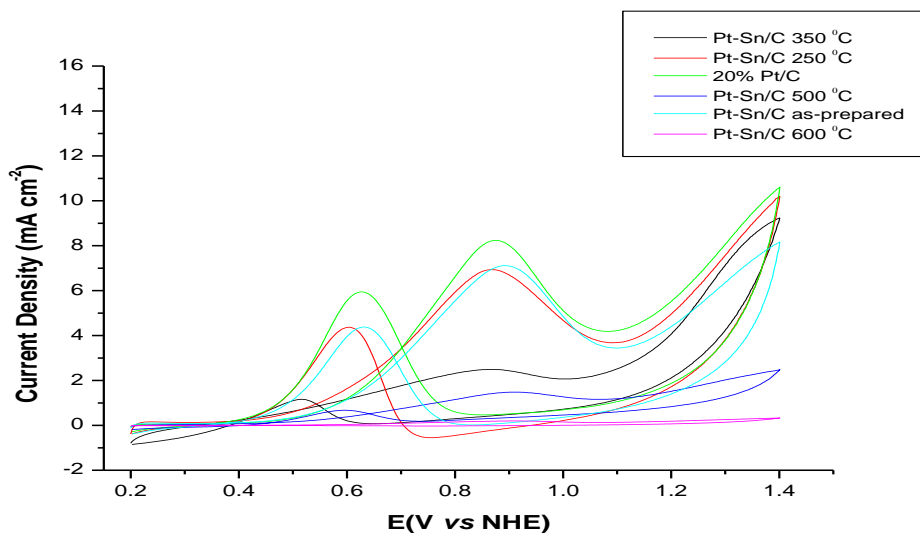


Fig. 5.19 CV of methanol oxidation obtained on a Pt-Sn/C electrode and compared with that of Pt/C in $0.5 \text{ M H}_2\text{SO}_4 + 0.5 \text{ M}$ methanol solution scan rate 20 mV s^{-1} (b)

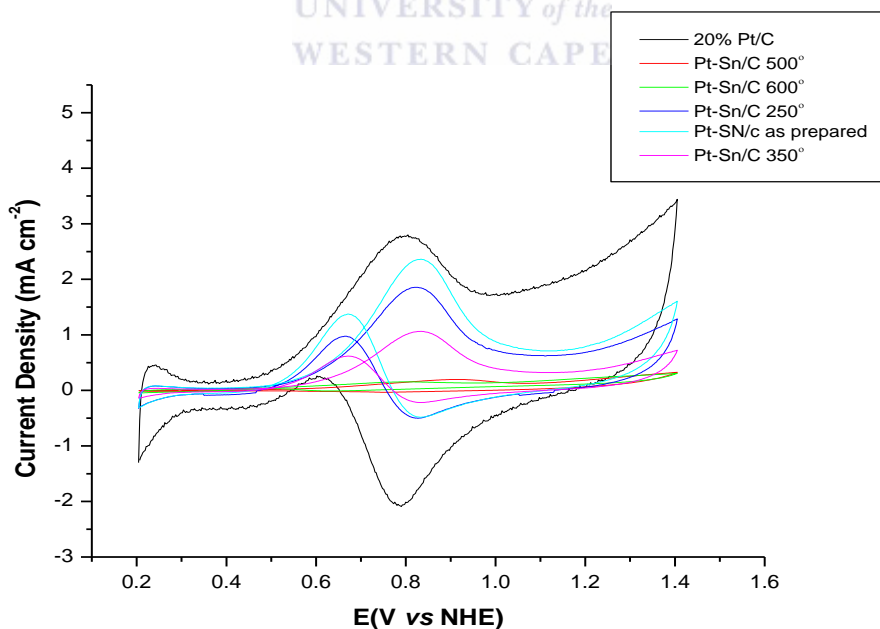


Fig. 5.20 CV of methanol oxidation obtained on a Pt-Sn/C electrode after adding $50 \mu\text{l}$ methanol to $0.5 \text{ M H}_2\text{SO}_4$ and compared to Pt/C; scan rate 20 mV s^{-1} , room temperature.

Table 5.8 MOR properties of Pt/C and Pt-Sn/C HA Slurry pH3 series catalysts.

Catalyst Pt-Sn/C	MOR current @ 0.86 V (mA cm⁻²)	MOR current (mA cm⁻²) after 50 µl methanol	MOR current (mAcm⁻²) after 200 µl methanol
HA Slurry pH3	7.11	4.74	13.43
250°C	6.98	3.63	10.88
350 °C	2.4	1.98	7.02
500 °C	1.76	0.53	2.12
600 °C	0.11	0.04	0.07
20% Pt/C	8.25	5.96	19.28
40% Pt/C	13.03	7.35	27.89
46% TKK	13.55	8.02	34.21

Compared to the ORR in pure H₂SO₄ solutions, all the catalysts for the ORR showed an increase in overpotential. This increase is due to the simultaneous oxidation of methanol and oxygen reduction on the surface of the catalyst. When compared to all the catalysts the increase of the overpotential for the pure Pt/C catalyst was the highest and such a high mixed potential at the cathode will negatively affect the performance of the catalyst when tested in DMFC. Fig. 5.21 showed that all the Pt-Sn/C HA Slurry pH3 catalysts are less affected by the presence of methanol in solution than Pt/C under the same conditions. For Pt-Sn/C 500°C and 600 °C the methanol oxidation current is completely absent. This therefore implies that the Pt-Sn/C catalyst system might be a good potential active cathode catalyst for application in the direct methanol fuel cell with methanol tolerant capabilities. The ability of the catalysts to show methanol tolerant behaviour can in part be described by the so-called geometric “ensemble” effect [15,24-26]. The second metal or metal oxide (Sn, SnO₂) atoms surrounding the Pt active sites, could potentially block methanol oxidation on the Pt sites due to the ensemble effect. Therefore, methanol oxidation on the binary system can be possibly be suppressed. On the other hand only two adjacent Pt sites are required for the dissociative chemisorption of oxygen and Pt is thus less affected by the presence of Sn or SnO₂.

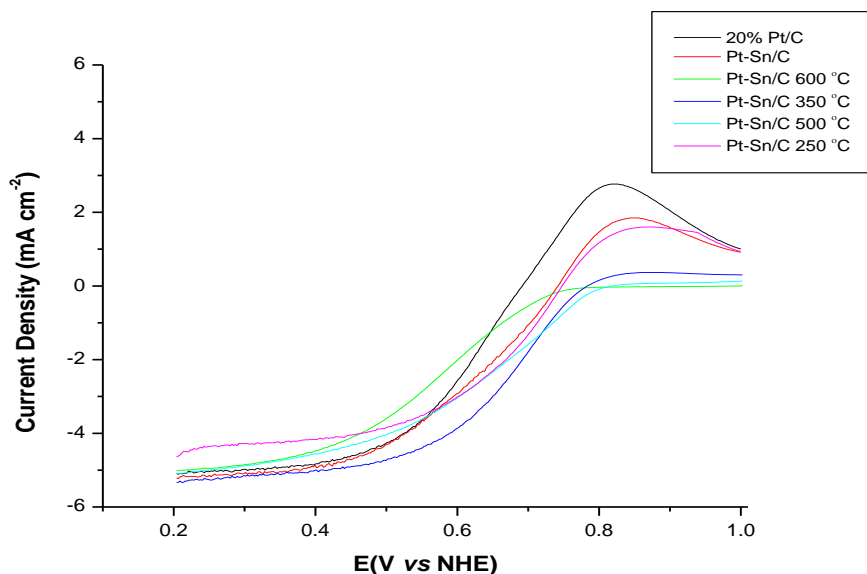


Fig 5.21 Polarization curves for Pt/C and Pt-Sn/C HA Slurry pH3 in 0.5 M H₂SO₄ + 0.5 CH₃OH under oxygen atmosphere and at a scan rate of 5 mV s⁻¹, rotating speed 1500 rpm.

The composition of the as-prepared Pt-Sn/C bi-metallic catalyst – is 3:1 and results in a low activity towards methanol oxidation and therefore represents a high methanol tolerance during ORR [15,24-26]. The order of electrocatalytic resistance towards methanol is as follows: Pt-Sn/C 600°C > Pt-Sn/C 500 °C > Pt-Sn/C 350 °C > Pt-Sn/C 250 °C > Pt-Sn/C as-prepared.

5.8 Accelerated durability studies

Accelerated durability studies were conducted to investigate the catalyst performance over a long period (10-12 hours) to observe how the ECSA will be effected if exposed to long hours of operation in a DMFC. First we applied accelerated square wave potential cycling between +0.6 and +1.10 V vs NHE in N₂ purged 0.5 M H₂SO₄ solutions at room temperature for 1200 cycles after which the procedure was stopped and then the CV required for calculation of ECSA was recorded at a scan rate of 25 mV s⁻¹ form +0.05V – +1.10V vs NHE. The cycle was then repeated and a CV scan recorded after every 1200 cycles. The study was performed overnight and lasted for up to 12 hours. The CVs showed a loss of 14% and 18% in ECSA for 20% Pt/C and the as-prepared Pt-Sn/C HA Slurry pH3 catalysts respectively for the first 1000 cycles suggesting the lower durability of Pt-Sn/C HA Slurry pH3 for long term operation. As

the number of cycles increased, so the ECSA decreased for both catalysts. After 7200 cycles the overall loss in ECSA was 49% for Pt/C and 51% for Pt-Sn/C HA Slurry pH3. The bad performance of the Pt-Sn/C HA Slurry pH3 catalysts during the initial stages of the durability test may be related to the incomplete alloying of Pt with Sn for the as-prepared catalyst. Also, Sn may dissolve or leach out of the surface under the operation conditions and long exposure in the acidic environment. Fig.5.22 shows the comparison of the different Pt catalysts after performing the accelerated durability tests for 15 000 cycles. The 46% TKK catalysts showed the worst durability capabilities of all the commercial catalysts with an overall lost in ECSA of 83%.

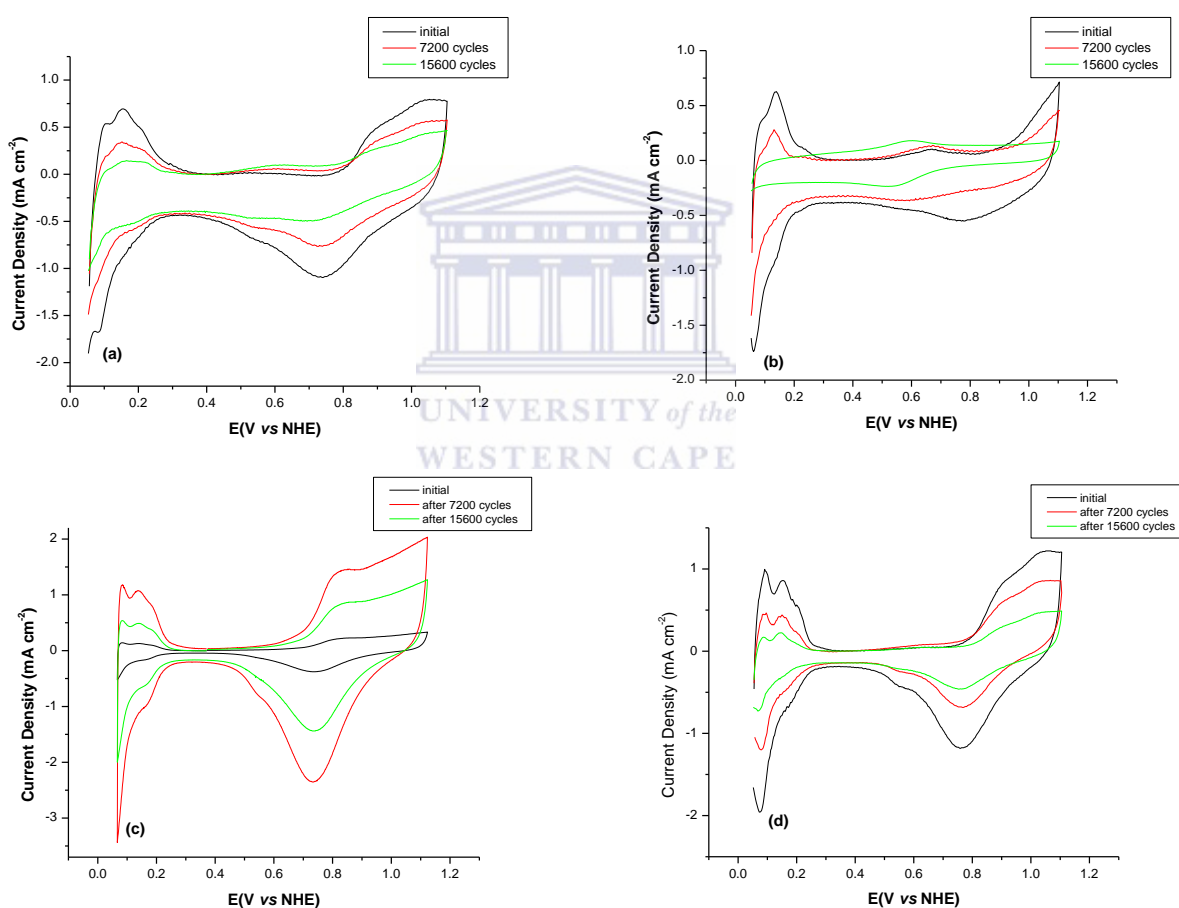


Fig. 5.22 CV of (a) 20% Pt/C (b) Pt-Sn/C HA Slurry pH3(c) 46% TKK and (d) 40% Pt/C before and after accelerated durability test at 25 mV s^{-1} in $0.5 \text{ M H}_2\text{SO}_4$.

Although the initial ECSA for TKK was the highest, there was a steep drop in ECSA value after 3000 cycles. For the Pt-Sn/C as-prepared catalyst the ECSA in the beginning was higher than that of Pt-Sn/C 250 °C catalyst but after 15 000 cycles the overall lost in ECSA was much lower for the heat-treated catalyst when compared to the as-prepared catalyst and commercial Pt/C catalysts. This proves that heat-treatment of the Pt-Sn/C catalyst is beneficial when it comes to the catalyst's durability properties and that the catalyst is more stable under ADT conditions in comparison with the commercial catalyst. It was observed that after 9000 cycles a plateau appears for all the catalysts (except TKK) indicating that after a certain amount of cycles the ECSA values do not change much as seen during the initial stages of the test (1- 7200 cycles). After completion of the ADT runs post analysis of selected catalysts samples by TEM revealed changes in the morphology of the catalysts. The TEM micrographs in Fig. 5.24 show significant increase in particle size and agglomeration for TKK and the as-prepared Pt-Sn/C.

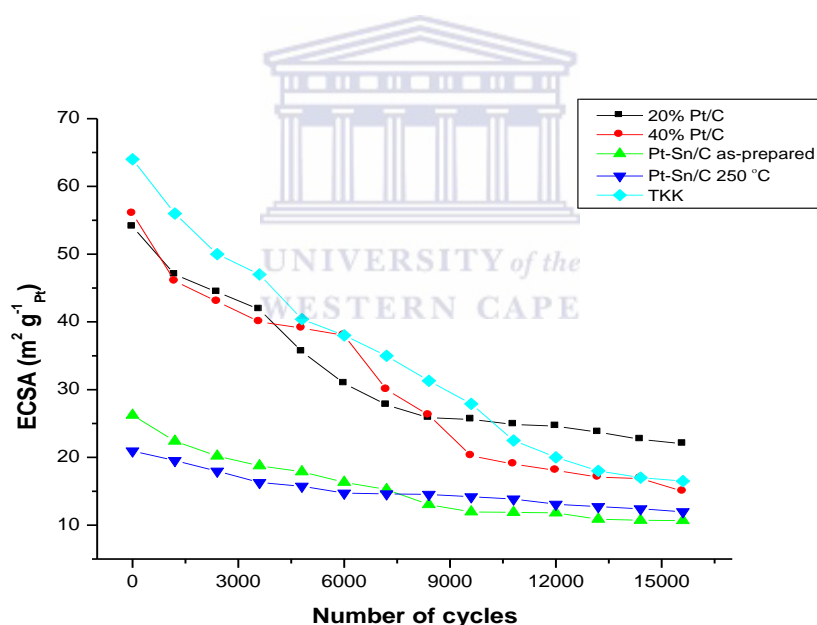


Fig. 5.23 Durability test of different Pt/C and Pt-Sn/C catalysts.

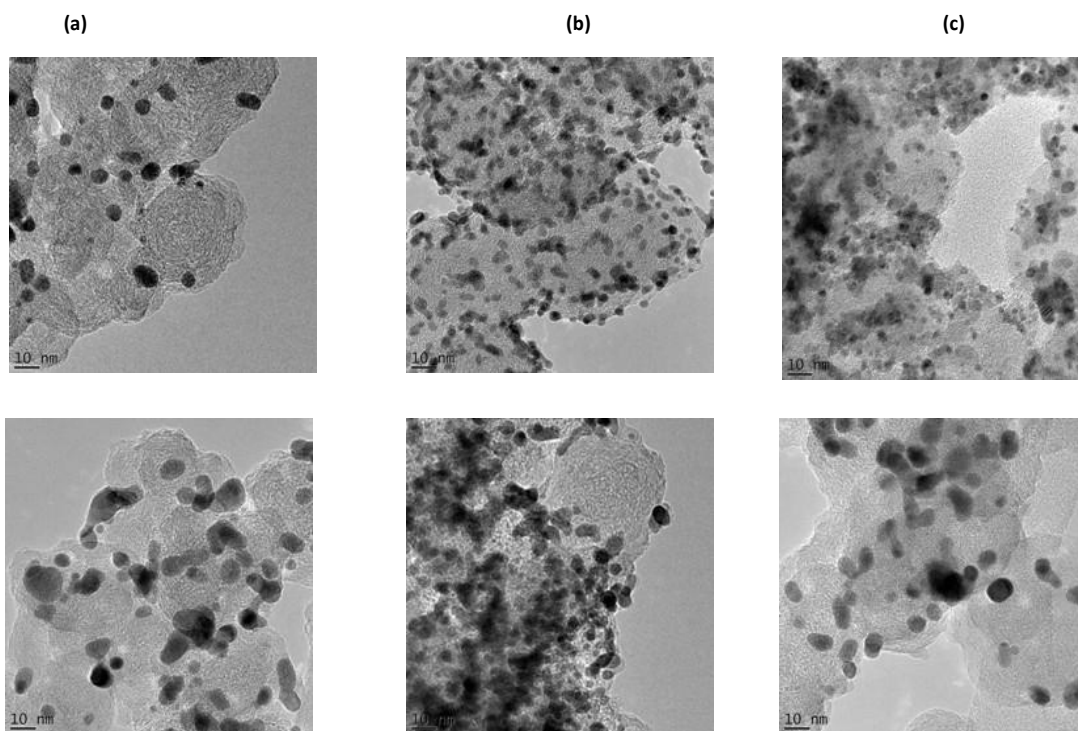


Fig. 5.24 (top) Pre-TEM images of (a) Pt-Sn/C, (b) TKK and (c) Pt-Sn/C 250°C (bottom) post TEM images.

The increase in particle size and the widening of the particle size distributions shown in Fig. 5.25 are characteristic of Ostwald ripening and is a major degradation mechanism for Pt/C catalysts at the cathode [27]. The as-prepared Pt-Sn/C and TKK catalyst both showed the smallest particle size distribution before cycling but the effect of Ostwald ripening was more severe on both when compared to the other catalysts. It's known that smaller Pt nanoparticles are more easily subjected to dissolution than larger ones making the effect of Ostwald ripening bigger and hence the bigger lost in ECSA for the two catalyst in comparison with the other catalyst that showed a bigger particle size distribution [27,28]. On the other hand, there was no significant change in particle size for the Pt-Sn/C 250 °C catalyst. This enhanced durability is more likely due to inhibition of Ostwald ripening as a result of heat treatment of the catalyst. Table 5.9 summarizes the data collected after the ADT run.

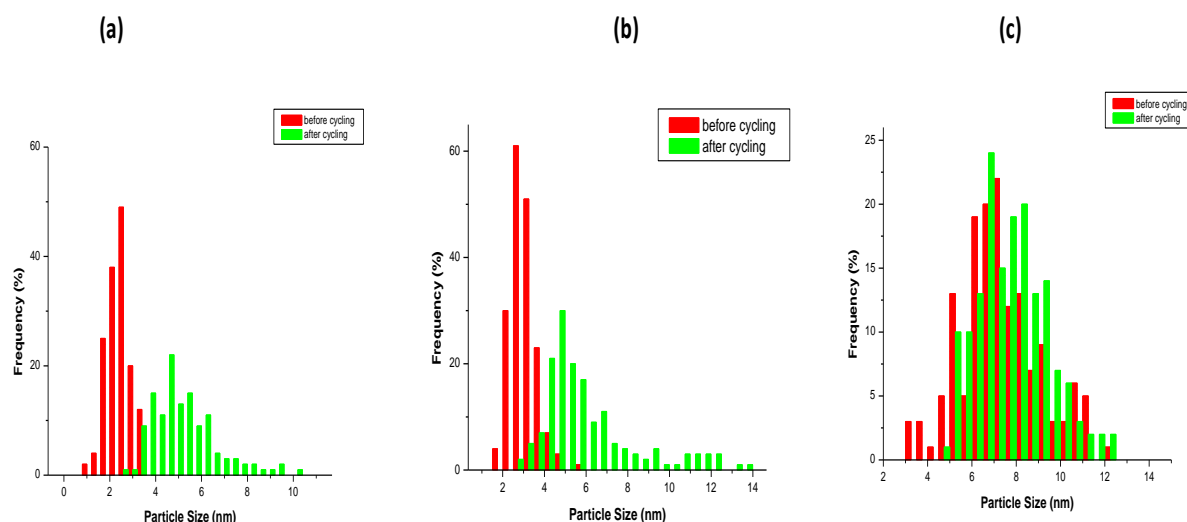


Fig. 5.25 Particle size distribution of pre -and post ADT TEM images of (a) Pt-Sn/C, (b) TKK and (c) Pt-Sn/C 250°C.

Table 5.9 Summary of catalyst properties and ADT data

Catalyst	Particle Size (nm)	Particle Size after ADT (nm)	ECSA before ADT ($\text{m}^2\text{g}^{-1}\text{Pt}$)	ECSA after ADT ($\text{m}^2\text{g}^{-1}\text{Pt}$)	% ECSA lost
20% Pt/C	3.94	5.32 ± 1.87	53.98	22.34	58.61
40% Pt/C	3.80	5.67 ± 2.02	56.08	15.54	72.28
46% TKK	2.97	7.23 ± 2.62	64.35	10.76	83.27
Pt-Sn/C	2.49	4.56 ± 2.24	26.24	11.87	54.76
Pt-Sn/C 250°C	5.08	5.98 ± 1.65	20.98	10.65	49.23

5.9 Conclusions

Carbon supported Pt-Sn alloy electrocatalysts synthesized with the polyol method were characterized electrochemically by CV, MOR and ORR. All the Pt-Sn/C catalysts showed different degrees of resistance towards MOR and can be attributed to the alloying of Pt with Sn. Of the as-prepared catalysts, the Pt-Sn/C HA Slurry pH3 catalyst showed superior performance when compared to 20% Pt/C for ORR and MOR and was comparable to 40% Pt/C. Subtracting background scans for raw ORR data and IR-Drop correction for ohmic

resistance of electrolyte solutions proved to be an important factor in producing accurate i_k and Tafel slope values. The thin-film method proved to be a satisfactory method to screen catalyst before DMFC testing. Heat-treatment of the Pt-Sn/C HA Slurry pH3 catalyst showed an increase in methanol tolerance but mixed performances towards ORR were observed. The Tafel slopes of Pt-Sn/C HA Slurry pH3 heat-treated catalysts suggest that the ORR mechanism is similar to that of Pt/C and that the alloying of Pt with Sn does not negatively influence the catalyst kinetic properties. From the initial screening of the synthesized catalysts, the as prepared Pt-Sn/C HA Slurry pH3 and Pt-Sn/C 250 °C fulfilled the criteria for the search of a methanol tolerant cathode catalyst as both catalysts showed methanol resistance as well as faster kinetics for the ORR. However, an area in which the two catalysts performance were not up to standard was during the durability testing where it was demonstrated that both catalysts showed a loss in ECSA of more than ca. 50% which is not satisfactory for a cathode catalyst which needs to be operational for long hours in a DMFC. The improvement of the durability properties is critical and further work is needed in this area to lower the percentage lost in ECSA.



REFERENCES

1. M. Piet, MSc Thesis, Synthesis and characterization of cathode catalysts for use in direct methanol fuel cell, UWC 2010
2. A. J. Bard, L. R. Faulkner, *Electrochemical Methods - Fundamentals and Applications* (2nd edition), John Wiley & Sons, Inc., New York (2001)
3. H. Angerstein-Kozłowska, B.E. Conway, W.B.A Sharp, *Electroanal. Chem. Interfacial Electrochem.* 43 (1973) 9
4. A. Hamnett, in: A. Wieckowski (Ed.) *Interfacial Electrochemistry - Theory Experiments and Applications*, Marcel Dekker, Inc., New York (1999)
5. I. Takahashi, S.S Kocha *J. Power Sources* 195 (2010) 6312
6. Y. Garsany, O.A Baturina, K.E Swider-Lyons, S.S Kocha, *Anal. Chem.* 82 (2010) 6321
7. H.A Gasteiger, S.S Kocha, B. Sompalli, F.T Wagner, *Appl. Cat. B* 56 (2005) 9
8. M. Hayes, A.T. Kuhn, W. Patefield, *J. Power Sources* 2 (1977) 121.
9. G.S. Popkirov, *J. Electroanal. Chem.* 359 (1993) 97
10. D. van der Vliet, D.S Strmcnik, C. Wang, V.R Stamenkovic, N.M MARKovic, M.T Koper, *J. Electroanal. Chem.* 647 (2010) 29
11. C. Coutanceau M.J Croissant, T. Napporn, C.Lamy, *Electrochim. Acta* 46 (2000) 579
12. F. Colmati, E. Antolini. E.R Gonzalez, *Electrochim. Acta* 50 (2005) 5496
13. E. Lee, I. Park, A. Mathiram, *J. Phys. Chem. C* 114 (2010) 10634

14. S. Rani, A. Jayaraman, L.D. Sharma, G. MuraliDhar, T.S.R PrasadaRao, *J. Electroanal. Chem.* 495 (2000) 62
15. C. Jeyabharathi, P. Venkateshkumar, J. Mathiyarasu, K.L.N Phani, *Electrochim. Acta* 54 (2008) 448-454.
16. K. Kinoshita *J. Electrochem. Soc* 137 (1990) 845
17. A.N Haner, P.N Ross, *J. Phys. Chem.* 95 (1991) 3740
18. E. Antolini, E.R. Gonzalez, *Catal. Today* 160 (2011) 28
19. V.S Murthi, C. Urian, S.Mukerjee, *J.Phys. Chem. B* 108 (2004) 11011
20. Y. Takasu, Y.Fujii, K.Yasuda, Y.Iwanaga, Y.Matsuda, *Electrochim. Acta* 34 (1989) 453
21. P. Briot, A. Auroux, D.J ones, M. Primet, *Appl. Catal.* 59 (1990) 141
22. C. Wang, C. Yeh, *J Catal.* 178 (1998) 450.
23. M. Nesselberger, S. Ashton, J.C Meier, I. Katsounaros. K.J.J Mayrhofer, M. Arenz, *J. Am. Chem. Soc.* 133 (2011) 17428
24. C. Lamy, A. Lima, V. Le Rhun, C. Coutanceau, J.M. Leger, *J. Power Sources* 105 (2002) 283
25. H. Gasteiger, N. Markovic, P. Ross, E.J Cairns, *Electrochim. Acta* 39 (1994) 1825-1832.
26. D. Jong You, K. Kwon, K. Pak, H. Chang, *Catal. Today* 146 (2009) 15–19.
27. C. Hu, K.Y Liu, *Electrochim. Acta* 44 (1999) 2727-2738.

28. C. Bezerra, L. Zhang, H. Liu, K.Lee, A.L Marques. H. Wang, J. Zhang, *J. Power Sources* 173 (2007) 891



Chapter 6

Performance of Pt-Sn/C electrocatalysts in DMFC

6.1 Introduction

As discussed in Chapter 2 the search for more active cathode electrocatalysts with reduced Pt content is progressing in two major directions a) focusing on Pt-based catalysts and b) focusing on non-Pt catalysts [1,2]. As mentioned before, it is more beneficial for groups in South Africa to focus on Pt-based catalysts as South-Africa is the world's largest supplier of PGMs. As for real applications in PEMFC and DMFC, Pt rich catalysts have shown significant improvement of 2-3 fold when compared to pure Pt catalysts interms of performance based on activity [3,4].

To develop new electrocatalysts with improved activity for fuel cell applications, well defined measurements are required to quantitatively determine and compare the electrocatalytic activities under fuel cell relevant conditions (i.e., steady state, 60-80 °C, continuous reactant flow). The most common method for this approach is to produce a MEA and to measure the catalytic activity in a single cell configuration in spite of the fact that such an evaluation of catalysts in the form of a MEA in fuel cells is a very time consuming process. Therefore, a facile alternative was developed on the basis of the RDE method used in the previous chapter [5]. Therefore, only the 2 catalysts with the best performance from the thin-film RDE studies (i.e., as-prepared Pt-Sn/C HA Slurry pH3 and the Pt-Sn/C 250 °C) were considered for DMFC testing.

6.2 Testing of Pt-Sn/C electrocatalysts in a fuel cell environment.

DMFC electrodes were fabricated using the synthesized Pt-Sn/C HA Slurry catalysts and electrochemical performance was evaluated as described in Chapter 3. Commercial Pt/C catalysts were also fabricated and evaluated for comparison. The polarization curves of 20% Pt/C (Pt1 MEA) and 40% Pt/C (Pt2 MEA) (JM) of the prepared electrodes are presented in Fig.6.1. The two cells differed only on the cathode side depending on which commercial Pt/C catalysts were used. It is also important to point out that it was never our aim to optimize the DFMC testing conditions. The aim was to investigate how the best synthesized Pt-Sn/C

catalyst prepared via the improved methodology would perform under true conditions compared to the commercial Pt/C catalysts. The reason for doing this was due to as the fact that results and conclusions made from RDE testing could differ substantially from fuel cell testing results since conditions are not quite the same and will thus influence the performance of the catalyst. From Fig. 6.1 it should be noted that the open circuit voltage (OCV) for typical DMFC catalysts is expected to be in the 0.65-0.9V range [6]. For both cases the OCV is significantly lower than the expected value but similar to each other. However, these typically higher OCV values were obtained with catalysts having loadings of 1.5 – 2.5 mg Pt cm⁻² and frequently even up to 5 mg Pt cm⁻² which is much higher than the 0.5 mg Pt cm⁻² for our catalysts used in this study. These high catalyst loadings are needed for DMFC when compared to PEMFC (which is normally 0.2- 0.5 mg Pt cm⁻²) due to slow reaction kinetics found in DMFC operations [6,7].

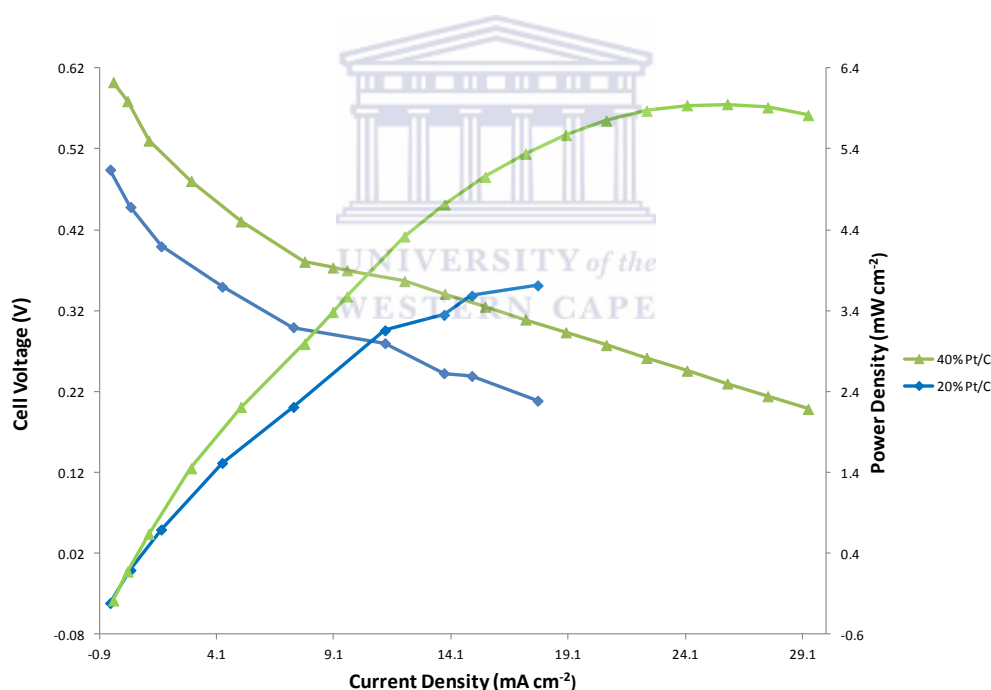


Fig. 6.1 Polarization curves of the Pt/C catalysts MEAs after conditioning cell temperature, 70°C; methanol concentration and flow rate, 1.0 M and 20.0 ml min⁻¹; dry oxygen, 50 ml min⁻¹ at ambient pressure.

Since it is of interest to compare the performance of Pt/C and the Pt-Sn/C catalysts the OCV baseline is considered to be less important than having similar OCV. It may also be noted in Fig. 6.1 that the cell made of 40% Pt/C cathode exhibits a higher performance although both commercial electrodes have similar Pt loading (0.5 mg Pt cm⁻²). At a fixed voltage of 0.35 V,

the current density of Pt2 MEA was nearly 17.2 mA cm^{-2} which is higher than 7.4 mA cm^{-2} for Pt1. The polarization curves also demonstrated that the Pt2 electrode has a higher limiting current density than Pt1 and therefore the mass transport properties of the Pt2 electrode are better than that of Pt1. To determine the exact reason for this better performance, further electrochemistry studies need to be performed on the different MEAs. From a MEA assemble point of view, human error can have an influence on every MEA and there is no guarantee that every MEA assembled is done in the same manner. Therefore this could also make a contribution and be one of the reasons why the performance of Pt2 was better. By comparing the two commercial catalysts the importance of performing single cell fuel cell testing to determine the real activities of the catalysts for real fuel cell applications is easy to be understood. Additionally, we also compared the best synthesized Pt-Sn/C electrocatalysts based on ORR using the RDE method to the commercial Pt/C catalysts and the results are illustrated in Fig.6.2.

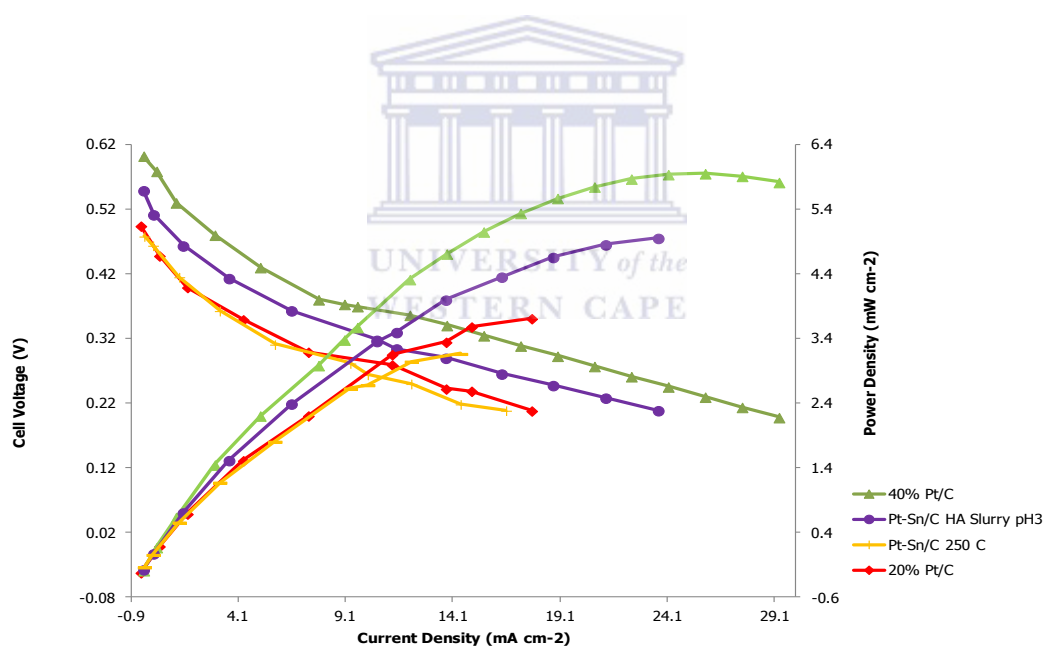


Fig. 6.2 Polarization curves of the Pt/C and Pt-Sn/C catalysts MEAs after conditioning. Cell temperature, 70°C ; methanol concentration and flow rate, 1.0 M and 20.0 ml min^{-1} ; dry oxygen, 50 ml min^{-1} at ambient pressure.

The polarization curves indicated that the as-prepared Pt-Sn/C HA Slurry pH3 showed a higher OCV than Pt1 but lower than Pt2 whereas in the case of the Pt-Sn/C 250°C a decline in performance was observed. Table 6.1 summarizes the results gathered from single cell

DMFC testing. The importance of single testing was noted in these results since in the RDE testing the Pt-Sn/C 250°C catalysts showed better performance than the commercial 20% Pt/C catalyst, whereas for the DMFC testing performed under our laboratory conditions the opposite was observed. This decline could be attributed to several factors including the way the catalyst ink was prepared and the manner in which the MEA was actually assembled. However, after repeating the Pt-Sn/C 250 °C catalyst evaluations twice more, the same observations were made where a decrease in performance was observed. This proved that in order to make a proper conclusion of a newly prepared electrocatalyst, both RDE and fuel cell testing is absolutely essential. The 40% Pt/C catalyst (0.5 mg Pt cm⁻² loading) showed the best performance of the MEAs. From CV results (Chapter 5) it showed the highest ECSA which means that the 40% Pt/C catalyst has a higher active surface area. Another reason for the improved performance could be that the catalyst layer of the MEA is much thinner as less catalysts (less carbon) is needed for the 40% Pt/C catalyst to achieve the desired loading of 0.5 mg Pt cm⁻². The path that the reactants (methanol and O₂) move through to come in contact with the catalysts is much shorter due to the thinner catalyst layer on the cathode and anode. This results in a shorter path that leads to lower resistance and therefore a higher activity. The order of performance for DMFC testing was found to be: Pt₂ >Pt-Sn/C HA Slurry pH3 > 20% Pt/C >Pt-Sn/C 250°C.

Table 6.1 DMFC polarization data

Catalysts	OCV (V)	Current Density @0.35V (mA cm⁻²)	Power Density @0.35V (W cm⁻²)
20% Pt/C	0.502	4.33	1.51
40% Pt/C	0.62	12.11	4.33
Pt-Sn/C as-prepared	0.54	7.25	2.84
Pt-Sn/C 250 °C	0.47	3.47	1.98

The gas diffusion electrode (GDE) catalysts were prepared by machine spray on carbon paper. The advantage of doing this to enable different electrode sizes to be prepared i.e., 5x5, 10x10, 25x25 by the simple expedient of physically cutting out the size required from the paper. The second major advantage of preparing the catalysts in this manner is that several small MEAs can be prepared from the same paper sheet and also the machine sprays evenly and it is not labour intensive. However it was found that preparing the catalysts in this way

for DMFC gave very low currents when the cell was polarize during fuel cell testing. It was thus of interest to investigate how the performance would change if instead of spraying on the Toray carbon paper we directly sprayed on the Nafion membrane. This latter method in literature is referred to as the catalyst coated membrane (CCM) method. The catalysts prepared for fuel cell testing were prepared the same with the only difference in the CCM method being that we did not use the Asymtek instrument but rather the hand spray gun.



Fig. 6.3 Picture of a catalyst coated membrane (CCM).

The prepared membrane is very fragile and can easily tear and thus when preparing the catalysts employing the CCM method one needs to be extremely careful. During the drying process of the catalysts using the spray procedure, caution needs to be taken to ensure that the membrane is not placed too close to the infra-red lamp as this will cause the membrane to deform due to the heat. Fig 6.4 shows the comparative performances of the Pt1 and as-prepared Pt-Sn/C HA Slurry pH3 catalysts with the CCM method. The OCV for both catalysts parallel each other very closely and are also close to the values observed for the GDE technique. However the current observed with the CCM method during polarization of the cell was much higher than before. For 20% Pt/C the limiting current at 0.2 V was 17.7 mA cm⁻² by spraying on the carbon paper and 92 mA cm⁻² when using the CCM technique, which lead to 5 fold increase of current. For Pt-Sn/C HA Slurry pH3 catalyst the limiting current was 23.60 mA cm⁻² with GDE technique and 103.2 mA cm⁻² when the catalysts were directly sprayed on the membrane which led to a 4 fold increase of current. Table 6.2 shows the values found for the CCM technique. The big improvement on the catalysts performance can be attributed to several factors. In the CCM method the anode and cathode ink are sprayed on opposite sides of the membrane which results in better contact between catalyst and membrane and is thus able to provide an increase in performance.

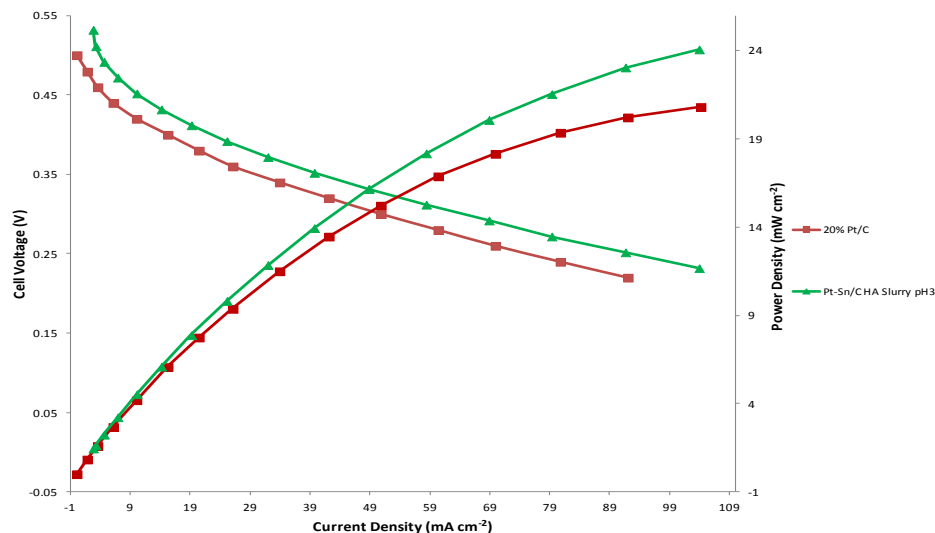


Fig. 6.4 Polarization curves of CCM Pt/C and Pt-Sn/C catalysts MEAs after conditioning cell temperature, 70°C; methanol concentration and flow rate, 1.0 M and 20.0 ml min⁻¹; dry oxygen, 50 ml min⁻¹ at ambient pressure.

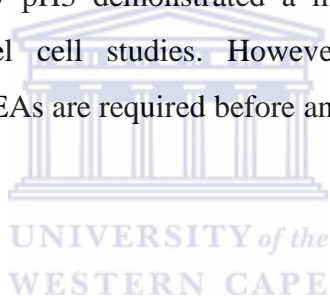
In the case for the GDE technique, the membrane is sandwiched between the catalyst sprayed carbon paper that influence the contact between the catalysts and membrane seeing that the catalysts is sprayed on only one side of the carbon paper. A further reason for the observed increase in performance for CCM could be that the structured setup for the measurements achieved a lower resistance. Thus by eliminating the carbon paper it ensured that there was nothing in the path of methanol/O₂ to inhibit these from coming into contact with the electrode surface and this further would contribute in a lower resistance with concomitant increase in current. At a potential of 0.35 V the current density of the Pt-Sn/C catalyst was 39.6 mA cm⁻² to the commercial catalyst which was 29.8 mA cm⁻² i.e., an improvement of 25%. Concerning the power density at 0.35 V the effect of tin was important with a power density of 18.13 mW cm⁻² compared to 15.82 mW cm⁻² for pure Pt an increase of 13% for Pt-Sn/C catalyst.

Table 6.2 DMFC polarization data of Pt/C and Pt-Sn/C with CCM

Catalysts	OCV (V)	Current Density @0.35V (mA cm ⁻²)	Power Density @0.35V (W cm ⁻²)
20% Pt/C	0.5	29.8	15.82
Pt-Sn/C as-prepared	0.53	39.6	18.13

6.3 Conclusions

The Pt-Sn/C catalysts with the best physical and electrochemical properties that were synthesized had their corresponding MEAs fabricated. For single cell DMFC testing commercial Pt/C was used and compared to our in-house catalysts. The OCVs were measured to be lower than what is reported in literature but were close to each other for catalysts having a loading of $0.5 \text{ mg Pt cm}^{-2}$. The as-prepared Pt-Sn/C HA slurry pH3 catalyst performed better than Pt1 and Pt-Sn/C 250 °C. However, during ORR testing the Pt-Sn/C 250 °C performed better than Pt1 but during real fuel cell testing it showed the lowest performance. This finding highlights the fact that in order to make an informed conclusion of the improved abilities of a new electrocatalysts, both RDE and fuel cell testing are required to observe how the catalyst is able to perform under real conditions. The GDE technique proved to be unsuitable for DMFC testing whereas the CCM testing technique showed that our best catalyst viz., Pt-Sn/C HA slurry pH3 demonstrated a much better performance with an increase in current during fuel cell studies. However, further more comprehensive electrochemical studies on the MEAs are required before an overall conclusion can be made.



REFERENCES

1. H.A. Gasteiger, S.S. Kocha, B. Sompalli, F.T. Wagner, *Appl. Catal. B* 56 (2005) 9.
2. S. Koh, J. Leisch, M.F. Toney, P. Strasser, *J. Phys. Chem. C* 111 (2007) 3744
3. K. Sasaki, J.X. Wang, H. Naohara, N. Marinkovic, K. Mored, H. Inadae, R.R. Adzica, *Electrochim. Acta* 55 (2010) 2645.
4. S. Ball, S. L. Burton, E. Christian, A. Davies, J. Fisher, R. O'Malley, S. Passot, B. Tessier, B.R.C. Theobald, D. Thompsett, *ECS Transactions* 25 (2009) 1011
5. M. Gattrell, B. MacDougall, in: W. Vielstich, H.A. Gasteiger, A. Lamm (Ed.), *Handbook of Fuel Cells: Fundamentals, Technology and Applications*, vol. 2, John Wiley & Sons Ltd., New York, 2003
6. E. Antolini, T. Lopes, E.R. Gonzalez, *J. Alloys Compd.* 461 (2008) 253–262
7. A.K. Shuka, R.K. Raman, *Annu. Rev. Mater. Res.* 33 (2003) 155-168

CHAPTER 7

Conclusions and Recommendations

The thesis describes work that originally set out to achieve three different objectives – a) to synthesize Pt-Sn/C catalysts with an improved polyol reduction method producing catalysts with high Pt loading that will be methanol resistant and promote the ORR, b) to characterize the Pt-Sn/C catalysts based on their physical and electrochemical properties and c) to evaluate the best synthesized Pt-Sn/C catalysts in a DMFC and compare the results to the commercial Pt/C catalysts.

7.1 Conclusions

Pt-Sn/C catalysts were successfully synthesized using a modified polyol reduction method. Different variations to the STD method were implemented to establish the best synthesis of the catalysts. It was found that adjusting the pH to above 12 initially helped with the reduction of the particle size and distribution. The influence of an experimental parameter viz., pH of the solution during the overnight stirring process, was explored. It was found that adding HCl which acted as a sedimentation promoter to adjust the pH to 3 after the reaction was completed resulted in the smaller Pt particle size and higher Pt loading. The role of sonication was also investigated and it was found that 30 – 60 min was sufficient for the reaction mixture to be sonicated before starting the reduction reaction procedure. The particle size of the catalysts were determined by XRD and TEM and found to be comparable to each other. The Pt size ranged from 2-4 nm for the as-prepared catalysts and 5-10 nm for the heat-treated catalyst. It was concluded that adjusting the pH after completion of the reaction was a key parameter. It was found that Pt-Sn nanoparticles were stabilized by the presence of glycolate ions whose content is affected by the pH.

Electrochemical characterization of the synthesized Pt-Sn/C catalysts was carried out by CV, MOR and ORR testing. From EC testing the as-prepared Pt-Sn/C HA Slurry pH3 and Pt-Sn/C 250 °C catalysts were found to be the best performing based on ORR studies. All the Pt-Sn/C catalysts showed resistance towards MOR. Electrochemical parameters like the Tafel slope, specific-and mass activity were determined from ORR in H₂SO₄. Two Tafel slope regions were observed in the low and high current density regions and values obtained

for the two best catalysts were comparable to literature reported values. However accelerated durability studies showed that improvement for long term operation still needs much attention as the Pt-Sn/C catalysts were found to be unstable after long hours of operation when compared to Pt/C.

As a final assessment the as-prepared Pt-Sn/C HA Slurry pH3 and Pt-Sn/C 250 °C catalysts were tested in a fuel cell environment. The electrodes were prepared by either spraying on the Toray carbon paper (GDE) with the Asymtek machine or by hand spraying directly on the Nafion membrane. Polarization curves were obtained that demonstrated that the as-prepared Pt-Sn/C HA Slurry pH3 catalyst performed better than the commercial 20% Pt/C with the same Pt loading for the GDE technique. The CCM technique showed a big improvement when the two catalysts were tested delivering much higher currents compared to GDE technique when the cell was polarized from ca. 0.5 V – 0.2 V. The importance of conducting electrochemical as well as real fuel cell studies were noted in order to make a proper assessment of the synthesized electrocatalyst.

In conclusion the polyol method may be viewed as an effective synthetic route for the synthesis of nanoparticles for FC applications. The strength of the method lies in its ability to effectively control the size and distribution of nanoparticles without necessitating complicated procedures. The Pt-Sn/C catalyst synthesized via the modified method has been extensively characterized for relevant electrochemical and physical properties such that it can be employed for fabrication by our research group for DMFC testing.

7.2 Recommendations:

It would be useful to investigate the influence of a third metal (Cu, Cr, Fe, Ni, Co) to observe if there possibly can be any further improvement towards ORR and methanol tolerance. It would also be useful to run long durability tests on the current Pt-Sn/C MEAs to determine the exact reasons why the Pt-Sn/C 250 °C catalysts performed worst during DMFC testing after showing enhanced performance during ORR testing. Also, more DMFC studies needs to be conducted to find the optimum parameters for the Pt-Sn/C catalyst to be used as cathode catalyst on a routine basis. Higher catalyst loadings for both anode and cathode should be investigated and compared to other commercial Pt bi-metal catalysts.



UNIVERSITY *of the*
WESTERN CAPE